

DOUBLET EMITTERS DERIVED FROM STABLE CARBENES FOR
POTENTIAL OLED APPLICATIONS

by

Gabrielle Eden Harmon, B.S.

A thesis submitted to the Graduate Council of
Texas State University in partial fulfillment
of the requirements for the degree of
Master of Science
with a Major in Chemistry
May 2020

Committee Members:

Todd W. Hudnall, Chair

William Brittain

Alexander Zakhidov

COPYRIGHT

by

Gabrielle Eden Harmon

2020

FAIR USE AND AUTHOR'S PERMISSION STATEMENT

Fair Use

This work is protected by the Copyright Laws of the United States (Public Law 94-553, section 107). Consistent with fair use as defined in the Copyright Laws, brief quotations from this material are allowed with proper acknowledgement. Use of this material for financial gain without the author's express written permission is not allowed.

Duplication Permission

As the copyright holder of this work I, Gabrielle Eden Harmon, authorize duplication of this work, in whole or in part, for educational or scholarly purposes only.

ACKNOWLEDGEMENTS

First, I want to thank my graduate advisor, Dr. Todd Hudnall, for accepting me into his lab as an undergraduate researcher and then a graduate researcher. He helped me grow as a chemist and an academic and for that I am truly grateful. He pushed me harder than any other professor or boss ever has, and that made me excel as a student and a scientist.

I also want to thank the Hudnall lab group for all of their help and support. Thank you Isaac Blythe and Dr. Tharushi Perera for staying late nights with me to help me run reactions, Michael Gildner for the DFT calculations and NMR help, and the rest of the group for overall support and random things I have asked for.

Lastly, I want to thank my soon to be husband, Dr. Eric Welch, for all of the amazing support he has given me the last 6 years throughout my undergraduate and graduate degrees. He saw many late nights of studying and working and kept me motivated. He saw many tears but was always there with kind words of encouragement. He has pushed me to not only be a better scientist, but overall a better person. I don't know how I would have done this without him.

TABLE OF CONTENTS

	Page
ACKNOWLEDGEMENTS	iv
LIST OF TABLES.....	vii
LIST OF FIGURES	viii
LIST OF ABBREVIATIONS	xiii
ABSTRACT	xv
CHAPTER	
1. INTRODUCTION	1
1.1 General Introduction.....	1
1.2 History of OLEDs.....	5
1.3 The Importance and Problems of Modern OLEDs.....	8
1.4 Doublet Emitters.....	11
1.5 Tuning Emissions by Incorporation of Carbenes	16
1.6 Objectives.....	19
1.7 General Procedures.....	21
1.8 Instrumentation	21
2. TRIARYLMETHYL RADICALS	22
2.1 Introduction	22
2.2 Synthesis and Characterization of IMes-Triarylmethyl Radical.....	23
2.3 Synthesis and Characterization of a CAAC-Triarylmethyl Radical.....	26
2.4 Synthesis and Characterization of a DAC-Triarylmethyl Radical	29
2.5 Discussion and Conclusion.....	32
3. TRIARYLBORYL RADICALS	33
3.1 Introduction	33
3.2 Synthesis of Potential Triarylborene Precursors and Previous Reactions of Carbenes with Fluorinated Borane Derivatives.....	34
3.3 Synthesis and Characterization of a CAAC-Triarylboryl Radical.....	38

3.4 Synthetic Efforts Toward an IPr-Triarylboryl Radical	51
3.5 Synthetic Efforts Toward a SIMes-Triarylboryl Radical	58
3.6 Synthetic Efforts Toward a DAC-Triarylboryl Radical	62
3.7 Experimental.....	64
3.8 Discussion and Conclusion.....	65
 4. FUTURE WORK	 67
4.1 Overview	67
4.2 Synthesis and Characterization of MAAC-Triarylboryl Radicals	69
4.3 Synthesis and Characterization of Cyclopropenyldiene-Triarylboryl Radicals	70
4.4 Synthesis and Characterization of BiCAAC-Triarylboryl Radicals ...	71
4.5 Synthesis and Characterization of a Carbene-Substituted Oxoboranthracene Derivatives	71
 APPENDIX SECTION	 73
 LITERATURE CITED	 98

LIST OF TABLES

Table	Page
1. List of OLED discoveries and new technologies from 1987-2013.....	7
2. HOMO and LUMO levels of selected carbenes (Gaussian(09):B3LYP/6-31G+(d).....	18
3. Comparison of HOMO/LUMO energy levels between MAAC, BiCAAC, cyclopropenylidene, CAAC, and SIMes	68

LIST OF FIGURES

Figure	Page
1. Components of a modern OLED device.....	1
2. Diagram of electron-hole recombination.....	2
3. Singlet and triplet excited states.....	3
4. Jablonski diagram describing various excitation and relaxation pathways.....	4
5. Jablonski diagram of TADF emission.....	4
6. Materials and structure of an OLED device reported by C.W. Tang et. al.....	5
7. First commercially available OLED display in car radios.....	6
8. Rollable OLED screen by LG corporation.....	8
9. Projected monetary growth of OLEDs over the next six years.....	9
10. Projected roadmap for future OLED displays includes foldable and rollable displays	10
11. Series of four brightly colored iridium phosphorescent materials used in OLED devices.....	11
12. Illustration of closed-shell versus open-shell systems, figure modified from reference 32.....	12
13. Molecular orbital energy levels of TTM-1Cz.....	13
14. Gomberg, Theile, and Tschitschibabin radical species, respectively.....	13
15. PTM, TTM, PyBTM, bisPyTM, and PTM-3NCz radical systems.....	15
16. Series of synthesized doublet emitters.....	15
17. Left vial: chloroform solution of compound 1 , right vial: cyclohexane solution of compound 2	16
18. Buchner's ethyl diazacetate reaction with carbene intermediate.....	17

19. Wanzlick and group's NHC and dimer	17
20. Bertrand's isolated carbene.....	17
21. HOMO/LUMO gaps of selected carbenes	18
22. Triaryl methyl radical with counter anion PF_6^-	20
23. Triaryl boryl radical.....	20
24. Compounds 5,6 , and 7	22
25. Synthesis to incorporate IMes into TPFM giving compound 5	24
26. Powder obtained from reaction of TPFM with IMes	24
27. Weak orange emission of compound 5 under hand-held UV lamp.....	25
28. HOMO of compound 5	25
29. Oxidation of compound 5 to give radical cation $\mathbf{5}^+$	26
30. Weak green emission of $\mathbf{5}^+$	26
31. Synthesis of triarylmethyl-CAAC compound 6	27
32. Solution of compound 6	27
33. Left: HOMO of compound 6 , Right: ChemDraw rendering of compound 6	28
34. Oxidation of 6 with Reaction of TPFM-CAAC and nitrosonium hexafluorophosphate to give radical cation $\mathbf{6}^+$	28
35. OLED device made with $\mathbf{6}^+$	29
36. Reaction scheme for the synthesis of compound 7	29
37. Compound 7 in C_6D_6	30
38. Room temperature EPR spectrum of compound 7 in benzene	30

39. Left: One singly occupied molecular orbital of 7 depicting density localized on the triarylmethyl carbon of the TPFM moiety.....	31
40. Left: The other singly occupied molecular orbital of 7 depicting density localized on the DAC moiety.....	31
41. Synthesis of tris-pentafluorophenyl borane	34
42. a) reaction of a-NHC with tris-pentafluorophenyl borane b) reaction of CAAC with tris-pentafluorophenyl borane	35
43. Left- Crystal structure of a-NHC with tris-pentafluorophenyl borane.....	36
44. Synthesis of dimesityl pentafluorophenyl borane	36
45. ¹⁹ F NMR of dimesityl pentafluorophenyl borane in chloroform	37
46. Left: Triaryl borane in DCM.....	37
47. Proposed structures of 8–11	38
48. Reaction of CAAC with dimesityl, pentafluorophenyl borane to synthesize compound 8–Fa and 8–Fb	39
49. Left: Compound mixture of 8–Fa,b in dry DCM.....	39
50. ¹⁹ F NMR spectrum of product 8–Fa,b obtained by addition of CAAC to dimesityl pentafluorophenylborane	41
51. ¹¹ B NMR of mixture of 8–Fa and 8–Fb	42
52. UV-Vis spectrum of 8–Fa,b mixture in dry DCM.....	42
53. Fluoride abstraction from mixture of 8–Fa,b with TMS-OTf to give the cation 8⁺	43
54. Left: 8⁺ in dry DCM.....	44
55. ¹⁹ F NMR of 8⁺ in CD ₂ Cl ₂	44
56. ¹⁹ F NMR spectrum of 8⁺ from approximately -126 ppm to -131 ppm in CD ₂ Cl ₂	45
57. ¹¹ B NMR spectrum of 8⁺ in CD ₂ Cl ₂	46

58. UV-Vis spectrum of 8 ⁺ in DCM.....	46
59. Reduction of 8 ⁺ with potassium graphite to afford radical 8 [•]	47
60. 8 [•] in dry benzene	47
61. Emission of a benzene solution of 8 [•] when irradiated with a hand-held UV lamp	48
62. Top: Simulated EPR spectrum of 8 [•] : g _{iso} = 1.956, hyperfine coupling constants (G): ¹⁵ N1: 4.31, ¹⁹ F1: 4.00, ¹⁹ F2: 3.90, ¹¹ B1: 0.96	49
63. Left: Skeletal formula of 8 [•]	50
64. Photoluminescence spectra of 8 [•] processed and encapsulated in N ₂	50
65. Photoluminescence spectra of 8 [•] processed in N ₂ but no encapsulation (exposed to air)	51
66. Projected synthesis of 9 [•]	52
67. Left: 9 – F in dry DCM.....	52
68. ¹⁹ F NMR of product 9 – F obtained from reaction of IPr and triaryl borane.....	53
69. Close up of triplet peak at -164.15 from figure 68.....	53
70. ¹¹ B NMR spectrum (CD ₂ Cl ₂) of the product obtained from addition of IPr to the triaryl borane	54
71. Example of a double C-F activation	55
72. Potential product 9 ⁺ of double addition of triaryl borane to IPr.....	55
73. Left: Product obtained from addition of TMS-OTf to the product of the addition of IPr to the triarylborane in dry DCM.....	56
74. ¹⁹ F NMR of product obtained from the addition of TMS-OTf to the product obtained from the addition of IPr to the triarylborane.....	57
75. ¹¹ B NMR spectrum of the addition of TMS-OTf to the product obtained from addition of IPr to the triarylborane.....	58

76. Addition of SIMes to the triaryl borane to form product 10-F	58
77. Left: 10-F in dry DCM	59
78. ¹⁹ F NMR spectrum of 10-F in CD ₂ Cl ₂	59
79. ¹¹ B NMR in CD ₂ Cl ₂ of 10-F	60
80. Lewis adduct 10	60
81. ¹⁹ F NMR spectrum of the product obtained from the addition of TMS-OTf to Lewis adduct 10	61
82. ¹¹ B NMR spectrum of the product obtained from the addition of TMS-OTf to Lewis adduct 10	62
83. Unsuccessful reaction pathways of DAC and the triaryl borane	63
84. Okamoto, Takeya, and Yamaguchi's boron stabilized neutral π -radical system.....	68
85. π -radical system with carbene	68
86. Future carbenes to attach to triaryl borane	69
87. Proposed synthesis of MAAC-triaryl borane radical.....	70
88. Proposed synthesis of cyclopropenylidene-triaryl borane radical.....	70
89. Proposed synthesis of BiCAAC-triaryl borane radical.....	71
90. Proposed synthesis of π -radical system with carbene.....	72

LIST OF ABBREVIATIONS

Abbreviation	Description
BiCAAC	bicyclic cyclic(alkyl)amino carbene
CAAC	cyclic(alkyl)amino carbene
CV	cyclic voltammetry
DAC	six-membered diamido carbene
DCM	dichloromethane
Dipp	2,6-diisopropylphenyl
HOMO	highest occupied molecular orbital
IPr	N, N'bis (dipp) imidazolylidene
IQE	internal quantum efficiency
LUMO	lowest unoccupied molecular orbital
MAAC	mono(amido)amino carbene
Mes	2,4,6-trimethylphenyl
NaHMDS	sodium hexamethyldisilyl amide
NMR	nuclear magnetic resonance
OLED	organic light emitting diode
OTf	triflate
SIMes	saturated N,N'dimesitylimidazol-2-ylidene
SOMO	singly Occupied Molecular Orbital
SUMO	singly Unoccupied Molecular Orbital

TPFM	tris(pentafluorophenyl)methane
TMS	trimethylsilyl or trimethyl silane
UV-Vis	ultra-violet-visible spectroscopy

ABSTRACT

Organic light emitting diodes (OLEDs) typically exhibit low quantum efficiencies (~19%) due to quantum mechanical limitations and spin statistics. In traditional OLEDs, the emitting excitons are either singlet (25%) or triplet (75%) spin states. Because decay from triplet states is spin forbidden, the internal quantum efficiency of fluorescent devices is limited to a theoretical maximum of 25%. To circumvent this problem, modern OLEDs rely on triplet, phosphorescent emitters, that require the incorporation of often expensive heavy atoms to facilitate intersystem crossing between the singlet and triplet excited states, thus increasing triplet emission. In contrast to the widely explored triplet emitters, this thesis will describe our recent efforts to prepare cationic and neutral doublet emitters derived from carbenes and triarylmethyl- or triarylboryl-centered radicals, respectively. In principle, doublet emitters have theoretical quantum efficiencies of up to 100%, making them ideal candidates for next-generation light-emitting devices. Carbenes will be incorporated into the triarylmethyl- and triaryl boryl- compounds in order to change the emission color as well as stabilize the radical.

A series of cationic doublet emitters were synthesized and one (CAAC-TPFM radical) was layered onto a device. This device was found to be very inefficient, possibly due to anionic emission dampening.

A series of neutral doublet emitters were attempted with one doublet emitter (CAAC-triaryl boryl radical) being layered onto a device. This OLED device was tested for efficiency and found to be subpar due to degradation; however, carbenes were found to be

successful in changing the emission colors of each molecule. Colors that were recorded were orange, yellow, green, and blue.

1. INTRODUCTION

1.1 General Introduction

Organic materials have been known to show very high fluorescent quantum efficiencies in the visible region which has made them a candidate for light emitting devices.^{1,2} Organic light emitting diodes, otherwise known as OLEDs, are a competitive technology used in the display and lighting field.¹ OLEDs differ from their LED predecessor by using organic materials for light emission rather than solid state inorganic materials commonly used in LEDs.² OLEDs are comprised of organic layers that are sandwiched between an anodic electrode and a cathodic electrode, as shown below in Figure 1.³ Generally, there are multiple organic layers between the electrodes, and each have a purpose. The most common uses for these organic layers are for transport and emission.

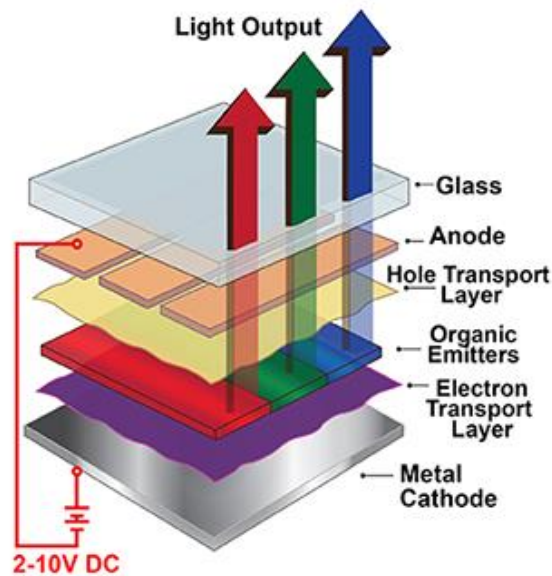


Figure 1. Components of a modern OLED device.³

When voltage is applied to the system, charge carriers, which are particles that can

freely move and possess a charge, are injected into the organic layers from their respective electrodes. The anode injects a hole, also known as a positive charge, and the cathode injects an electron, which holds a negative charge. These charge carriers travel through the transport layers and recombine in the emissive layer. When this recombination event occurs, a photon is released, and light is emitted.⁴ This idea is shown in Figure 2.

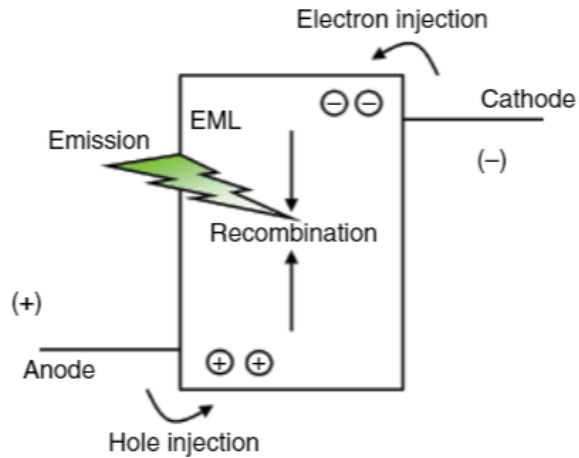


Figure 2. Diagram of electron-hole recombination²

Emission in OLEDs is the production and discharge of light. Emission can be represented by the following equation;

$$h\nu = |E_m - E_n| = \Delta E$$

where E_m and E_n are different states with different energy levels, h is Planck's constant, and ν is the frequency of emission.² This equation shows that the emission frequency in OLEDs depends on the energy gap between ground and excited states. Thus, emission colors are able to be tuned by the various gap distances between ground and excited stages. There are three main types of emission in OLEDs; thermally activated delayed fluorescent (TADF) OLEDs, phosphorescent OLEDs, and fluorescent OLEDs.^{5,6,7}

When some outside stimulus is applied to the system, such as voltage, one of the electrons in the ground state, otherwise known as the highest occupied molecular orbital (HOMO), are promoted to a higher energy excited state, which is typically the lowest unoccupied molecular orbital (LUMO). After the electron is excited, it can either then form a singlet or triplet excited state (Figure 3). If the spin of the excited state electron is opposite that of the electron in the ground state, this is known as a singlet state. A triplet state is when both the excited electron and ground state electron have matching spin states. A triplet state is said to be forbidden due to the Pauli Exclusion Principle, which is the assertion that no two identical fermions can exist in the same quantum state.⁸

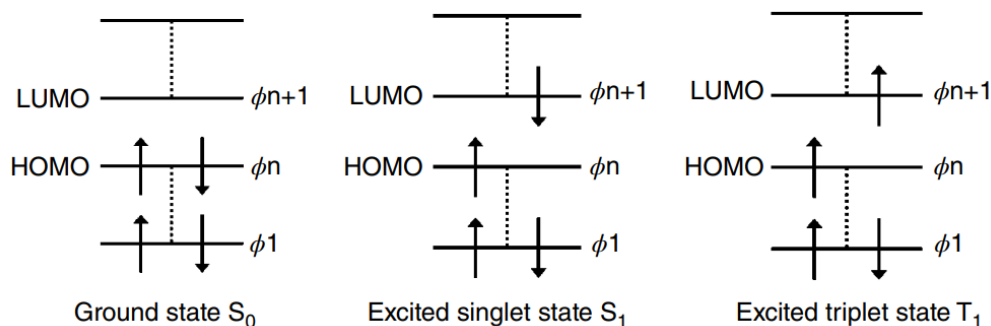


Figure 3. Singlet and triplet excited states²

Fluorescence occurs when the singlet state excited electron relaxes back down to its ground states and emits a photon. Phosphorescence occurs whenever a triplet state excited electron relaxes back down to its ground state and emits a photon. Due to this spin state being forbidden, this process must happen radiatively so that the electron spin of the excited electron does not match the spin of the electron that remained in the ground state. This is illustrated in the Jablonski diagram shown below (Figure 4).

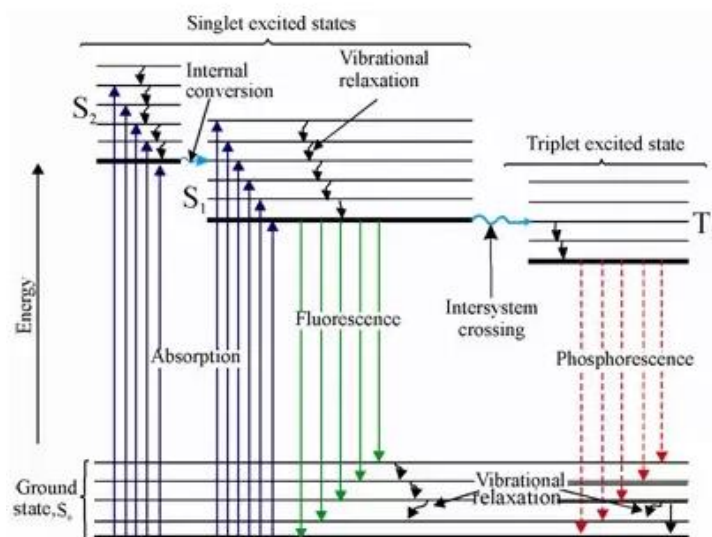


Figure 4. Jablonski diagram describing various excitation and relaxation pathways⁹

Thermally activated delayed fluorescent (TADF) OLED work by having singlet and triplet excited states that are very close to energetically. This promotes both intersystem crossing (ISC) and reverse intersystem crossing (RISC), the latter of which enables the triplet excited electrons to convert back into singlet excited electrons which then relax normally to give off light (Figure 5).^{5,10}

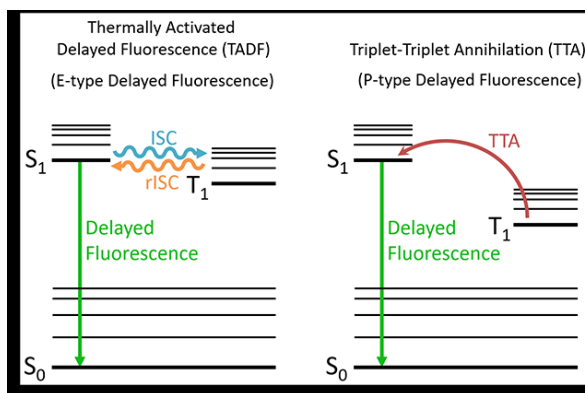


Figure 5. Jablonski diagram of TADF emission

1.2 History of OLEDs

OLEDs were first discovered by Andre Bernanose et al in 1953 when a cellulose film doped with acridine orange emitted light.¹¹ It was not until ten years later that another discovery was made with OLEDs, by Martin Pope et al.¹² This group documented that when a single crystal of anthracene was placed in a high electric field, the crystal would show light emission. Unfortunately, OLEDs were not seen as a potential technology during this time due to the need of a very high electric field while exhibiting very low efficiency and luminescence. Another impactful discovery with OLEDs didn't occur until 1987 when C.W. Tang and S. A. VanSlyke reported bright emission from a device which sandwiched two organic layers between an anode and cathode.⁷ This reported device consisted of a bottom emission structure coupled with small molecular fluorescent monochrome organic material that was evaporated onto glass substrates (Figure 6).

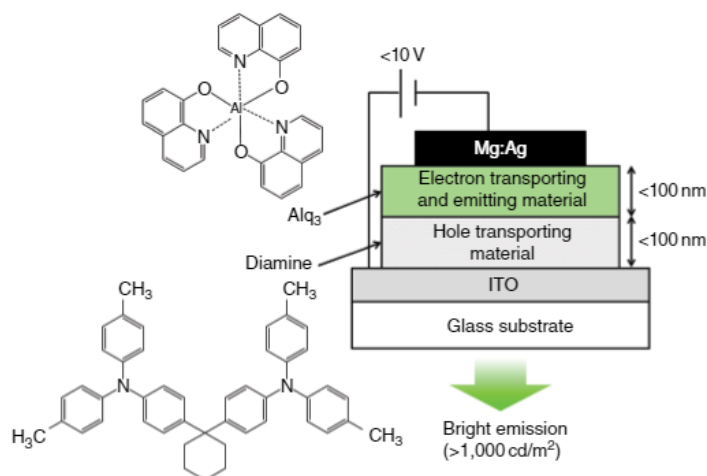


Figure 6. Materials and structure of an OLED device reported by C. W. Tang et al.⁷

This was an incredible discovery because of how it differed from the discoveries before it. Tang and S. A. VanSlyke created two new technologies that were very innovative,

once which used organic layers with extremely low thicknesses as well as the implementation of a bi-layer structure in devices. Tang and S. A. VanSlyke also reported that the voltage requirement was only 2.5 V for emission to occur, whereas before the voltage required for emission in some devices was upwards of 100V. The external quantum efficiency was still very low, approximately 1%, but the discovery itself of this was enough to spur the movement towards OLED technology, both academically and commercially. In 1990 Cavendish Laboratories synthesized a light emitting polymer that could be used with devices.¹³ In 1994, white emissive OLEDs were reported by Kido et al. of Yamagata University.¹⁴ This report led to making full- color OLED displays by the use of white OLED emission with color filters. In 1997 the world's first commercially available OLED device was made available by the Pioneer corporation. This device was a green emissive passive-matrix OLED display used for car radios. An example of such is shown below in Figure 7.¹⁵



Figure 7. First commercially available OLED display in car radios¹⁵

Phosphorescent OLEDs were reported by the Thompson and Forrest's group at Princeton university.¹⁶ These OLEDs had a critical role in the development of modern OLEDs due to their theoretical internal quantum efficiency (IQE) of 100%, which before then was unheard of. Many more discoveries were made after this time up to the present, which are listed in the detailed in table 1 below.

Table 1. List of OLED discoveries and new technologies from 1987-2013²

1987	Invention of two layered OLED (Eastman Kodak/ Tang and VanSlyke)
1990	Invention of polymer OLED (Cavendish Lab. / Burroughes et al. of Friend's group)
1994	First reported white emissive OLED (Yamagata Univ. / Kido et al.)
1997	World's first commercial OLED (Pioneer Corporation)
1998	Discovery of Phosphorescent OLED (Princeton Univ./ Baldo et al. of Thompson and Forrest's group)
1999	Prototype of a full-color polymer AM-OLED display fabricated by ink-jet printing (Seiko- Epson)
2001	Prototype 13" full color AM-OLED display (Sony)
2002	Invention of multi-photon OLED (Yamagata Univ./Kido et al.)
	Prototype 17" full-color polymer AM-OLED display fabricated by ink-jet printing (Toshiba)
2003	World's first commercial polymer OLED display (Philips)
	World's first commercial active-matrix OLED display (SK Display)
2006	Prototype of 3.6" full-color polymer AM-OLED display with the world's highest resolution (202 ppi) (Sharp)
2007	World's first application of AM-OLED displays for main displays of mobile phones (Samsung)
	World's first commercial AM-OLED-TV (Sony)
2009	Discovery of TDAF (Thermally Activated Delayed Fluorescence) (Kyushu Univ. / Endo et al. of Adachi's group)
2011	World's first commercial OLED lighting (Lumiotec)
2012	Flexible OLED display prototype (Semiconductor Energy Laboratory & Sharp)
	Prototype of 55" OLED-TV (Samsung;LG)
2013	Prototype of 56" TV (Sony) (Panasonic)
	World's first commercial flexible OLED displays (Samsung) (LG display)

1.3 The Importance and Problems of Modern OLEDs

OLEDs are very important for modern technology. They are a very versatile type of technology that can be used in flat panel displays for consumer electronics ranging from television screens, tablets, phones, computer monitors, and portable gaming systems.¹⁷

OLEDs are theoretically cheaper to produce than liquid crystal display (LCD) or plasma displays. This is because OLEDs have the ability to be printed on plastic substrates. These plastic substrates often are lightweight and flexible which cause them to be much more shatter resistant than typically fragile LCD displays.¹⁸ If a material like polyethylene terephthalate (PET) were used as a substrate for the OLEDs to be printed onto, the screen would be incredibly inexpensive to produce, as well as having the advantage of being so flexible it could be rolled up (Figure 8).



Figure 8. Rollable OLED screen by LG corporation¹⁹

OLEDs can be made into solid and planar device structures which allows them to be used for thin and lightweight flat panel display systems. Due to the fact that every OLED pixel is self-illuminating rather than working with a backlight, the color contrast ratio is higher than LCDs. Each pixel can also turn off completely, which gives a much darker black,

and increases the power efficiency. TVs that are comprised of OLEDs not only achieve darker black levels than LCD, they are also thinner and lighter, caused by the lack of a backlight.²⁰ This higher contrast ratio grants a better picture quality than previous display technologies. OLED TVs give a much wider viewing angle when compared to LCD or LED crystals. Also, OLEDs have a faster response time than LCDs do, due to the lack of a shutter array.²¹ Collectively, these many excellent attributes when compared to other light emitting devices, are why OLEDs have become such a popular technology. To illustrate this further, Figure 9 shows the projected monetary growth of the OLED display market over the next six years.

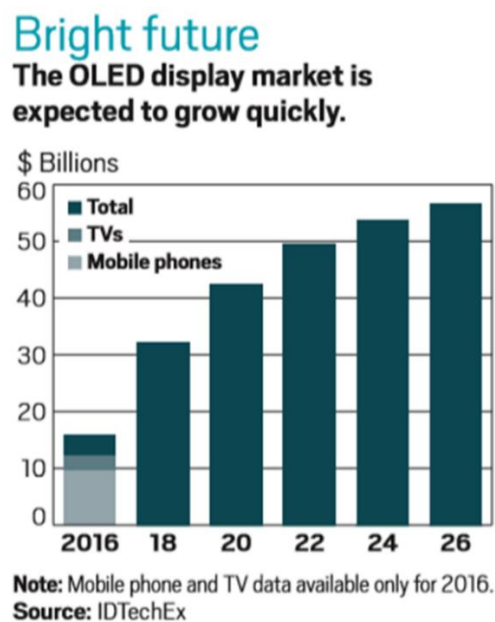


Figure 9. Projected monetary growth of OLEDs over the next six years²²

It is projected that more than 70% of smartphones will have adopted OLED technologies by this year.²³ Because OLEDs can be layered on to flexible plastic substrates, many companies are already working on making rollable TVs and foldable phones and tablets, as shown below in Figure 10. These types of technologies contribute to the quickly

growing market.

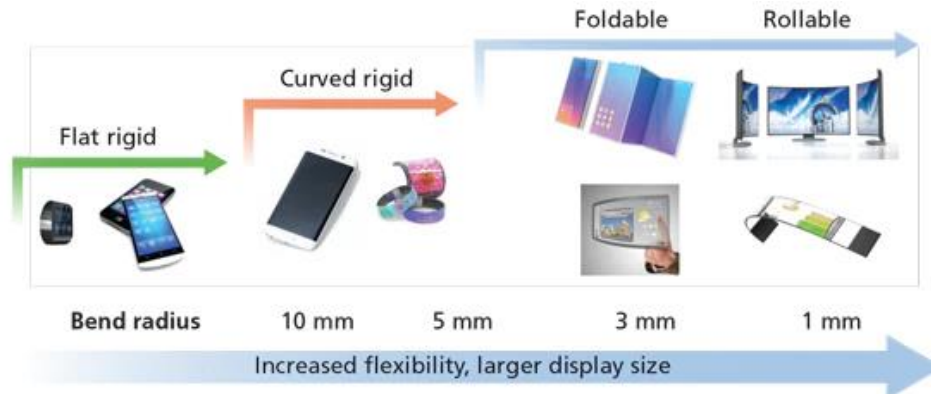


Figure 10. Projected roadmap for future OLED displays includes foldable and rollable displays²³

Unfortunately, modern OLEDs do have their share of problems. Because of spin statistics the ratio of singlet versus triplet state is 1:3, giving emission from the singlet excited state only a 25% chance of occurring. Decay from triplet states is spin forbidden so the maximum theoretical quantum efficiency on these devices is 25%.²⁴ In actual fluorescent devices, the highest efficiency achieved without the introduction of a heavy atom is approximately 19%.²⁵ For this reason, phosphorescent OLEDs have emerged to circumvent this limitation. Phosphorescent OLEDs work by using the heavy atom effect to change the triplet excited from non-radiative to radiative by spin orbit coupling.²⁶ Unfortunately, the heavy atoms used in these OLEDs are often iridium, platinum, or osmium, which are very costly, often toxic, nonrenewable sources.²⁷ Four well known phosphorescent organic emitters used in OLEDs are shown in Figure 11. It is clear that these compounds are capable of very bright emissions and an IQE that has reached almost 100%, however they are extremely expensive and come from non-renewable sources.²⁸

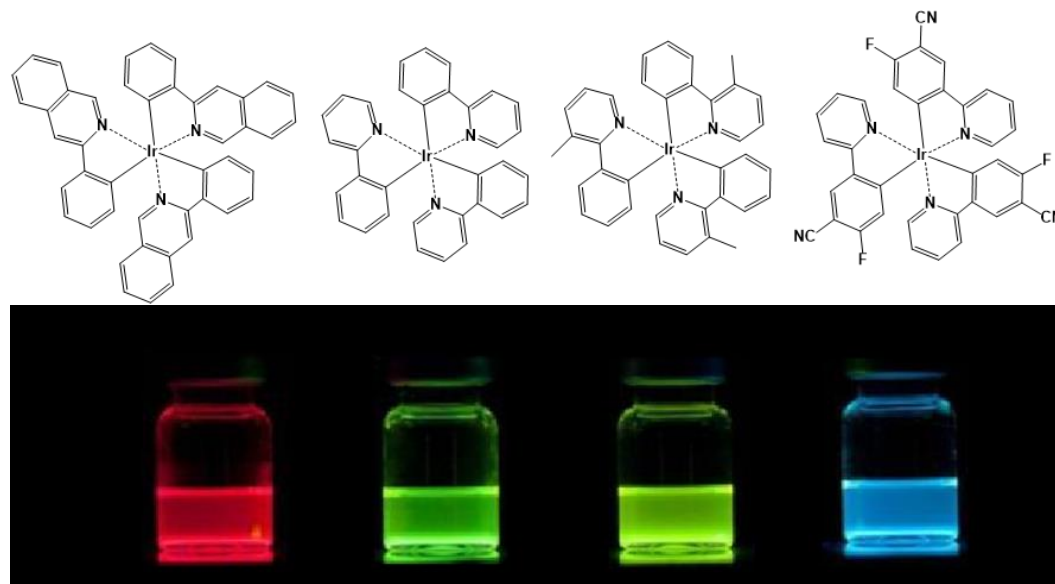


Figure 11. Series of four brightly colored iridium phosphorescent materials used in OLED devices²⁹

1.4 Doublet Emitters

Because both fluorescent and phosphorescent OLRD emitters have advantages and disadvantages, new strategies are being explored to reduce the cost of triplet emitters while maintaining the high theoretical IQEs. One more affordable and renewable strategy to bypass these issues has focused on the implementation of doublet emitters, which are compounds that have only one electron in the highest occupied molecular orbital.³⁰ The fluorescent, phosphorescent, and TDAF based materials that were mentioned previously are all closed shell systems.³¹ These systems have a pair of electrons in the HOMO/LUMO states. Unlike the closed shell systems, doublet emitters are open shell systems due to the lone electron. This lone electron, or radical, exists in a singularly occupied molecular orbital (SOMO) at its ground state energy level, and a singularly unoccupied molecular orbital (SUMO) once excited. The illustrations of closed-shell and open-shell systems are shown below in Figure 12.

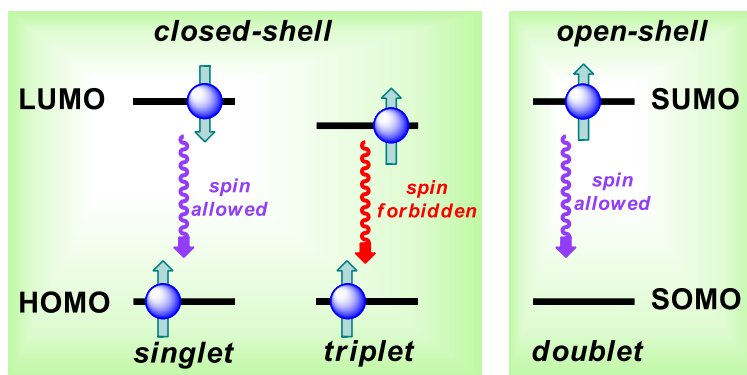


Figure 12. Illustration of closed-shell versus open-shell systems, figure modified from reference 32

Doublet emitters take advantage of radicals that are capable of emission of light upon excitation. Whenever the radical is excited, just like in the closed shell systems, the electron is promoted into an unoccupied molecular orbital. The important difference between closed shell and open shell systems is that no matter which spin the radical has when it reaches the doublet excited state, it can always relax down into the ground state and emit a photon. Closed shell systems must have opposing spins before the electron can relax back down and emission occur. Energetically, the SOMO and SUMO generally lie somewhere in between the HOMO and LUMO level. For example, as shown below in Figure 13, the SOMO of the emitters TTM-1Cz lies just above the HOMO, while the SUMO lies approximately midway between the HOMO and LUMO.³³

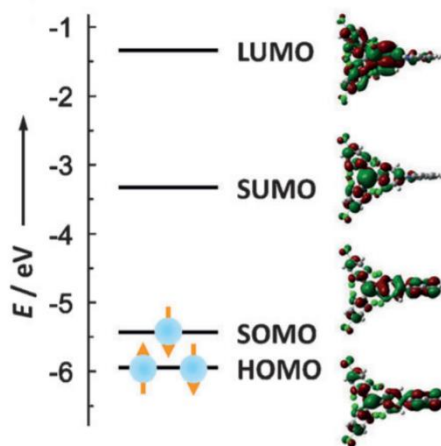


Figure 13. Molecular orbital energy levels of TIM-1Cz³³

Doublet emitters have a theoretical quantum efficiency of 100% as relaxation from a doublet excited state is not limited by the Pauli exclusion principle like closed-shell systems. The term doublet state in these radical emitters derives from the fact there are two possible spin states.³² The first persistent organic radical was discovered by Gomberg in 1900 (Figure 14), which marked the birth of paramagnetic chemistry.^{34,35} In 1905, Theile discovered a biradical bridged by a phenylene group, and later in 1907 Tschitschibabin reported a biradical bridged by a biphenylene group.^{36,37}

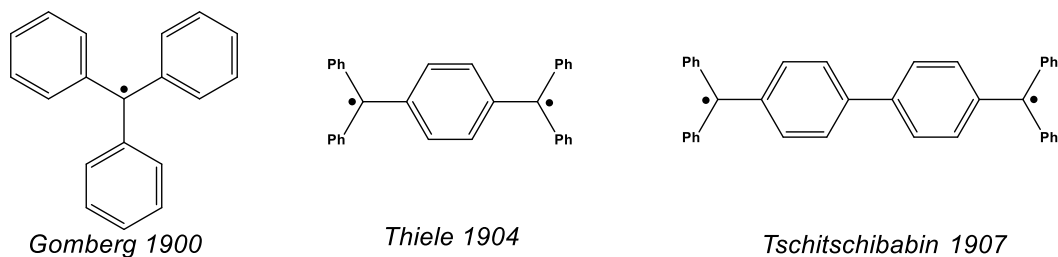


Figure 14. Gomberg, Theile, and Tschitschibabin radical species, respectively^{34,35,36,37}

After that discovery many intriguing organic radical systems have been synthesized and tested for numerous applications. Radicals have been used in many technologies such as

molecular magnets, organic rechargeable batteries, and organic field-effect transistors (OFETs), as well as accelerating the rate of chemical reactions.^{38,39,40,41} More recently though, radicals have been used in various OLEDs.³³ Four organic radicals that are isolable at room temperature and stable to ambient atmosphere are shown below in Figure 15. From left to right the figure shows the perchlorotriphenyl methyl (PTM) radical derivatives, tris (2,4,6-trichlorophenyl) methyl (T⁺TM) radical derivatives, pyridal-containing triarylmethyl (PyBTM), bis-pyridal triarylmethyl (bisPyTM) radicals derivatives, and a *N*-naphthylcarbazole substituted PTM (PTM-3NCz) radical derivative. These are all considered to be in the triphenylmethyl radical family.^{42,43,44,45}

Currently Li and coworkers have the record for a doublet emitter with the highest quantum yield (53%) and external quantum efficiency (EQE, 5.3%) with PTM-3NCz.⁴⁵ This doublet emitter features a donor-acceptor (D-A) ensemble where the electron-rich *N*-naphthylcarbazole unit serves as a donor moiety which is attached to the electron-poor tris-pentachlorophenylmethyl radical acceptor. This unique D-A ensemble results in a doublet emitter that does not obey the Aufbau principle. For this particular molecule, a combination of DFT, cyclic voltammetry (CV) and ultraviolet photoelectron spectroscopy (UPS) studies revealed that SOMO is localized primarily in the PTM acceptor moiety which is lower lying than the HOMO which is localized primarily in the donor carbazole moiety. This compound not only exhibits high luminescent quantum yields but is also exceptionally photostable.

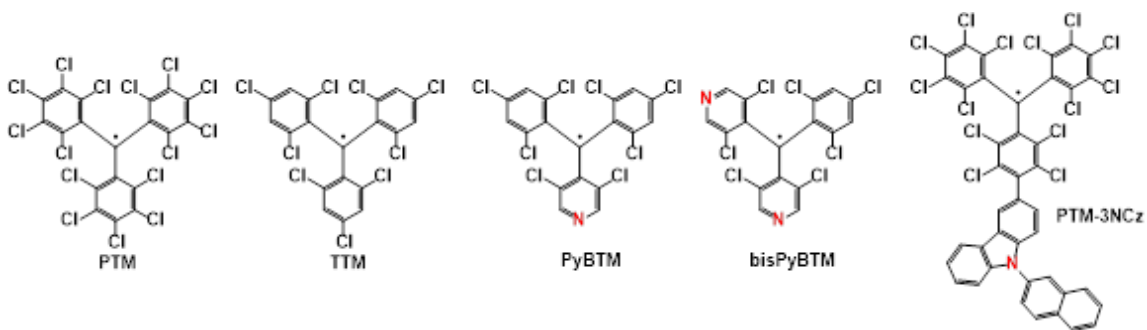


Figure 15. PTM, TTM, PyBTM, bisPyBTM, and PTM-3NCz radical systems^{42,43,44,45}

More specific examples of radical molecules use in OLED devices that have been tested are shown in Figure 16. The compounds **1** and **2** were synthesized by Feng Li et. al, compound **3** was synthesized by Nishihara et. al, and compound **4** by Okamoto, Takeya, and Yamaguchi. Compounds **1**, **2**, and **3** were fabricated into OLED devices that had comparable reported efficiencies to current devices that emit the same color.^{33,42,43}

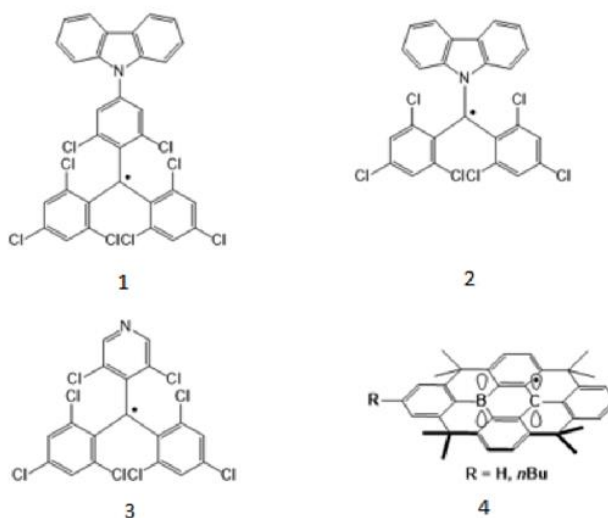


Figure 16. Series of synthesized doublet emitters^{33,42,43,46}

Unfortunately, the only color that would emit from these OLED devices was red.

Two of the emitted colors are shown in Figure 17, the left vial was a chloroform solution of

compound **1** from Figure 16 under a hand held UV light, and the right vial was a cyclohexane solution of compound **2** from Figure 16 under 365 nm irradiation.^{33,42}



Figure 17. Left vial: chloroform solution of compound **1**, right vial: cyclohexane solution of compound **2**.^{33,42}

1.5 Tuning Emissions by Incorporation of Carbenes

Carbenes are molecules that contain a neutral, divalent carbon with six valence electrons. Carbenes have an unpaired set of electrons which can be spin paired (singlet ground state) or unpaired (triplet ground state).⁴⁷ Triplet carbenes are very reactive compounds that are typically utilized as transient intermediate in organic reactions such as Buchner ring expansion reactions. Indeed, carbenes were first postulated by Buchner in 1903 from cyclopropanation studies of ethyl diazacetate with toluene (Figure 18).⁴⁸ In contrast to their reactive triplet counterparts, singlet carbenes are quite stable and feature a lone pair and empty π orbital at the carbene carbon. These singlet carbenes have been used in many chemical fields including catalysis, main group chemistry, and transition metal chemistry.^{49,50,51}

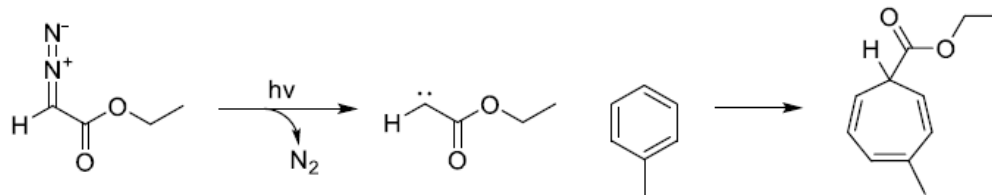


Figure 18. Buchner's ethyl diazacetate reaction with carbene intermediate⁵²

Wanzlick and group synthesized the first N-heterocyclic carbene, otherwise known as an NHC, in 1961 but unfortunately, was unsuccessful in isolating the free carbene. He found that the carbene would dimerize with itself, but none the less he had synthesized a carbene.⁵³

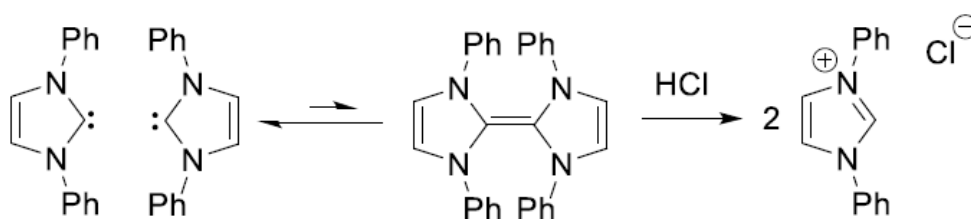


Figure 19. Wanzlick and group's NHC and dimer⁵³

The first singlet carbene that was isolated was done so by Bertrand and group in the late 1980s. Bertrand's carbene is shown below in Figure 20. This carbene is stabilized by the hetero atoms that surround the carbene carbon due to their push-pull effect.⁵⁴

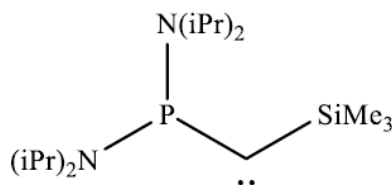


Figure 20. Bertrand's isolated carbene⁵⁴

Carbenes are incredible because the frontier molecular orbitals (FMOs) can be

modified by changing the backbone of the molecule as well as the atoms or groups flanking the carbene carbon. For example, the calculated HOMO and LUMO energy levels of a variety of carbenes (IPr, SIMes, cyclopropenyliidene, CAAC, MAAC, BiCAAC, and DAC.^{55,56,57,58,59,60}) all differ greatly depending on the structure of the carbene.

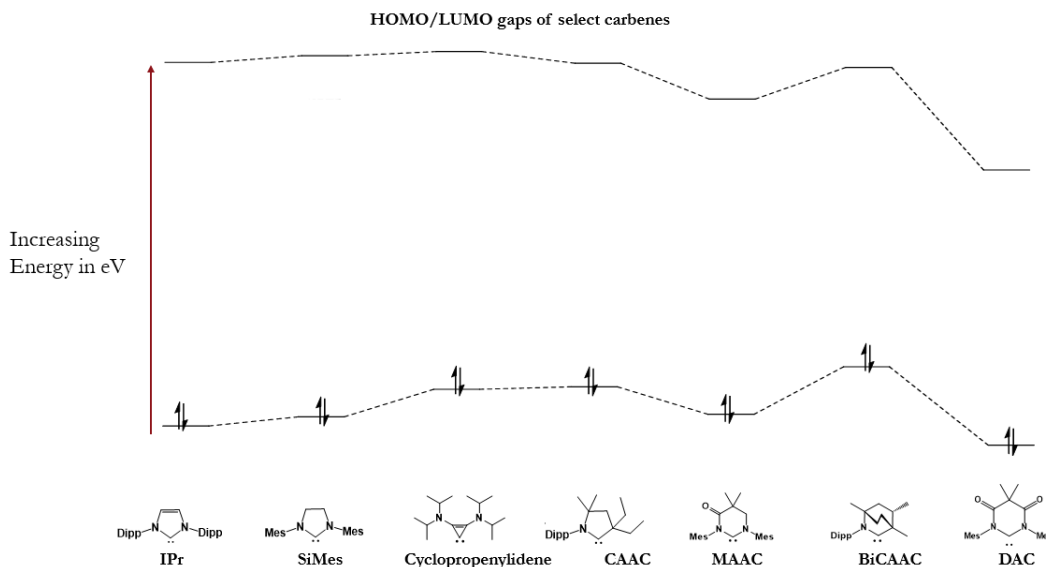


Figure 21. HOMO/LUMO gaps of selected carbenes

Table 2. HOMO and LUMO levels of selected carbenes (Gaussian(09):B3LYP/6-31G+(d))

Carbene	HOMO (eV)	LUMO (eV)	Gap Difference (eV)
BiCAAC	-4.971	-0.503	4.468
CAAC	-5.279	-0.433	4.845
cyclopropenyliidene	-5.306	-0.260	5.046
MAAC	-5.683	-0.985	4.698
SIMes	-5.723	-0.329	5.394
IPr	-5.864	-0.432	5.432
DAC	-6.105	-2.036	4.069

From the calculated data shown in Figure 21 and Table 2, it is clear that BiCAAC has

the highest HOMO level, cyclopropenyliene has the highest LUMO level, and DAC has both the lowest HOMO and LUMO level, therefore, DAC is the most electrophilic of this grouping.

Not only would carbenes tune the emission for these devices, they would also theoretically stabilize the molecule due to the captodative effect.⁶¹ Carbenes have been widely studied for stabilization of highly reactive, low oxidation state, main group molecules.⁶² The captodative effect is where a radical or radicals are stabilized in a molecule by a synergistic effect between an electron donating substituent and an electron withdrawing substituent that are near the radical center. The surrounding substituents prevent other molecules or radical species from reacting with any radicals on the molecule.⁶³ This is incredibly important for these doublet emitters as the emission comes entirely from the radical's relaxation from the excited state. If the radicals in these molecules are easily reacted with, the emission of the potential OLEDs can decrease dramatically.

1.6 Objectives

The primary objective of this research is to incorporate a variety of carbenes into triarylmethyl and triarylboryl emissive radical scaffolds. It is hypothesized that the use of carbene ligands will serve to: i) stabilize the desired radicals, an important consideration for applications in OLEDs, and ii) to tune the color of the emission.

The first radical system to be studied is the triarylmethyl radical scaffold that has been coupled to a carbene (Figure 22). This doublet emitter is structurally similar to the aforementioned published doublet emitters due to the triarylmethyl radical with the surrounding aromatic groups decorated with electronegative atoms. Our triarylmethyl radicals possess fluorine atoms in place of the chlorine atoms in the previously described

molecules. The three carbenes that were successfully attached to these triarylmethyl radicals were six-membered diamido carbene (DAC), cyclic (alkyl) amino carbene (CAAC), and N,N'-dimesitylimidazol-2-ylidene (IMes).

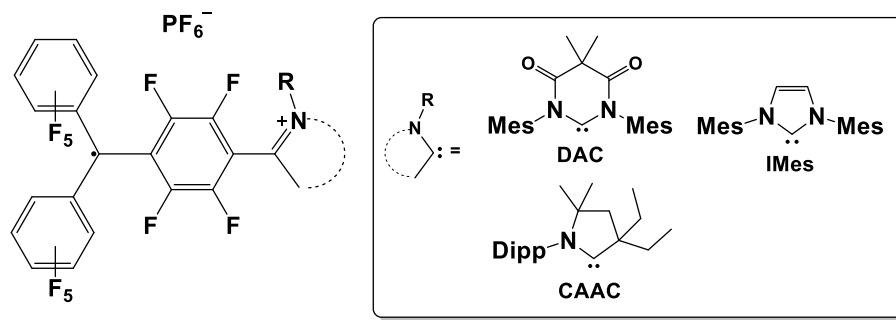


Figure 22. Triaryl methyl radical with counter anion PF_6^-

After these were synthesized and studied, a second iteration focused on triarylboryl centered radicals instead of a triarylmethyl centered radicals. A triarylboryl system was chosen as an alternative to triarylmethyl for reasons that will be discussed in the third chapter of this thesis. The carbenes added successfully to the triaryl boron compound were CAAC, N,N'-bis-(2,6-diisopropylphenyl) imidazole-2-ylidene (IPr), and saturated N,N'-dimesitylimidazolylidene (SIMes). DAC was attempted but did not successfully add.

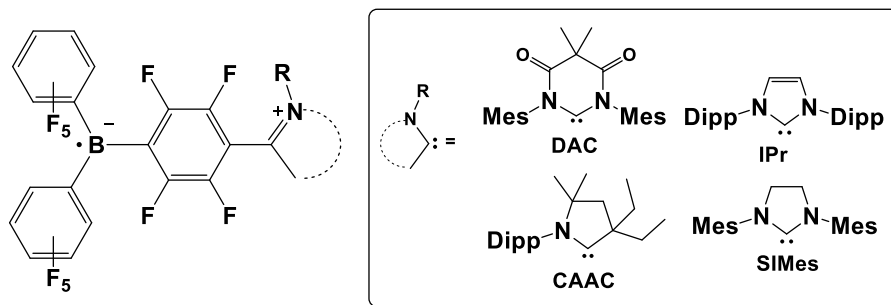


Figure 23. Triaryl boryl radical

1.7 General Procedures

All air free procedures were performed using standard Schlenk techniques under an inert atmosphere of either nitrogen or argon or in a nitrogen filled glove box unless otherwise noted. Hexanes, benzene, pentane, and diethyl ether were dried over sodium metal, distilled, and degassed by three freeze-pump-thaw cycles. Dichloromethane (DCM) was dried over calcium hydride, distilled, and degassed over three freeze-pump-thaw cycles. Each dried and degassed solvent was stored in a glovebox in a glass bottle that contained 3Å molecular sieves.

1.8 Instrumentation

NMR spectra were recorded on both Bruker Avance 400 MHz and Bruker Avance 500 MHz spectrometers. Chemical shifts are reported in ppm in relation to the solvent peak for ^1H and ^{13}C NMR and given in δ (^1H : CDCl_3 , δ 7.26; CD_2Cl_2 , δ 5.32; ^{13}C : CDCl_3 , δ 77.16; CD_2Cl_2 , δ 53.84). ^{11}B and ^{19}F NMR shifts were referenced to external $\text{BF}_3 \cdot \text{Et}_2\text{O}$ and CFCl_3 , respectively. UV-Vis spectra were recorded on a PerkinElmer Lambda 365 UV-Vis spectrophotometer in a dry DCM solution. EPR spectra were recorded on an X band Active Spectrum Benchtop Micro ESR spectrometer (9.5 GHz, 300 Gauss sweep range).

2. TRIARYLMETHYL RADICALS

2.1 Introduction

The first three compounds that were synthesized for this overarching project were based on the triphenylmethyl radical systems synthesized by Li et al. and Kunishihara et al., specifically Li's TTM radical.^{32,39,40} The difference in these radicals in comparison to Li's TTM radical is that instead of attaching a carbazole group, the addition was a carbene. The idea behind this was that the color emission of the radical species would change due to the differences in the HOMO/LUMO gaps. Interestingly, addition of the various carbenes into the triarylmethyl manifold resulted in redox chemistry such that sacrificial carbene, or addition of exogenous base, which served as a reductant was needed for the reaction to be high yielding. For this reason, once the initial compounds were isolated, they were then oxidized to give the desired radicals. This made these compounds cationic species, so a counter anion was necessary to balance the overall charge. The counter anion in this series of molecules was hexafluorophosphate (PF_6^-). The below figure shows the specific structures that were targeted in this portion of the research.

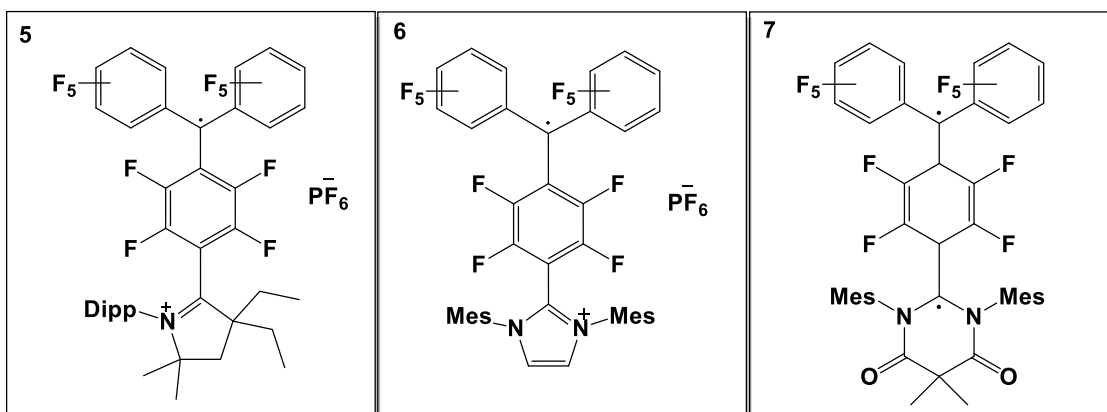


Figure 24. Compounds 5,6, and 7

Another difference in these molecules in comparison to Li's radicals are that they

possess fluorine atoms on the aromatic groups instead of chlorine atoms. Replacement of the chlorine atoms with the fluorine effectively enhances the electrophilicity of the triarylmethyl precursor toward nucleophilic attack of the carbene. The enhanced electronegativity of the fluorine atoms over chlorine, coupled with the fact that fluorine is a better leaving group in nucleophilic aromatic substitution (NAS) reactions overall improve the reactions of the carbenes with the triarylmethyl precursor. Additionally, fluorine atoms are significantly smaller than the chlorine atoms, which potentially provide more room for the carbene to insert.

The compounds discussed in this chapter of the thesis were synthesized by Dr. Renzo Arias and Christopher Barragan, and further characterized by me.

The DFT calculations for the compounds in this chapter were performed by Dr. Shane Yost using the Q-Chem software with the omega-b97x-d functional and the 6-31G* basis set for all atoms.

2.2 Synthesis and Characterization of IMes-Triarylmethyl Radical

The first carbene that will be discussed is IMes (N, N'-dimesitylimidizolyidene). Two equivalents of both IMes and tris(pentafluorophenyl)methane (TPFM) were added together dry, degassed benzene and stirred.⁶⁴ The synthesis and product of this reaction, compound **5**, is shown in Figure 25.

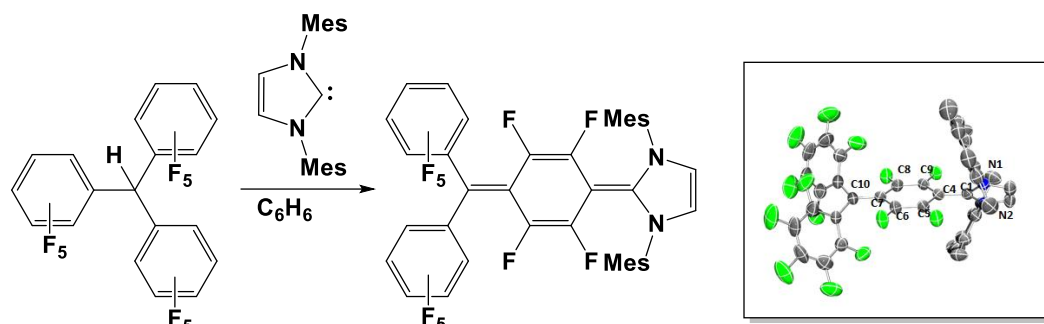


Figure 25. Synthesis to incorporate IMes into TPFM giving compound **5**

Compound **5** was isolated as a bright red, air and water stable solid after column chromatography (Figure 26). Gratifyingly, we were also able to obtain single crystals suitable for an X-ray diffraction analysis (see Figure 25, far right) by slow evaporation of an acetone solution saturated with compound **5**. Importantly, compound **5** adopts the highly conjugated quinoidal structure as depicted in Figure 25. Specifically, the C10–C7, C6–C5, C8–C9, and C4–C1 bond distances are indicative of multiple bond character (1.395(5), 1.347(5), 1.352(5), and 1.434(5) Å, respectively). Under a hand-held UV lamp, compound **5** exhibited a weak orange emission (Figure 27). Remarkably, this compound can be considered as an air stable analogue of Thiele’s biradical, which is quite sensitive to oxygen. The intense color of this compound can be attributed to the almost completely conjugated structure throughout the entirety of the molecule.



Figure 26. Powder obtained from reaction of TPFM with IMes

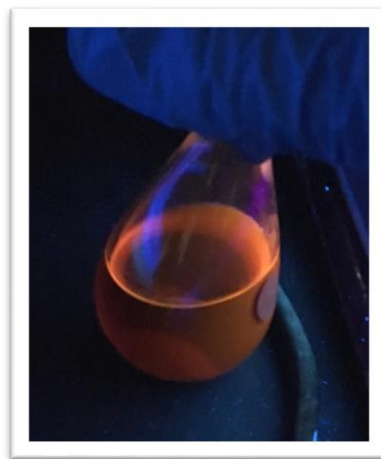


Figure 27. Weak orange emission of compound **5** under hand-held UV lamp

Looking at the HOMO of compound **5**, it is clear that there is electron density around each of the double bonds as well as the two nitrogens. This suggests the electron density is spread out throughout the majority of the molecule, not just localized on one central atom.

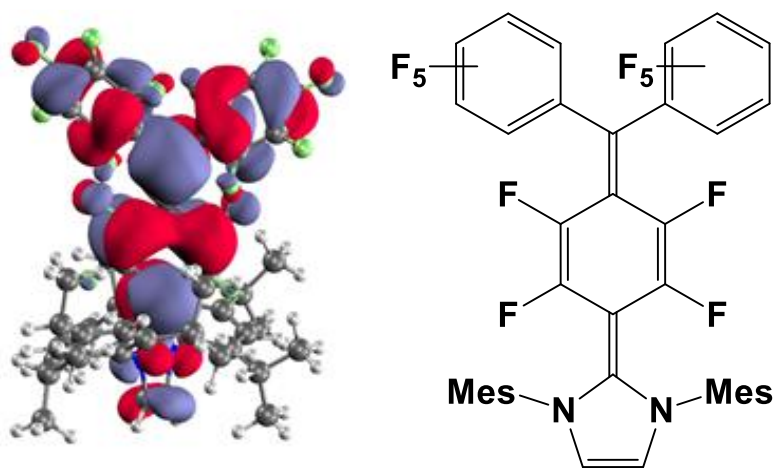


Figure 28. HOMO of compound **5**

To obtain the desired emissive radical cation, compound **5** was then oxidized using nitrosonium hexafluorophosphate ($[\text{NO}][\text{PF}_6]$) to give the radical cation $\mathbf{5}^{\bullet+}$ (Figure 29).

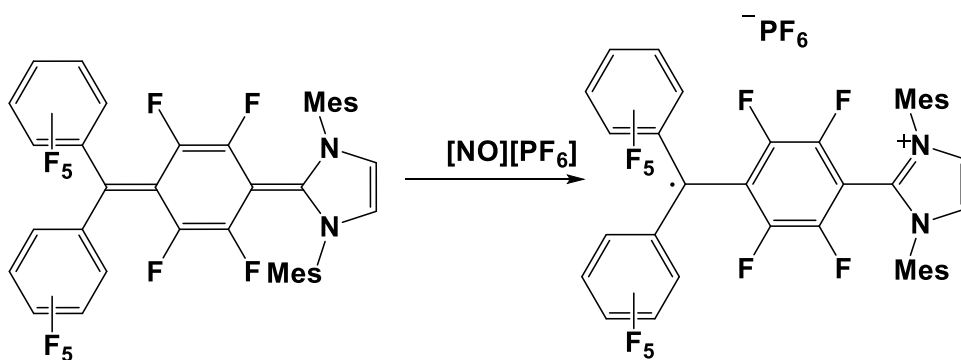


Figure 29. Oxidation of compound **5** to give radical cation $5^{\bullet+}$

Radical cation $5^{\bullet+}$ was obtained as a brown solid which gave a greenish emission under hand-held UV lamp. Unfortunately, this emission was also weak indicating poor potential quantum efficiency (Figure 30).

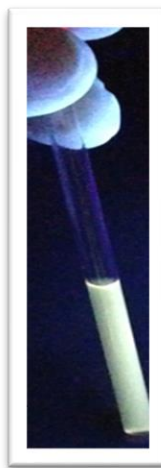


Figure 30. Weak green emission of $5^{\bullet+}$

2.3 Synthesis and Characterization of a CAAC-Triarylmethyl Radical

Next, compound **6** was prepared in a similar fashion to **5** by treating one molar equivalent of TPFM with two equivalents of the CAAC in benzene (Figure 31).

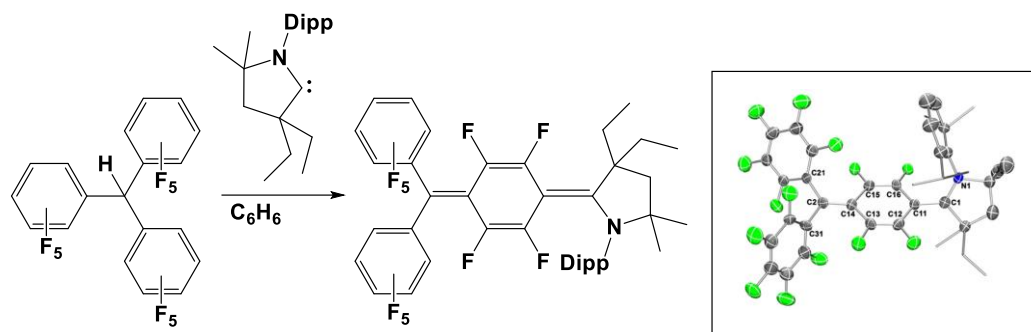


Figure 31. Synthesis of triarylmethyl-CAAC compound **6**

Compound **6** was isolated as a dark blue solid which gives a deep blue solution when dissolved in DCM (Figure 32). This proves that changing the carbene can change the physical properties of a molecule, such as color.



Figure 32. Solution of compound **6**

Gratifyingly, we were also able to obtain single crystals suitable for an X-ray diffraction analysis (see Figure 31, far right) by slow evaporation of a DCM solution saturated with compound **6**. In the crystal, **6** is a dark purple with a metallic green luster. Similar to **5**, compound **6** adopts a highly conjugated quinoidal. Specifically, the C1–C11, C12–C13, C15–C16, and C14–C2 bond distances all exhibit multiple bond character (1.4299(17), 1.3570(18), 1.3509(17), and 1.3903(17) Å, respectively). It's worth noting that

the carbene carbon to tetrafluoroaryl carbon bond is shorter in compound **6** (C1–C11: 1.4299(17) Å) when compared to the analogous bond in **5** (C1–C4: 1.434(5) Å) which is consistent with the CAAC in **6** being more π -acidic or electrophilic than the NHC in **5**. The HOMO of compound **6** is very similar to what was observed for **5**. The electron density in compound **6** is again distributed throughout virtually the entire compound (Figure 33).

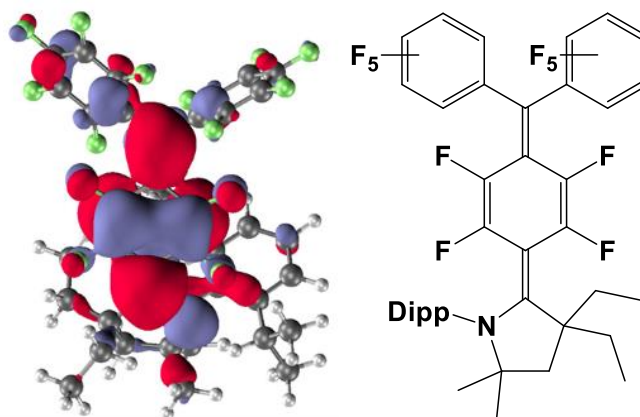


Figure 33. Left: HOMO of compound **6**, Right: ChemDraw rendering of compound **6**

Next, compound **6** was oxidized with nitrosonium hexafluorophosphate [NO][PF₆] similar to compound **5** to give the desired radical cation **6**^{•+} (Figure 34).

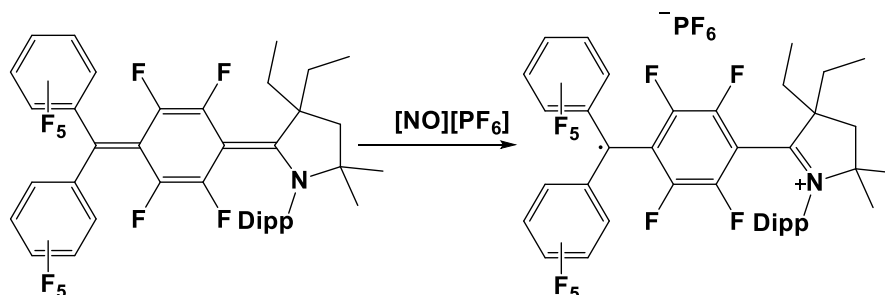


Figure 34. Oxidation of **6** with Reaction of TPFM-CAAC and nitrosonium hexafluorophosphate to give radical cation **6**^{•+}

In collaboration with Dr. Alexander Zakhidov's group, **6**^{•+} was layered onto an

OLED device and tested for efficiency (Figure 35). Unfortunately, the molecule was not emissive enough to reach modern OLED standards.



Figure 35. OLED device made with 6⁺

2.4 Synthesis and Characterization of a DAC-Triarylmethyl Radical

Finally, compound **7**, which utilized DAC, was prepared similarly to compounds **5** and **6** (Figure 36). Also similar to compound **6**, **7** was isolated as a dark blue solid which is highly soluble in benzene (Figure 37), however unlike compounds **5** and **6**, **7** was found to be very sensitive to air and water. Interestingly, it was found that this compound was NMR silent. This prompted an EPR analysis to be run on the compound, which produced the spectrum shown in Figure 38. This spectrum revealed that at room temperature compound **7** is paramagnetic and EPR active, and the lack of NMR activity hints that the system was actually a biradical at room temperature.

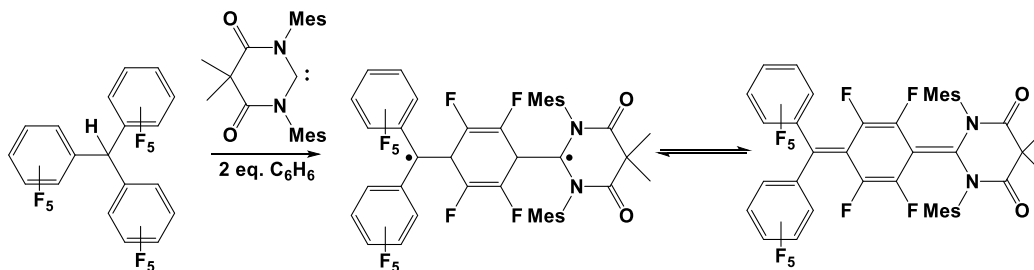


Figure 36. Reaction scheme for the synthesis of compound **7**.

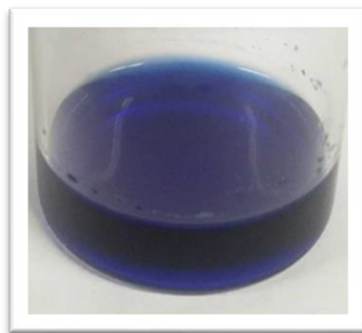


Figure 37. Compound **7** in C_6D_6 .

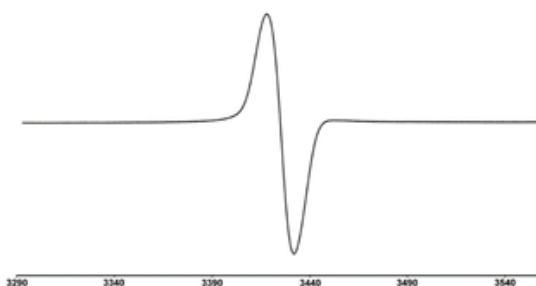


Figure 38. Room temperature EPR spectrum of compound **7** in benzene

Unfortunately, the lack of hyperfine coupling in the EPR makes it difficult to simulate and identify where the unpaired electron(s) are localized. Additionally, our benchtop model EPR spectrometer is not capable of observing a half-field signal at approximately 1700 G, which would be expected if **7** is a triplet biradical at room temperature. If we could observe this half-field signal, we could spectroscopically identify this compound as a triplet biradical as opposed to a singlet biradical which would not exhibit such a signal. Regardless, we believe the room temperature structure of compound **7** can best be described as the biradical shown in Figure 36.

Computational analysis of **7** revealed that the lowest energy state is an open-shell singlet biradical state. As a result, the FMOs of **7** are different than compounds **5** and **6**.

Instead of a HOMO, compound **7** has two energetically degenerate singly occupied molecular orbitals as shown in Figure 39 and Figure 40. In these images, the radicals are shown to reside in two different positions. One radical resides in the methyl carbon of the TPFM portion of the molecule, and the other resides close to the carbene carbon of the DAC portion.

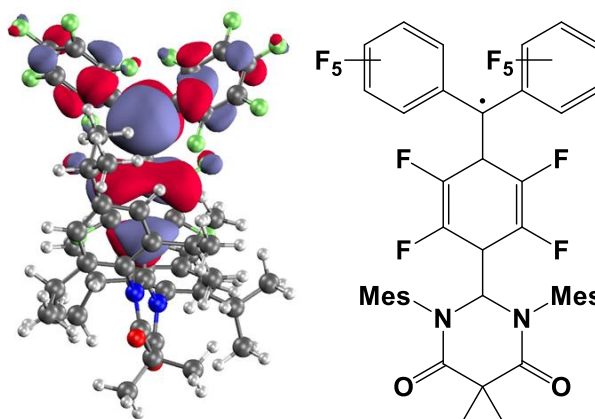


Figure 39. Left: One singly occupied molecular orbital of **7** depicting density localized on the triarylmethyl carbon of the TPFM moiety. Right: ChemDraw depiction of this molecular orbital.

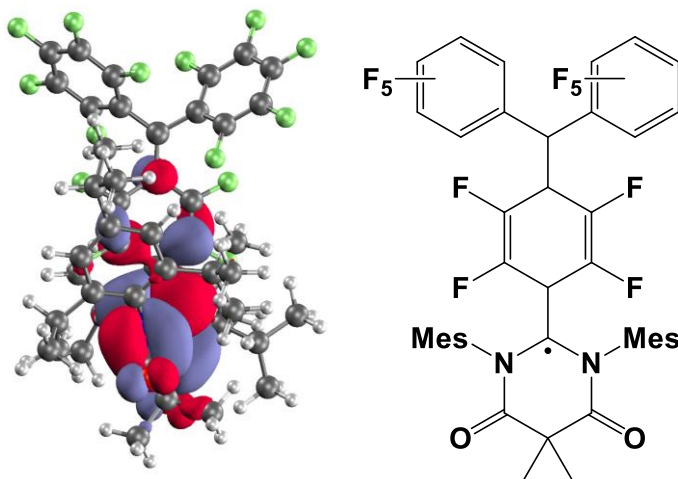


Figure 40. Left: The other singly occupied molecular orbital of **7** depicting density localized on the DAC moiety. Right: ChemDraw depiction of this molecular orbital.

2.5 Discussion and Conclusion

Radical cations $5^{+\bullet}$ and $6^{+\bullet}$ were prepared using IMes and CAAC with a counter PF_6^- anion to balance overall net charge. DAC was successfully added to TPFM but the resulting product, **7** was found to exhibit an open-shell singlet biradical ground state. Both $5^{+\bullet}$ and $6^{+\bullet}$ were emissive; unfortunately, the emission of these radicals was subpar for incorporation into competitive OLED devices.

An OLED device was successfully made with the triarylmethyl-CAAC radical system. However, it was not efficient enough to be comparable to today's technologies. The reason the OLED incorporating $6^{+\bullet}$ was not as efficient as was anticipated may be due to the PF_6^- anion. Past studies have shown that anions can induce quenching of aromatic materials.⁶⁵ In many cases the presence of an ion would increase the chance of conversion of the excited molecule to a triplet state. This occurs because of a quantum mechanical coupling that can induce radiationless transitions from the excited state of the organic compound to a triplet state. This may very well be the reason that these methyl radicals were not very emissive in comparison to known methyl radicals in literature. Further studies will be focused on completing the characterization of compound **7** which features the DAC. Specifically, we plan to probe the temperature dependence on the biradical electronic structure in order to discover how the behavior of the compound may change.

3. TRIARYLBORYL RADICALS

3.1 Introduction

Due to the subpar results of the synthesized triarylmethyl radicals discussed in chapter two, which we believe may be due to anion quenching of the emission, we next decided to focus on neutral radical scaffolds. With this in mind, we envisioned a series of radicals where the triarylmethyl center was replaced by an isoelectronic and isolobal triarylboryl center. Such replacement would result in an anionic boryl radical which would offset the cationic carbene functional group to give an overall neutral radical as opposed to the neutral triarylmethyl radicals functionalized with cationic carbene functional groups to give the radical cations **5**⁺ and **6**⁺ described above. Additionally, triarylboranes are highly luminescent compounds, which is promising for applications in OLEDs.^{66,67,68} Due to the unique property of having lower LUMO energy levels comparatively, the HOMO levels of triaryl boranes are able to be tuned by electron donor groups.⁶⁹ As discussed earlier, many of the carbenes chosen for this project are electron donors. Theoretically speaking, adding different carbenes to the synthesized triarylborane will give different emission colors. When triaryl boranes are accompanied by an electron donor unit, such as carbazoles or amines, excellent fluorescent emissions have been recorded by research groups.^{70,71,72,73} These types of compounds have been investigated by numerous groups as electron transporting and emissive materials in OLED devices and were found to be highly efficient.

3.2 Synthesis of Potential Triarylborane Precursors and Previous Reactions of Carbenes with Fluorinated Borane Derivatives

Initially, we planned to incorporate the carbenes into the well-known tris(pentafluorophenyl) borane which could be synthesized as shown below in Figure 41. This borane was very attractive due to its remarkably electrophilic nature and known susceptibility to undergo nucleophilic aromatic substitution reactions at one of the para-positions of a pentafluorophenyl ring.⁷⁴ Boron complexes like these are often used as Lewis acids because of this. In this specific case the electron withdrawing effects of the surrounding fluorinated aryl rings cause tris(-pentafluorophenyl) borane to be a powerful Lewis acid.

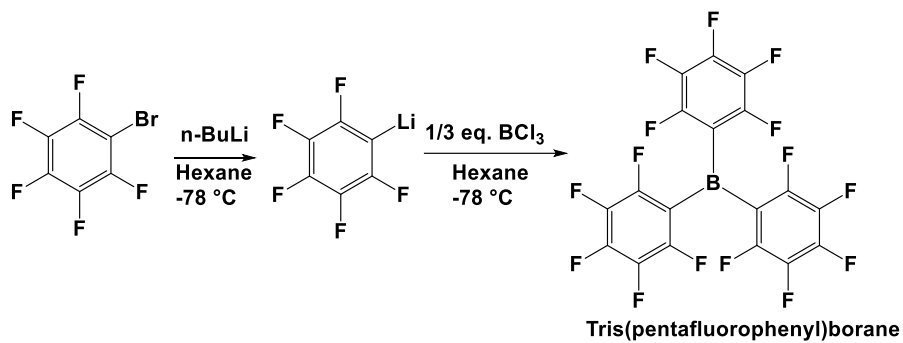


Figure 41. Synthesis of tris-pentafluorophenyl borane

Using a similar protocol to what Stephan developed in 2006, it was hypothesized that a carbene would be added into one of the para-positions of tris(pentafluorophenyl)borane followed by reduction to give the desired neutral radical, similar to the TTM radical Li's group made. Unfortunately, it was found that the carbenes studied added directly to the boron center of tris(pentafluorophenyl)borane to give a typical Lewis adduct with a four-coordinate boron atom. Bhatta, Vijaykumar, Vardhanapu, and Thakur observed similar

reactivity when adding how CAAC and an abnormal N-heterocyclic carbene (a-NHC) to tris(pentafluorophenyl)borane in inert conditions.⁷⁵ This group added these carbene to the tris(pentafluorophenyl)borane in toluene at room temperature under nitrogen. What they obtained from these reactions were compounds in which the carbene directly attached to the boron atom as shown below in Figure 42.

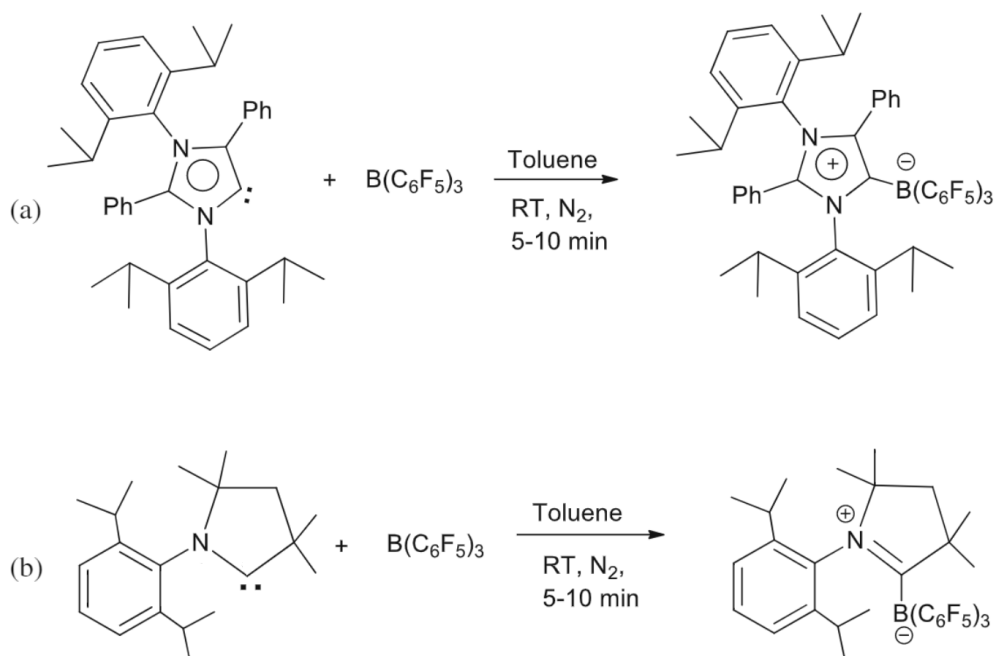


Figure 42. a) reaction of a-NHC with tris-pentafluorophenyl borane b) reaction of CAAC with tris-pentafluorophenyl borane⁶⁵

To further corroborate this assessment, the group was able to obtain x-ray crystal structures of these compounds (Figure 43). It is clear that instead of attaching to one of the pentafluorophenyl groups, the carbenes are instead coordinating to the boron atom. This is an undesirable product because the empty p-orbital at the boron center where the desired radicals would form is effectively neutralized by donation of the carbene lone pair.

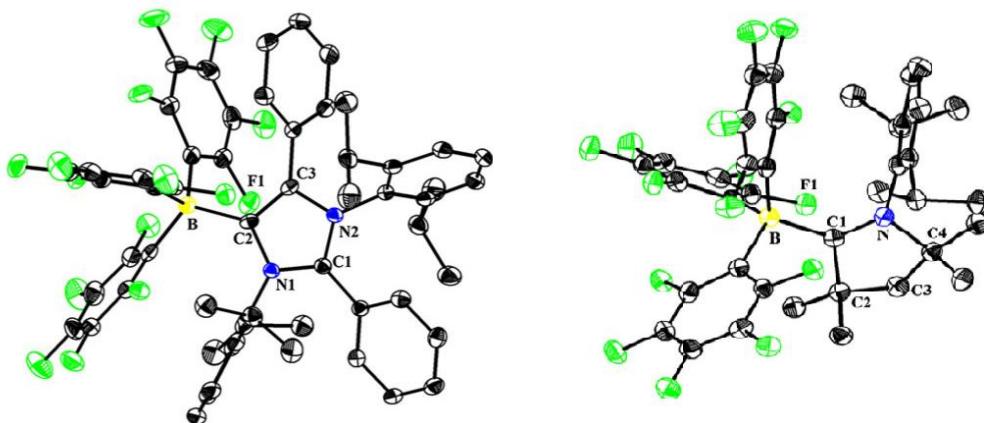


Figure 43. Left- Crystal structure of α -NHC with tris-pentafluorophenyl borane. Right- Crystal structure of CAAC with tris-pentafluorophenyl borane⁷⁴

Due to this undesirable product another route to obtain the desired compounds was envisioned. To decrease the Lewis acidity at the boron center and increase steric bulk to preclude coordination of the carbene to the boron atom, two of the pentafluorophenyl groups were replaced with 2,4,6-trimethylphenyl (mesityl, Mes) groups. This new triarylborane precursor, dimesityl pentafluorophenylborane, was synthesized according to a procedure reported by Jäkle and co-workers (Figure 44).⁷⁶

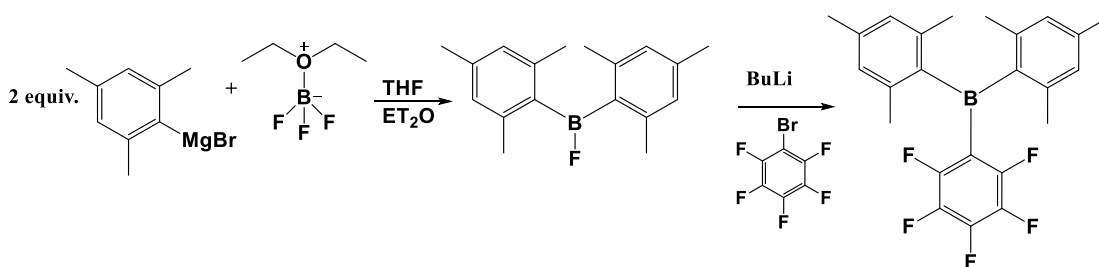


Figure 44. Synthesis of dimesityl pentafluorophenyl borane⁷⁶

The following figure shows the ¹⁹F NMR (CDCl₃) of the dimesityl pentafluorophenyl borane that was synthesized. There are three major peaks shown in the NMR, the first at approximately -130 ppm, the second around -150 ppm, and the third -161 ppm. This is reasonable because there should be 3 signals from this compound. One signal is

from the two equivalent fluorine atoms in the ortho position, another signal is from the two equivalent fluorine atoms in the meta positions, and the third signal is from the fluorine in the para position.

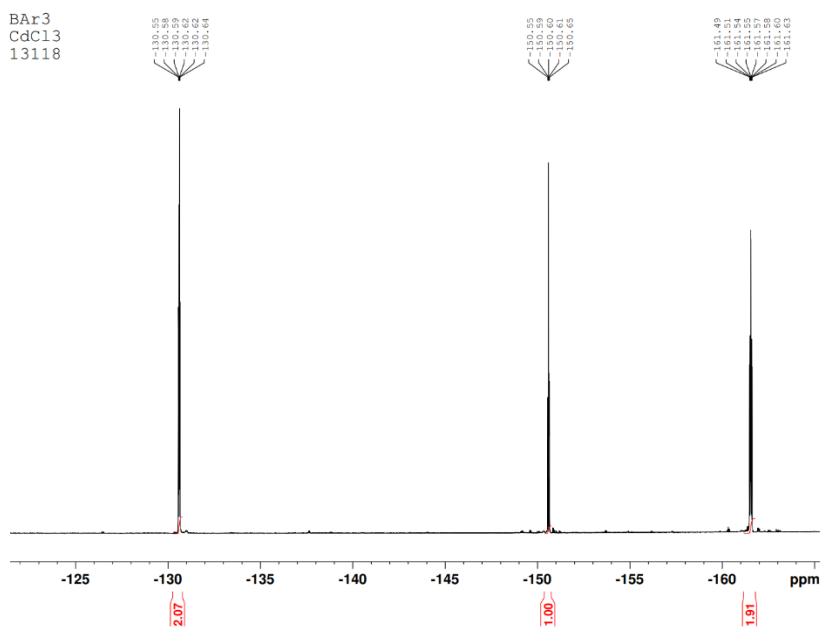


Figure 45. ^{19}F NMR of dimesityl pentafluorophenyl borane in chloroform



Figure 46. Left: Triaryl borane in DCM. Right: Triaryl borane in DCM under UV lamp

Once dimesityl pentafluorophenylborane was isolated, we investigated the

nucleophilic addition of four carbenes: CAAC, N,N'-bis(2,6-diisopropylphenyl)imidazole-2-ylidene (IPr), N,N'-dimesitylimidazol-2-ylidene (SIMes), and DAC with the intention of preparing the neutral radicals **8'**–**11'** (Figure 47).

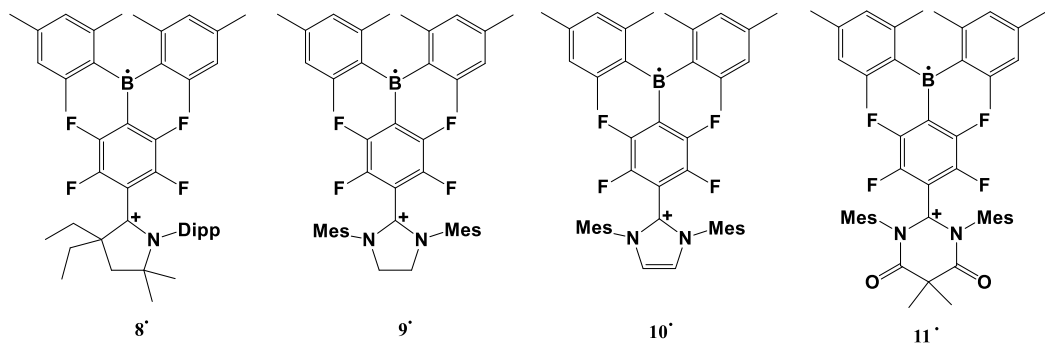


Figure 47. Proposed structures of **8'**–**11'**

3.3 Synthesis and Characterization of a CAAC-Triarylboryl Radical

The first carbene that was added to the triarylborane was CAAC. We started with CAAC because it's the most nucleophilic of the carbenes that we had previously synthesized in our lab, which would facilitate the desired nucleophilic aromatic substitution into the pentafluorophenyl ring of the triarylborane. This was completed by adding a 1:1 ratio of triarylborane to CAAC in a solution of hexane and stirring at room temperature overnight (Figure 48) The proposed end product, compound **8-Fa**, should be zwitterionic, where the fluorine that was in the para position to the boron would migrate to the boron and the carbene would covalently bond to the para carbon similar to what Stephan observed with the reaction of dimesitylphosphine with tris(pentafluorophenyl)borane.⁷⁴ This would cause a negative charge on the boron atom and a positive charge on the carbene carbon, but overall, the molecule would be neutral. While a single product, **8-Fa**, was expected, NMR spectroscopic data obtained on the product of this reaction revealed that two products, **8-**

Fa and **8-Fb**, where fluorine migration to the carbene carbon of the CAAC was observed were formed (*vide infra*). The migration of a fluorine from the para-position of pentafluoropyridine to the carbene carbon of a CAAC had previously been reported by Bertrand, and is consistent with what we observed in the reaction described in Figure 48.⁷⁵

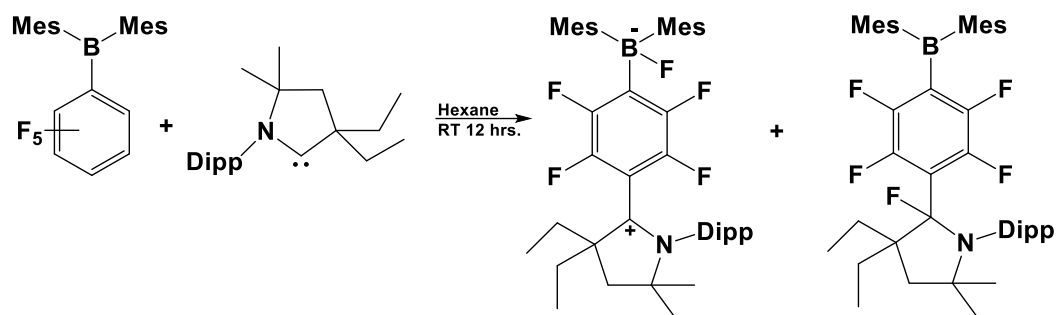


Figure 48. Reaction of CAAC with dimesityl, pentafluorophenyl borane to synthesize compound **8-Fa** and **8-Fb**

The product of the reaction described in Figure 49 was a light seafoam green powder that could be easily isolated by filtration. This powder was then washed with hexanes and ether. In solution the product of this reaction is a pale tan color which emits a weak green light when irradiate with a hand-held UV lamp (Figure 49).

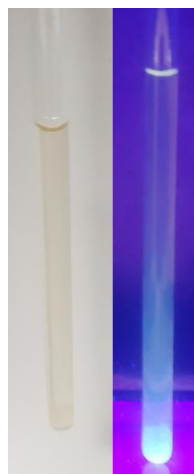


Figure 49. Left: Compound mixture of **8-Fa,b** in dry DCM. Right: DCM solution of **8-Fa,b** under hand-held UV light

Heteronuclear NMR spectroscopic measurements (^1H , ^{13}C , ^{11}B , and ^{19}F) were taken in deuterated DCM on the product obtained from the reaction described in Figure 48. Both the ^{11}B and ^{19}F NMR spectra are shown below in Figures 50 and 51, respectively. The most interesting NMR spectrum is the fluorine NMR due to how very messy it is which shows multiple groupings of very similar peaks. If compound **8-Fa**, where the fluorine atom migrated to the boron, was the only produce, then the fluorine NMR spectrum should only show three peaks, a doublet peak for the two almost identical fluorines ortho to the boron atom, a doublet peak for the two identical fluorines attached to the aromatic ring near the carbene, and the fluoroborate fluorine atom. It is clear by this NMR spectrum however, that there are more than three peaks. Due to these patterns we believe that there are actually two major compounds that are obtained after adding the carbene to the triarylborane, as shown in Figure 48. The second potential product is compound **8-Fb** (Figure 48). Indeed, the ^{19}F NMR spectrum also showed the fluorine nucleus attached to the carbene carbon at -139.42 ppm. Once the fluorine leaves the aromatic ring and the carbene is added successfully, it adds both to the boron as well as the carbene carbon.

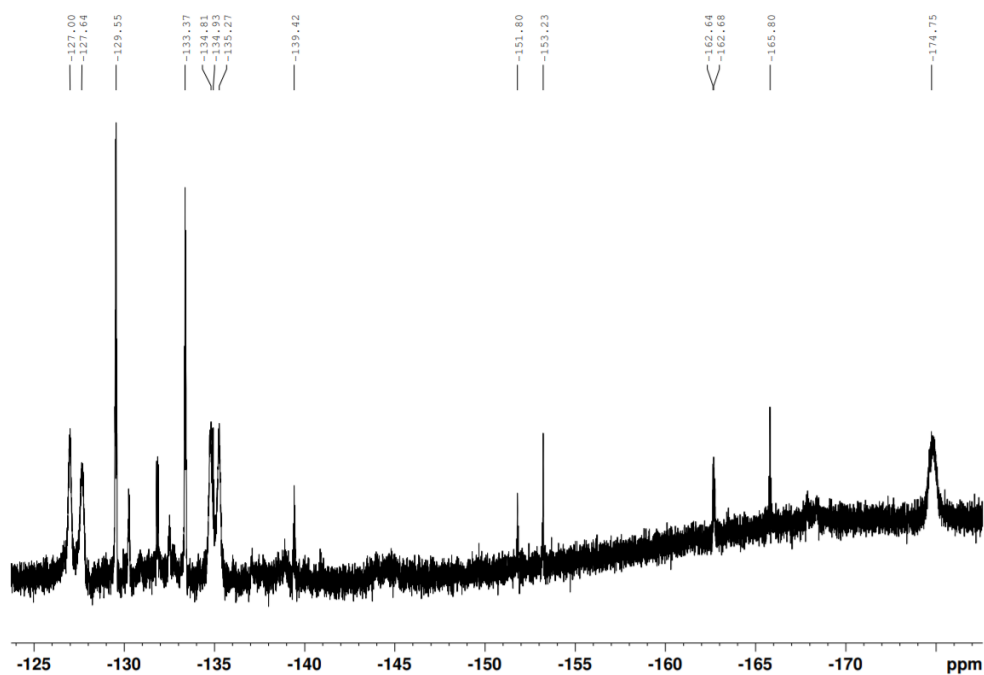


Figure 50. ^{19}F NMR spectrum of product **8-Fa,b** obtained by addition of CAAC to dimesityl pentafluorophenylborane

The doublets at approximately -127 ppm and -134 ppm both correspond to the same molecule (**8-Fa**). They both integrate in a 2:2 ratio and have the same coupling constant of approximately 200 Hz. Additionally, the broad peak at -174.75 ppm is consistent with a fluoroborate moiety.^{77,78,79} Looking at the ^{11}B NMR shown in Figure 51 there are two clear peaks, a broad peak at 50.66, consistent with a three-coordinate triarylborane, such as that in **8-Fb**, and a sharp peak at 1.34 ppm, consistent with a four-coordinate fluoroborate (**8-Fa**, the broad peak centered around zero ppm represents the borosilicate glass in the NMR tube and probe).

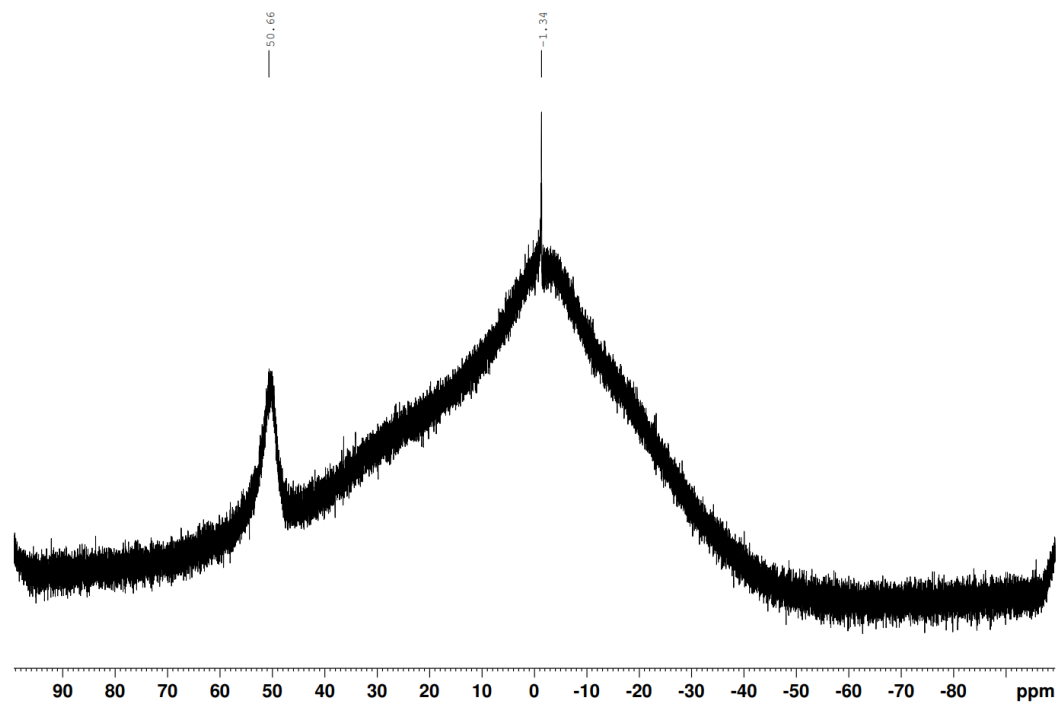


Figure 51. ^{11}B NMR of mixture of **8-Fa** and **8-Fb**.

A UV-Vis spectroscopy measurement was taken of the product in dry DCM (Figure 52) and the following data was collected.

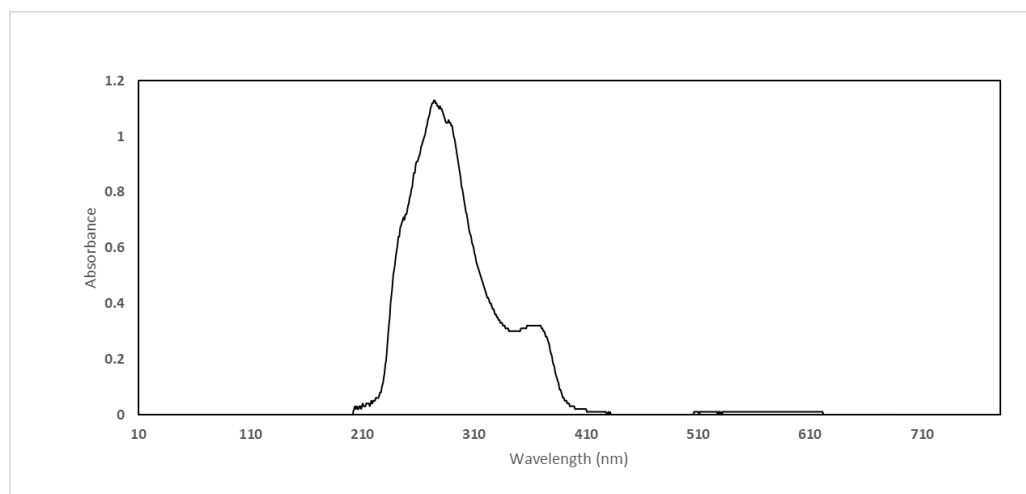


Figure 52. UV-Vis spectrum of **8-Fa,b** mixture in dry DCM

In the spectrum, there is a very large peak that is centered at approximately 240 nm.

This is in the ultraviolet portion of the spectrum. There is a second much smaller peak centered at approximately 390 nm. The larger peak may belong to the fluoroborate compound **8-Fa** while the small shoulder may belong to the three-coordinate triarylborane compound, **8-Fb**, which typically exhibit broad, featureless signals around 370 nm.^{80,81} The general location of the peaks is consistent with aromatic compounds.^{81,82,83}

Remarkably, addition of one molar equivalent of trimethylsilyl triflate (TMS-OTf) to the mixture of products obtained from the reaction shown in Figure 48 in DCM afforded a tan solid that by multinuclear NMR spectroscopy was a single compound (**8⁺**, Figure 53).

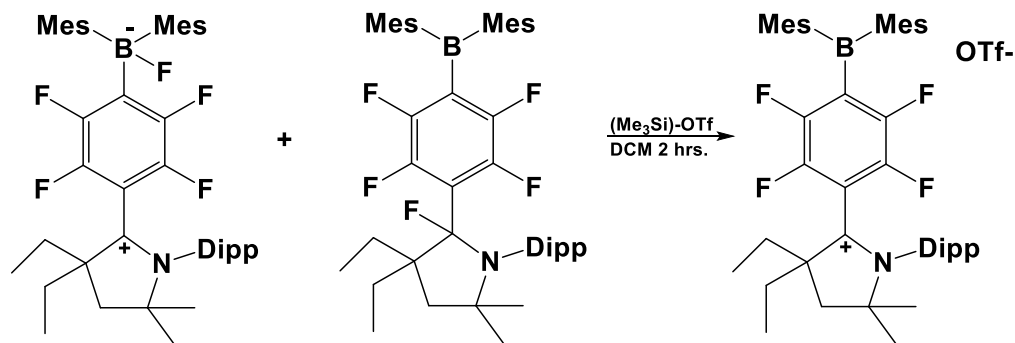


Figure 53. Fluoride abstraction from mixture of **8-Fa,b** with TMS-OTf to give the cation **8⁺**

In a solution of dry DCM, **8⁺** was a light tan, but under hand-held UV lamp the cation emitted a green yellow color, as shown in Figure 54. In comparison to the mixture of **8-Fa**, **8-Fb**, this emission appeared to be more intense with a naked eye.



Figure 54. Left: $\mathbf{8}^+$ in dry DCM. Right: Same solution under handheld UV lamp

The ^{19}F NMR spectrum of $\mathbf{8}^+$ clearly indicates the formation of a single product with 4 observed peaks. The tallest peak is at -78.10 ppm corresponds to the triflate counter anion which generally show a sharp peak around -78 ppm relative to CFCl_3 .⁸⁴

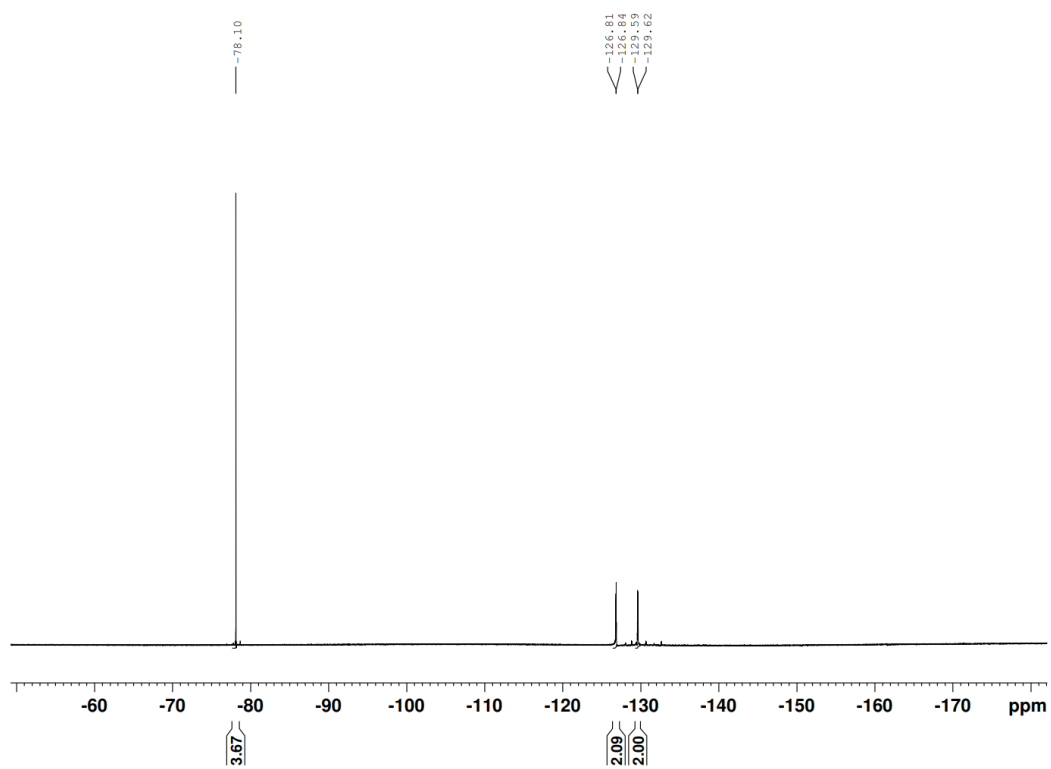


Figure 55. ^{19}F NMR of $\mathbf{8}^+$ in CD_2Cl_2 .

Zooming in on the peaks at approximately -126 ppm and -129 ppm, two distinct

doublets of doublets are observed owing to omega coupling (Figure 56). Importantly, the integration of the three signals: 3 for the CF₃ group in the triflate anion, 2, and 2 for the tetrafluorophenyl ring, are consistent with the formation of compound **8**⁺. Finally, the ¹¹B NMR spectrum exhibited a single broad peak at 78.7 ppm, consistent with triarylboranes (Figure 57).

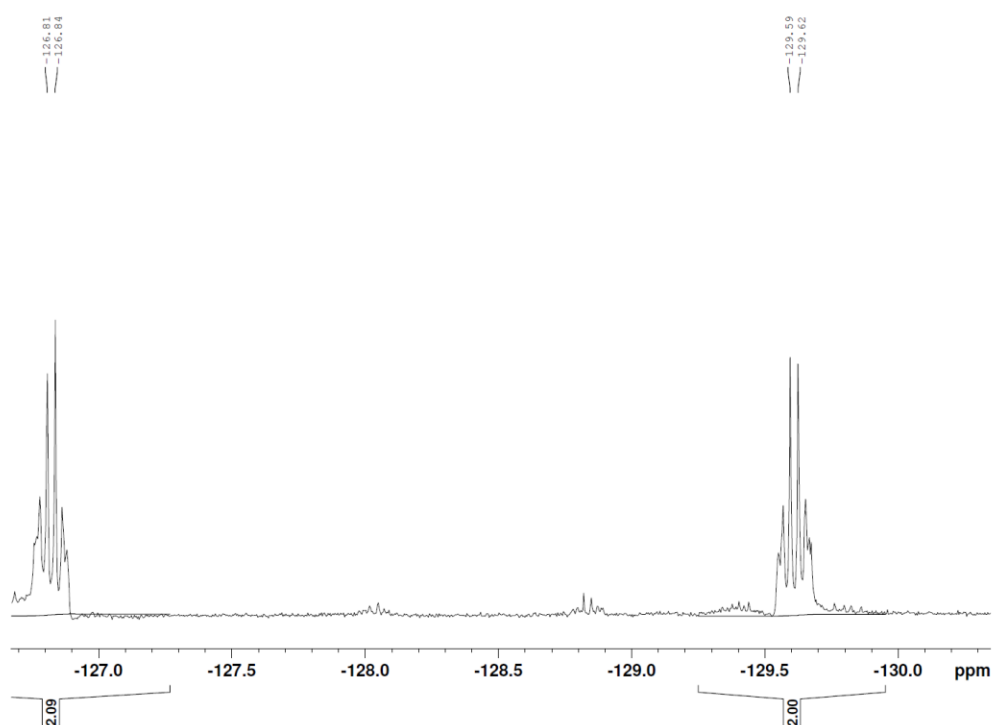


Figure 56. ¹⁹F NMR spectrum of **8**⁺ from approximately -126 ppm to -131 ppm in CD₂Cl₂.

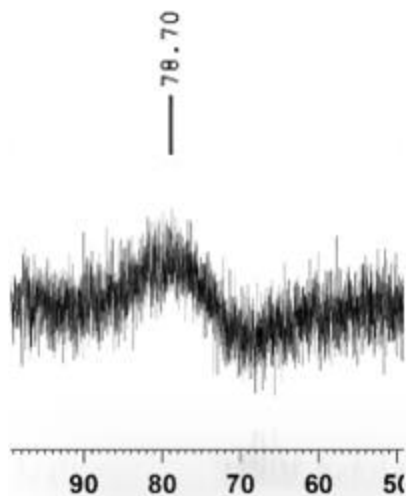


Figure 57. ^{11}B NMR spectrum of $\mathbf{8}^+$ in CD_2Cl_2

A UV-Vis spectrum of $\mathbf{8}^+$ product was taken in DCM (Figure 58). In comparison to the UV-vis spectrum of the mixture of $\mathbf{8-Fa}$ and $\mathbf{8-Fb}$, the spectrum of $\mathbf{8}^+$ clearly shows a λ_{max} centered around 340 nm, consistent with a triarylborane. Looking back to the UV-Vis data taken for the mixture of $\mathbf{8-Fa}$ and $\mathbf{8-Fb}$, it is apparent that the smaller peak centered around 390 nm was the three-coordinate boron in $\mathbf{8-Fb}$, and the larger peak around 270 nm was the fluoroborate product $\mathbf{8-Fa}$.

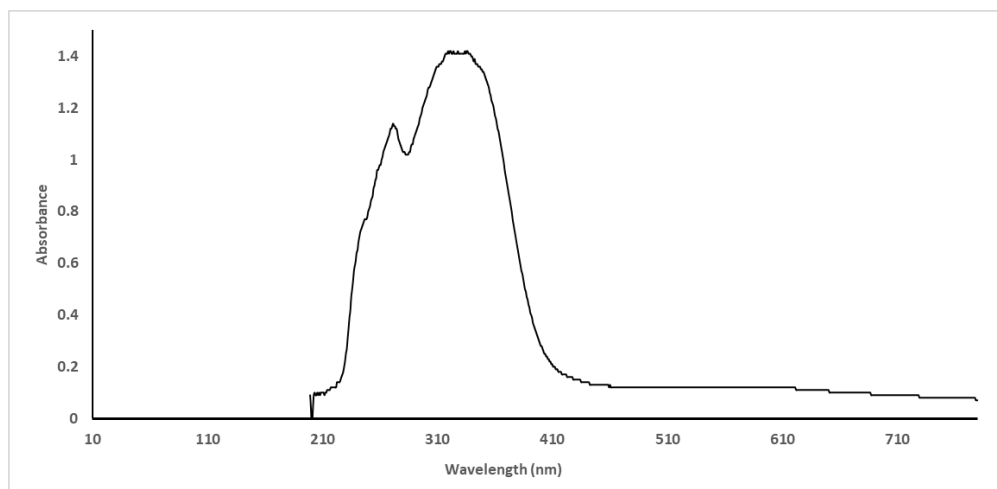


Figure 58. UV-Vis spectrum of $\mathbf{8}^+$ in DCM

With cation **8**⁺ in hand, we next focused on reduction to the desired neutral radical. This was accomplished by adding one equivalent of potassium graphite (KC₈) to **8**⁺ in a small vial inside of a nitrogen-filled glovebox. A few milliliters of benzene were added to the powders and the solution was stirred (Figure 59). Within a few minutes the dark suspension became an emerald colored solution with visible graphite suspended. This suspension was filtered after 1 hour using a 0.4-micron PTFE syringe filter inside the glovebox to remove graphite to give a deep emerald solution (Figure 60). The solvent was then removed *in vacuo* to give a green powder that was NMR silent.

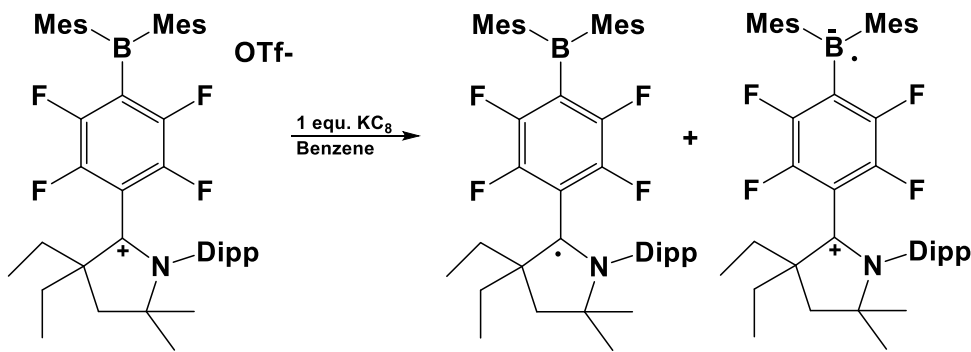


Figure 59. Reduction of **8**⁺ with potassium graphite to afford radical **8**[•]



Figure 60. **8**[•] in dry benzene

A benzene solution of **8**[•] was transferred into a borosilicate glass tube, removed from

the glovebox and then irradiated with a hand-held UV lamp to give an intense yellow green emission (Figure 61)



Figure 61. Emission of a benzene solution of **8**[•] when irradiated with a hand-held UV lamp.

As soon as this radical was obtained, it was observed that **8**[•] was NMR silent by ¹H NMR in deuterated benzene. This result prompted us to acquire an EPR spectrum of the compound in benzene at room temperature. To our delight, **8**[•] was EPR active and gave the spectrum shown as the bottom black line in Figure 62. To determine the localization of the unpaired electron in the radical, we simulated the EPR spectrum (top red line in Figure 62). Importantly, to simulate the experimental EPR spectrum, the following hyperfine coupling constants (G) were used: ¹⁵N1: 4.31, ¹⁹F1: 4.00, ¹⁹F2: 3.90, ¹¹B1: 0.96, which indicated that the unpaired electron is highly delocalized throughout the molecule.

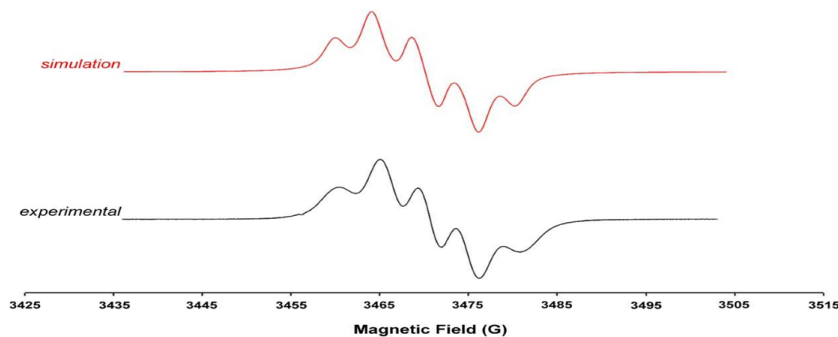


Figure 62. Top: Simulated EPR spectrum of **8**: $g_{\text{iso}} = 1.956$, hyperfine coupling constants (G): $^{15}\text{N1}$: 4.31, $^{19}\text{F1}$: 4.00, $^{19}\text{F2}$: 3.90, $^{11}\text{B1}$: 0.96. Bottom: Experimental EPR spectrum of **8** in benzene at room temperature

Specifically, it was noted that the unpaired electron couples to the boron atom, the carbene carbon and nitrogen atoms, and the two fluorine atoms meta to the dimesitylboryl group. This is further illustrated in the following spin density map and SOMO map of the radical that were determined using DFT calculations (Gaussian(09):B3LYP/6-31G+(d)), which is shown in Figure 63. The hydrogen atoms were omitted from both of these maps for clarity. From the spin density map (middle image), it is clear that the unpaired electron is delocalized over the atoms where hyperfine coupling was observed by the EPR measurement. The SOMO map (Figure 63, right) shows the probability of the location of the radical. The radical resides around the boron, the carbene carbon, the nitrogen, and the two fluorines closest to the carbene, labeled F1 and F2. Collectively, the computational data is in excellent agreement with the experimental EPR spectrum.

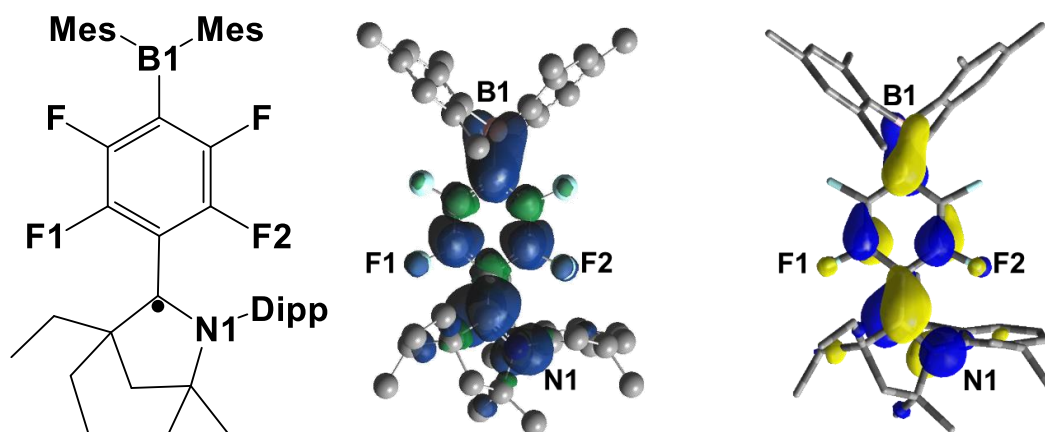


Figure 63. Left: Skeletal formula of **8**. Middle: Spin density map of the radical. Right: SOMO map of radical (H atoms omitted for clarity, atom colors: F: aqua, B: pink, C: gray, N: blue).

In collaboration with Dr. Zakhidov's group, **8** was successfully utilized as the emitter in an OLED device; unfortunately, the intensity was very low. Figure 64 shows the photoluminescence measurement taken from the fabricated device. There is a small peak at approximately 525 nm and a slightly larger peak at approximately 700 nm. The left peak sits at around 350 for intensity, and the right peak barely goes above 400 for intensity. These peaks are very broad which shows that this is very weak.

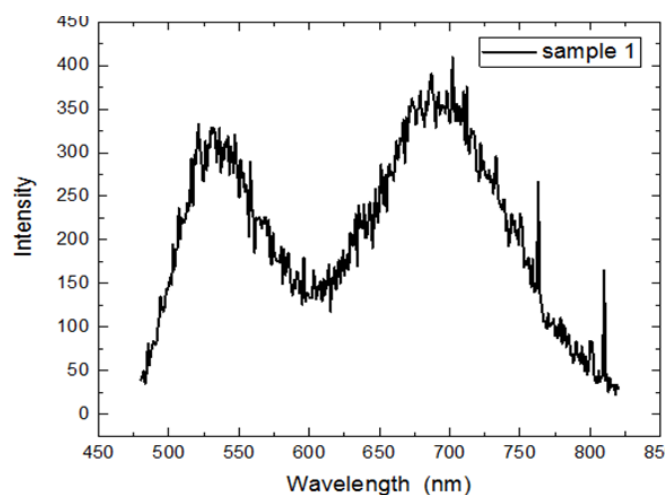


Figure 64. Photoluminescence spectra of **8** processed and encapsulated in N₂

When the **8** was exposed to air, the photoluminescence spectrum changed indicating some form of decomposition or oxidation. The peak at 525 nm did not appear to change while the peak at 700 nm shifted to about 725 nm, doubled in intensity, and gained additional features as it appeared as two unique signals (Figure 65).

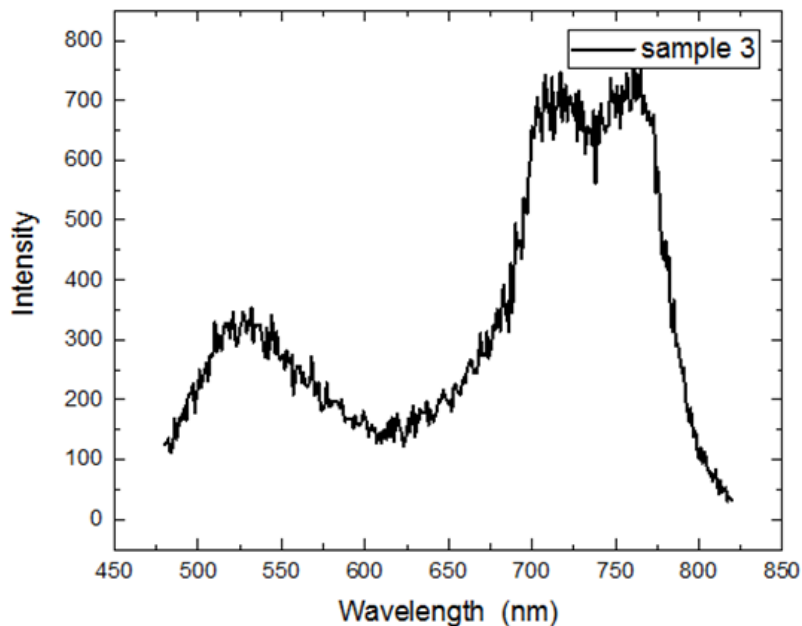


Figure 65. Photoluminescence spectra of **8** processed in N₂ but no encapsulation (exposed to air)

3.4 Synthetic Efforts Toward an IPr-Triarylboranyl Radical

Next, we focused on the incorporation of N, N'-bis(2,6-diisopropylphenyl)imidazole-2-ylidene (IPr) into the triarylborane. Similar to the synthesis of **8**, a 1:1 ratio of IPr and dimesityl pentafluorophenylborane were combined in hexanes and stirred for 12 hours (Figure 66). The assumption was that the reaction would proceed as shown to give the zwitterion **9-F** which could then be converted to cation **9⁺** by abstraction of the boron-bound fluoride using TMS-OTf. Once **9⁺** was isolated, reduction to give the neutral radical **9[•]** would be carried out similar to the chemistry described for **8**.

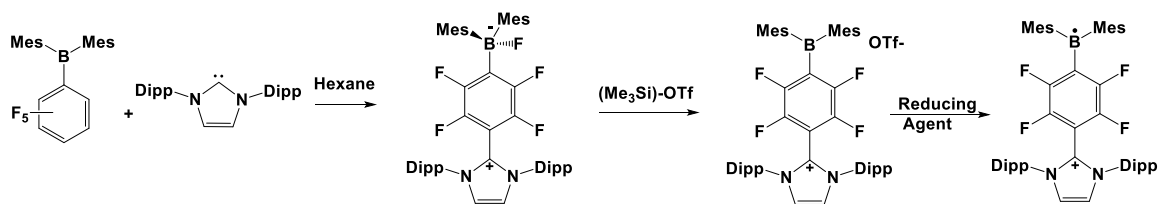


Figure 66. Projected synthesis of **9**

The product obtained from the first reaction shown in Figure 67 was a reddish orange powder. When this powder was dissolved in DCM, a brownish colored solution was observed (Figure 67, left). This solution was then held under a UV lamp, and an intense yellow emission was observed (Figure 67, right).



Figure 67. Left: **9-F** in dry DCM. Right: Solution under UV lamp

Unfortunately, the fluorine NMR spectrum of this product exhibited multiple signals indicative of the formation of several compounds (Figure 68). Specifically, there are two noticeable broad peaks around -170 ppm. This suggests that there are two different molecules that contain a B-F bond. Therefore, it is possible that the carbene added into multiple positions (ortho and para) on the pentafluorophenyl ring.

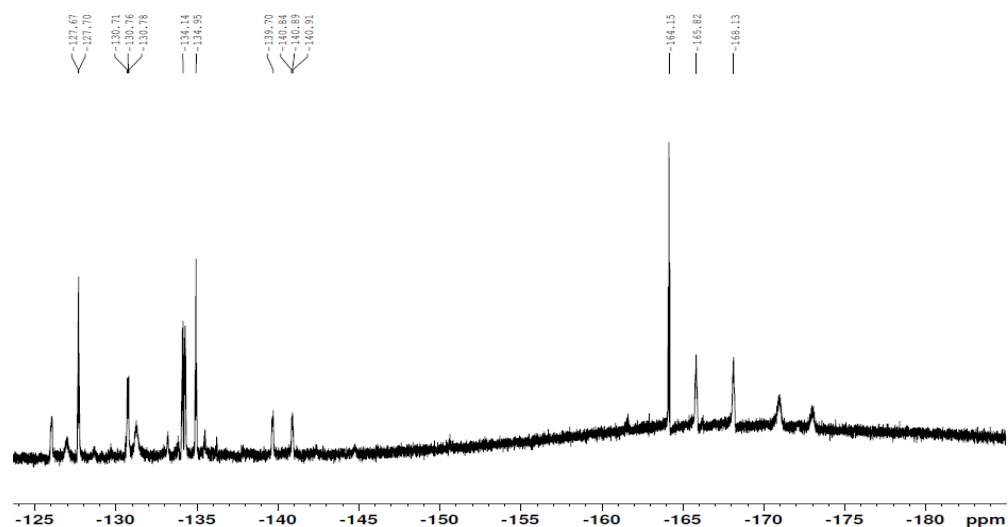


Figure 68. ^{19}F NMR of product **9-F** obtained from reaction of IPr and triaryl borane

Interestingly, when expanding upon the peak at -164.15 ppm, we can see that the peak is a triplet, with a similar chemical shift to the bifluoride (HF_2^-) anion (Figure 69).⁸⁵

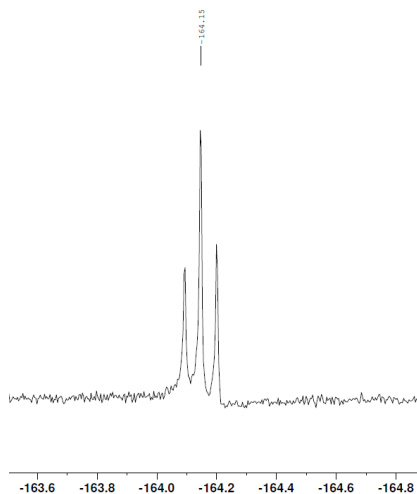


Figure 69. Close up of triplet peak at -164.15 from figure 68

The ^{11}B NMR spectrum of the product mixture in CD_2Cl_2 showed a solitary peak at -2.15 ppm (Figure 70), which is a stark difference from the boron NMR spectrum obtained for the analogous reaction with CAAC which appeared to be two products **8-Fa** and **8-Fb**

(*vide supra*).]The chemical shift of ^{11}B signal in Figure 70 is also sharp which suggested a 4-coordinate borate product, not a three-coordinate borane.

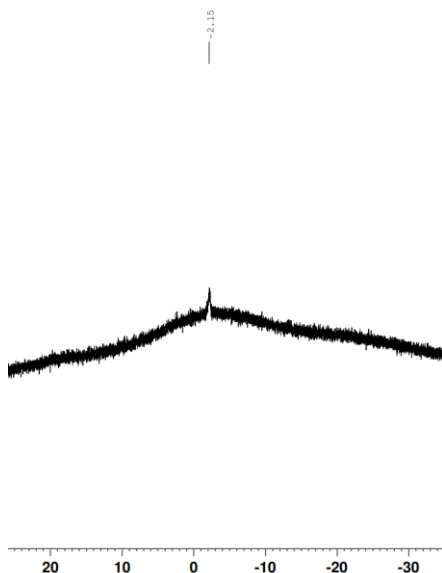


Figure 70. ^{11}B NMR spectrum (CD_2Cl_2) of the product obtained from addition of IPr to the triaryl borane

In a study done by Youngsuk Kim and Eunsung Lee, when 2 equivalents of a perfluorotoluene and an NHC are mixed in solution, double C-F activation occurs (Figure 71).⁸⁵ This occurs because the double bond in the backbone of the carbene can be used as a second carbene equivalent which can undergo nucleophilic aromatic substitution with another equivalent of perfluorotoluene. These “backbone” carbenes are known as abnormal carbenes (aNHCs). An indicator of this type of reaction is the appearance of an HF_2^- peak in the NMR spectra. This peak may be the triplet peak shown in Figure 69. This may be what is occurring in the reaction with IPr and the triaryl borane, due to IPr possessing the ability to become an abnormal carbene. However there is no indication of this occurring in the boron NMR. Further experiments need to be done in order to conclude what is actually happening in the reaction.

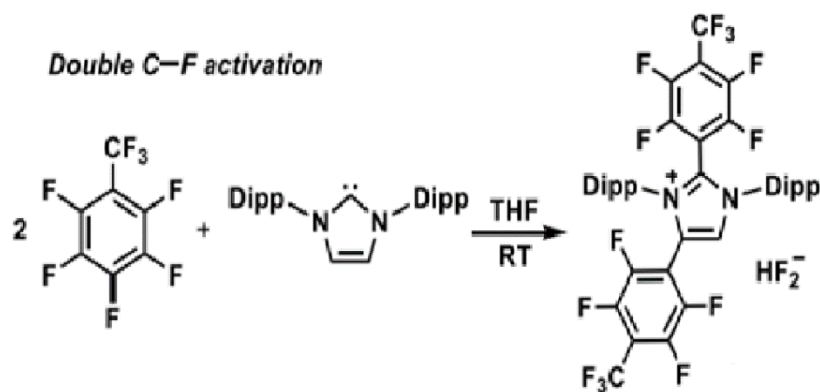


Figure 71. Example of a double C-F activation⁸⁵

If this double addition is occurring, then the reaction and product shown in Figure 72 below may be what we are isolating.

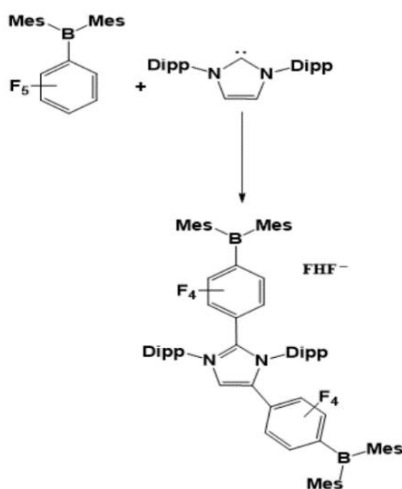


Figure 72. Potential product **9**⁺ of double addition of triaryl borane to IPr

Despite the complicated NMR spectra, the isolated product was added to a vial containing one molar equivalent of TMS-OTf in dry DCM, and the solution was stirred for 2 hours. After this occurred the product was precipitated out using a large excess of hexanes. The precipitated solid was isolated by filtration, then washed with hexanes, pentane, and diethyl ether to give a tan solid that tentatively may be compound **9**⁺ (see Figure 67). In

solution this compound is a golden tan color, and when placed under a hand-held UV lamp, gives off a soft green emission (Figure 73).

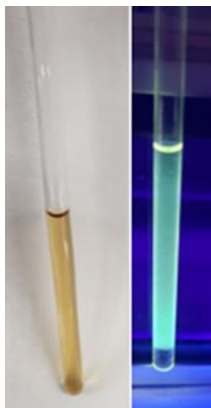


Figure 73. Left: Product obtained from addition of TMS-OTf to the product of the addition of IPr to the triarylborane in dry DCM. Right: Solution of this compound under hand-held UV lamp

After the solid was washed, both ^{19}F and ^{11}B NMR spectra were obtained in CD_2Cl_2 . Figure 74 shows the ^{19}F NMR. There is a large triflate peak at -78.83 ppm; however, there are also multiple peaks from -128.39 ppm to -162.49 ppm which are currently unassigned. While it looks as though there may be multiple compounds present, by ^{11}B NMR spectroscopy, there is only one boron-containing species as only a single peak was observed at -0.36 ppm (Figure 75).

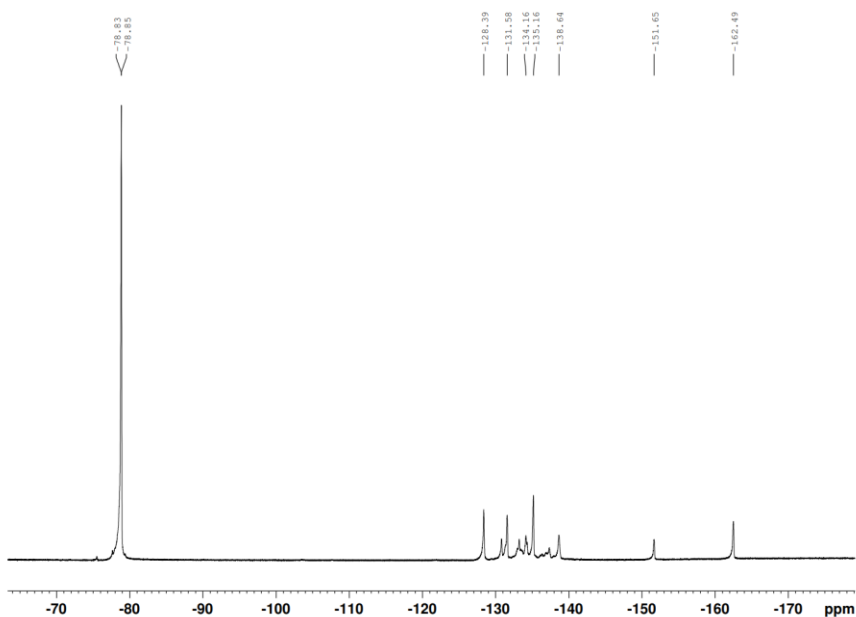


Figure 74. ^{19}F NMR of product obtained from the addition of TMS-OTf to the product obtained from the addition of IPr to the triarylborane

The single peak at -0.36 ppm in the ^{11}B NMR spectrum is sharp, which is different from what was observed for the CAAC analogue (compound $\mathbf{8}^+$) which exhibited a broad peak at 78.7 ppm. For $\mathbf{8}^+$, the broad signal near 80 ppm was consistent with a three-coordinate boron, whereas the sharp peak observed in Figure 75 is more consistent with a four-coordinate borate, as a result, further spectroscopic data or a single crystal X-ray diffraction analysis must be conducted.

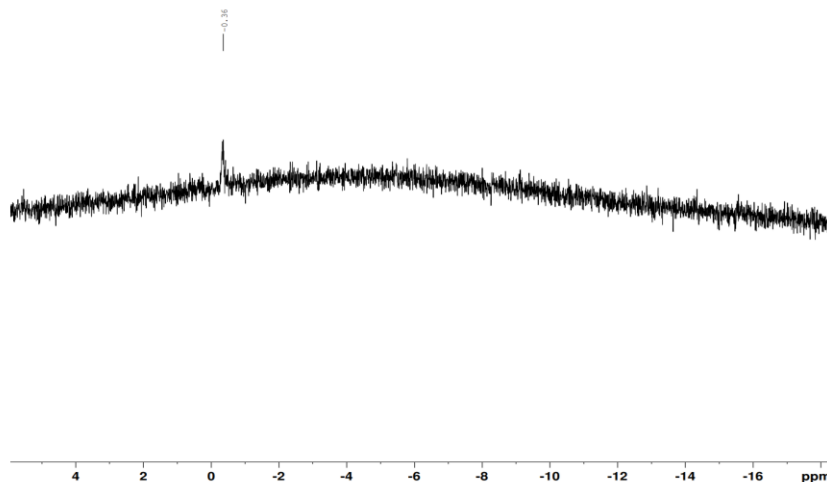


Figure 75. ^{11}B NMR spectrum of the addition of TMS-OTf to the product obtained from addition of IPr to the triarylborane

3.5 Synthetic Efforts Toward a SIMes-Triarylboryl Radical

Due to potential of IPr acting as an abnormal carbene and adding two equivalents of the borane, another route needed to be taken. Saturated N,N'-dimesitylimidizolin-2-ylidene (SIMes) is very similar to IPr; however, instead of a double bond in the backbone it is “saturated” with two CH_2 groups. This carbene was chosen to test because it was hypothesized that it would not act like an abnormal carbene and add the triarylborane twice. The SIMes carbene and triaryl borane were added in a 1:1 ration in hexanes and stirred for twelve hours after which a gray-tan solid (**10-F**) precipitated from the solution in (Figure 76).

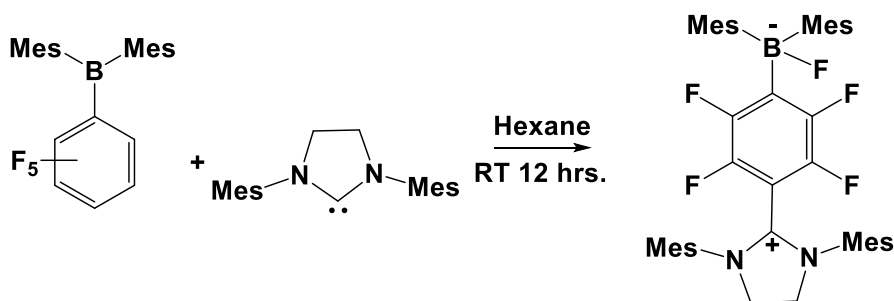


Figure 76. Addition of SIMes to the triaryl borane to form product **10-F**

A DCM solution of **10-F** was a dark tan in color that emitted an intense blue light when irradiated with a hand-held UV lamp (Figure 77). This emission was similar to what was observed for the analogous CAAC compounds **8-Fa** and **8-Fb** which indicated that this new compound may be isostructural with the other two.



Figure 77. Left: **10-F** in dry DCM. Right. DCM solution of **10-F** under a hand-held UV lamp.

In the ^{19}F NMR spectrum of **10-F** (CD_2Cl_2) there are only three peaks at -153.97, -134.57, and -132.98 ppm, respectively, which suggested that only one product was made in this reaction (Figure 78).

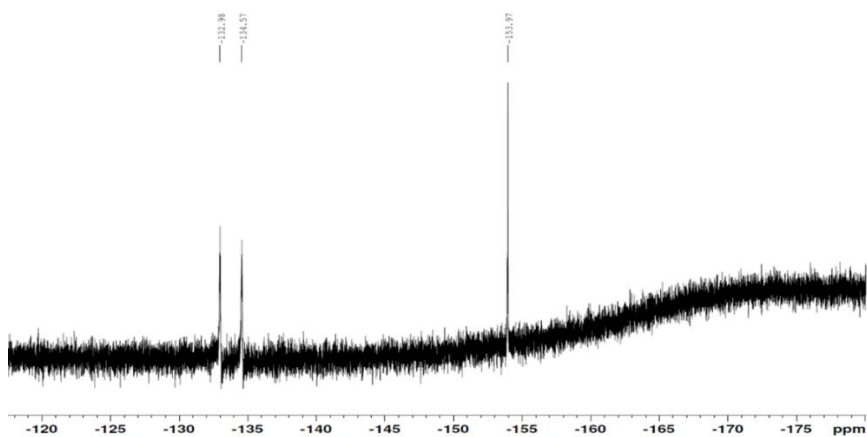


Figure 78. ^{19}F NMR spectrum of **10-F** in CD_2Cl_2 .

While the fluorine NMR spectrum indicated that only a single compound had been isolated, the ^{11}B NMR spectrum of **10-F** exhibited two peaks at 4.28 ppm and -0.83 ppm (Figure 79). It may be possible that the peak at 4.28 is borosilicate glass in the NMR tube and the NMR probe, and therefore, the only signal corresponding to **10-F** would be the sharp signal at -0.83. This peak is sharper and positioned below 0 ppm, which implies a 4-coordinate borate product. For this reason, we cannot rule out the possibility that the SIMes carbene simply coordinated to the boron center to give the Lewis adduct **10** (Figure 80).

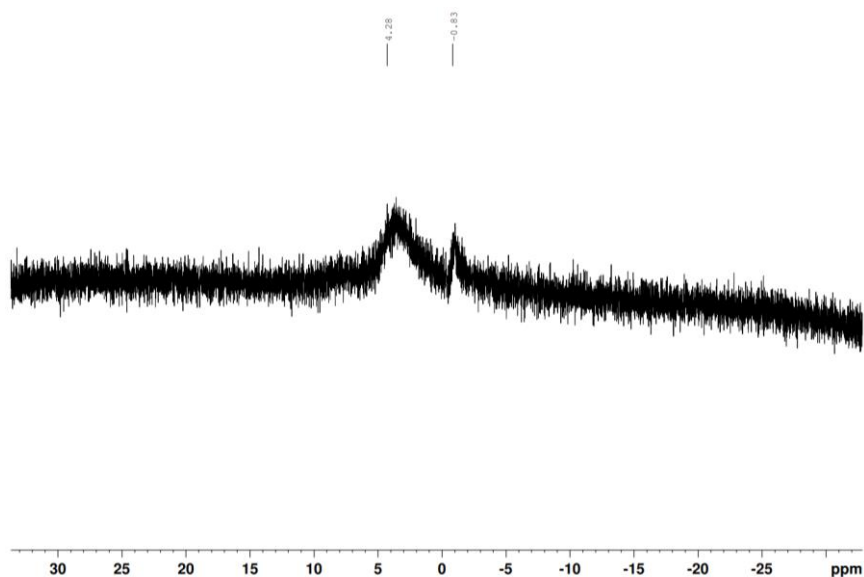


Figure 79. ^{11}B NMR in CD_2Cl_2 of **10-F**

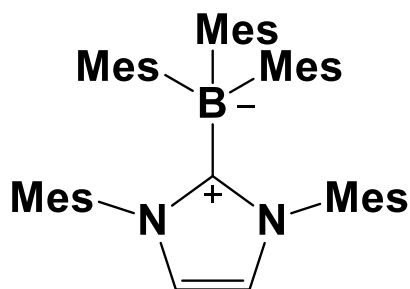


Figure 80. Lewis adduct **10**

The compound tentatively assigned as Lewis adduct **10** was subsequently stirred in a solution of DCM and one molar equivalent of TMS-OTf for two hours. The resulting product was precipitated out with an excess of hexanes. This precipitate was washed with dry hexanes, pentane, and ether to afford a reddish-tan powder.

The ^{19}F NMR spectrum of the solid isolated after addition of TMS-OTf was nearly identical to the NMR spectrum of the starting material with the exception of the appearance of a triflate peak at -79.06 ppm (Figure 81). The fact that the ^{19}F NMR spectrum did not change is excellent evidence that the identity of the compound isolated from the reaction shown in Figure 76 is indeed the Lewis adduct **10**. The fact that a triflate signal is present is not surprising given that triflate was added to this reaction, and some residual TMS-OTf could be present in the sample.

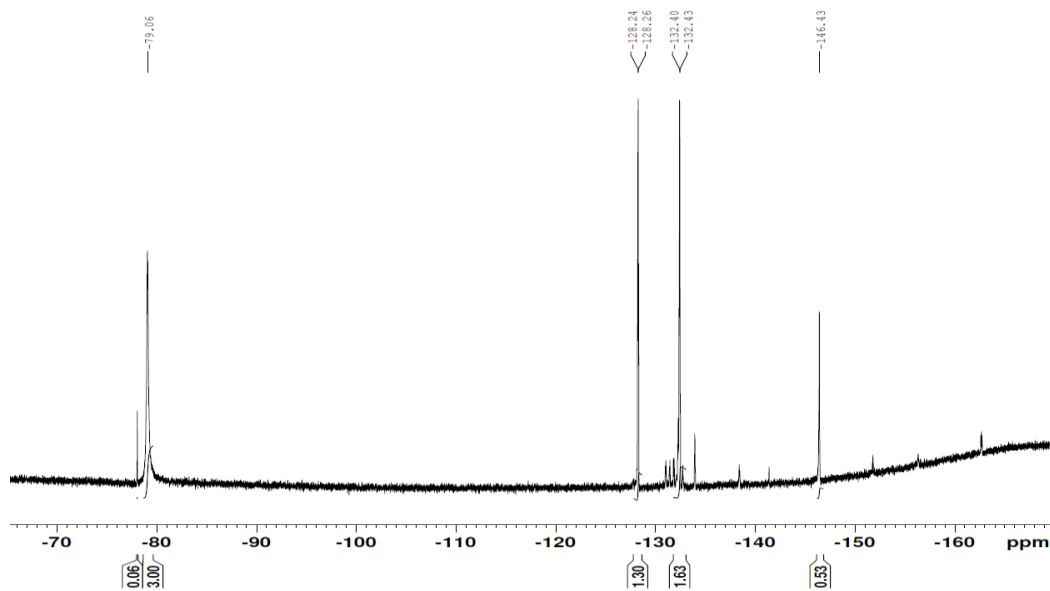


Figure 81. ^{19}F NMR spectrum of the product obtained from the addition of TMS-OTf to Lewis adduct **10**.

To further corroborate this, the ^{11}B NMR spectrum revealed only a single sharp peak at -1.02 ppm, consistent with a 4-coordinate borate (Figure 82).

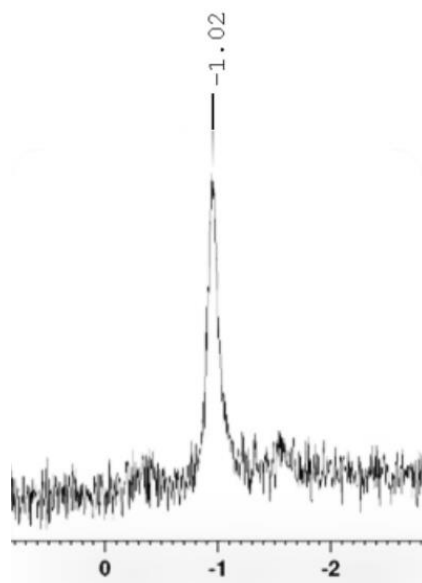


Figure 82. ^{11}B NMR spectrum of the product obtained from the addition of TMS-OTf to Lewis adduct **10**.

3.6 Synthetic Efforts Toward a DAC-Triarylboranyl Radical

Finally, the addition of the DAC to the triarylborane was attempted; however, the DAC-triaryl borane complex was unable to be synthesized. This is not surprising given that the DAC is the least nucleophilic of the four carbenes investigated. As such it appears that it not sufficiently nucleophilic to engage the triarylborane in a nucleophilic aromatic substitution reaction. The addition reaction was conducted in several ways to give compound **11-F** (Figure 83) The first attempt added DAC and the triarylborane to a vial with hexanes followed by stirring for 12 hours. After 12 hours only the two starting compounds were observed by NMR spectroscopy. Next, the mixture was heated at certain temperatures. Alas, this did nothing as well. The next attempts explored different solvents for the reactions including pentane, diethyl ether, DCM, and benzene. None of these changes were successful in adding the DAC to the triarylborane. Finally, we attempted to add the DAC to the triarylborane in the presence of a strong halide abstraction reagent. For

this reaction, the DAC was mixed with the triarylborane in the presence of silver(I) triflate in an effort to directly obtain **11**⁺(Figure 83). However, this was unsuccessful too.

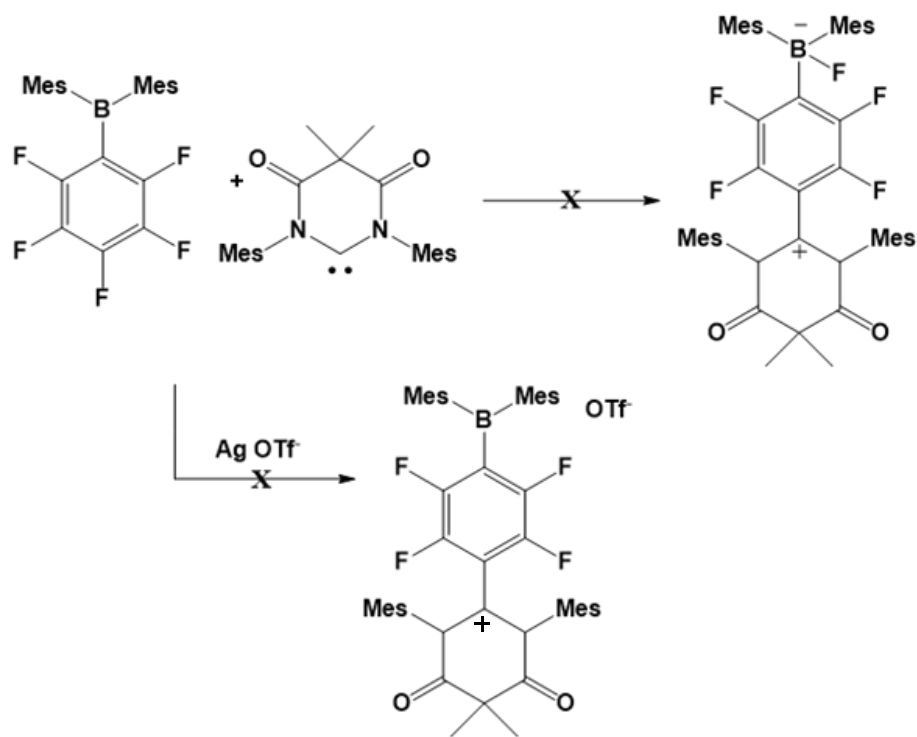


Figure 83. Unsuccessful reaction pathways of DAC and the triaryl borane

When comparing DAC to the other carbenes used there is one important difference, the HOMO level. The HOMO levels for CAAC, IPr, and SIMes are -5.279 eV, -5.864 eV, and -5.723 eV respectively. DAC's HOMO level is lower than each of these at -6.105 eV. As a result, the DAC is the least nucleophilic carbene in this series. Ultimately, this would hamper nucleophilic attack on the pentafluorophenyl ring.

3.7 Experimental

Synthesis of the mixture 8–Fa and 8–Fb

Dimesityl pentafluorophenylborane (1 g, 2.4 mmol) was added to a vial along with CAAC (.7526 g, 2.4 mmol) and a stir bar. These solids were then dissolved in 5 mL of dry hexanes and stirred at room temperature for 12 hours. A solid precipitated out, which was washed over a filter frit with dry hexane, pentane, and ether. A green-white solid was obtained (1.61 g, 94% yield).

Synthesis of 8⁺

The mixture of 8–Fa and 8–Fb (100 mg, .137 mmol) was dissolved in a vial that contained a stir bar, 5 mL of dry DCM, and TMS triflate (.025 mL, .031 mg, .137 mmol). This was stirred at room temperature for 2 hours. After this an excess of hexane was added to the system which allowed the product to precipitate out. This product was then washed with dry hexanes and ether. The powder produced was a tan color (.104g, 88% yield)

Synthesis of 8⁻

8⁺ (.1g, .116 mmol) was dissolved in 3 mL of dry benzene. KC₈ (.015 g, .116 mmol) was added to the vial. This solution immediately became a deep emerald color once the vial was shaken. This solution was filtered with a syringe and syringe filter to remove unused KC₈ or triflate salt formed.

Synthesis of 9–F

Dimesityl pentafluorophenylborane (1 g, 2.4 mmol) was added to a vial along with IPr (0.934g, 2.4 mmol) and a stir bar. These solids were then dissolved in 5 mL of dry hexanes and stirred at room temperature for 12 hours. A solid precipitated out, which was washed over a filter frit with dry hexane, pentane, and ether. An orange-red solid was obtained (1.64g, 85% yield).

Synthesis of 9⁺

9-F (100 mg, .124 mmol) was dissolved in a vial that contained a stir bar, 5 mL of dry DCM, and TMS triflate (.023 mL, .028 mg, .124 mmol). This was stirred at room temperature for 2 hours. After this an excess of hexane was added to the system which allowed the product to precipitate out. This product was then washed with dry hexanes and ether. The powder produced was a tan color (.081g, 70% yield)

Synthesis of Lewis adduct 10

Dimesityl pentafluorophenylborane (0.1 g, .24 mmol) was added to a vial along with SIMes (0.073g, 0.239 mmol) and a stir bar. These solids were then dissolved in 5 mL of dry hexanes and stirred at room temperature for 12 hours. A solid precipitated out, which was washed over a filter frit with dry hexane, pentane, and ether. A gray purple solid was obtained (0.152 g, 88% yield).

SIMes-Triaryl borane OTf-

SIMes-triaryl borane BF (100 mg, 0.138 mmol) was dissolved in a vial that contained a stir bar, 5 mL of dry DCM, and TMS triflate (.025 mL, .031 mg., mmol). This was stirred at room temperature for 2 hours. After this an excess of hexane was added to the system which allowed the product to precipitate out. This product was then washed with dry hexanes and ether. The powder produced was a light tan color (0.085g, 73% yield)

3.8 Discussion and Conclusion

The CAAC carbene successfully added to the triaryl borane. However, the NMR data suggests that at least two compounds were synthesized, a product where the removed fluorine added to the boron atom, and another where the removed fluorine added to the carbene carbon. These products were then successfully One OLED device was successfully

made with the CAAC- triaryl borane radical. However, this device was not comparable to today's devices due to its low luminescence. It also had decomposition when exposed to air. Even with the N₂ encapsulation there may have been some decomposition. This is not viable for an OLED device. These compounds do show a penchant for emission; however, the extreme air sensitivity makes them noncompetitive to on the market device until a more effective encapsulation method occurs.

IPr was successfully added, but it most likely added twice. Based on the NMR data, there is enough evidence that this is a reasonable possibility, especially because of the appearance of a potential HF₂⁻ peak in the fluorine NMR. The IPr carbene has the ability to act as an abnormal carbene which allowed for the double addition of the triaryl borane. The triflate reaction was carried out and it seems as if the B-F bond disappears and a new triflate peak appears, suggesting that that fluorine was replaced by the triflate counter anion.

The SIMes carbene successfully added as well, and the NMR data suggests two products just like with the CAAC-triaryl borane addition. This product gave a nice blue-white emission under UV lamp. The triflate complex was also synthesized, which is shown by the disappearance of the B-F peak in the fluorine NMR and the appearance of a triflate peak. This product gave off a bright white blue emission under a UV lamp, though a darker blue than the SIMes-triaryl borane product.

4. FUTURE WORK

4.1 Overview

More work needs to be done with the CAAC radical. The Stokes shift needs to be found in order to see the difference between the absorption and the emission of the molecule. This will be done with a photoluminescence spectrometer. As described in the introduction, Li has published promising results using doublet emitters that do not follow the Aufbau principle, which states that electrons fill lower energy atomic orbitals before filling higher energy atomic orbitals.⁸⁵ These radicals are more stable and more efficient than radicals that follow the Aufbau principle, however, are very rare. It will be very interesting to see if the radicals synthesized in this thesis as well as the potential radicals that will be synthesized follow the Aufbau principle or not. This will be tested by cyclic voltammetry (CV) and DFT calculations, and if available, ultraviolet photoelectron spectroscopy.

From an applications point of view, it may be of interest in looking at how the optoelectronic properties change for our radicals when adding in a conjugated polymer matrix (i.e. PVK) or a small molecule compound (i.e. TPBi) at different concentrations. Adding these into a film with our molecules may change the efficiency of the system. It will also be important to determine the Stokes shift for all compounds to be incorporated into an OLED device. Adequate separation of the absorption and emission bands of the emitter will be critical to minimize re-absorption of emitted photons to optimize device efficiency. Another future direction is for more carbenes to be tested with the triaryl borane as well as making a compound based off Okamoto, Takeya, and Yamaguchi's boron stabilized neutral π -radical system. This system is shown below in Figure 84.

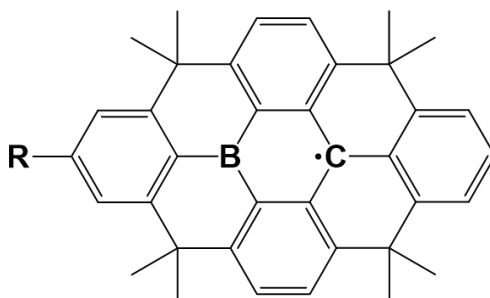


Figure 84. Okamoto, Takeya, and Yamaguchi's boron stabilized neutral π -radical system⁴²

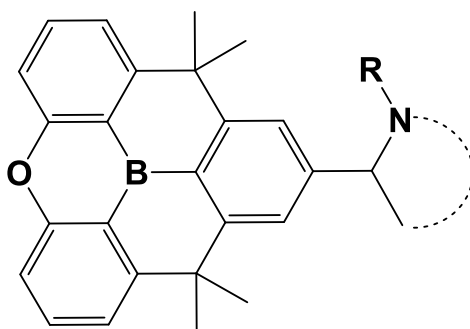


Figure 85. π -radical system with carbene

The next three carbenes that will be added are mono amido amino carbene (MAAC), cyclopropenylidene, and bicyclic alkyl amino carbene (BiCAAC). These three carbenes theoretically should add with no problem. Each one of them has HOMO/LUMO levels very similar to both CAAC and SIMes. The proposed radical products are shown below in Figure 86. The comparison between the HOMO/LUMO gaps of MAAC, BiCAAC, cyclopropenylidene, CAAC, SIMes are shown below in table 3.

Table 3. Comparison of HOMO/LUMO energy levels between MAAC, BiCAAC, cyclopropenylidene, CAAC, and SIMes

Carbene	HOMO (eV)	LUMO (eV)
BiCAAC	-4.971	-0.503
CAAC	-5.279	-0.433
cyclopropenylidene	-5.306	-0.260
MAAC	-5.683	-0.985
SIMes	-5.723	-0.329

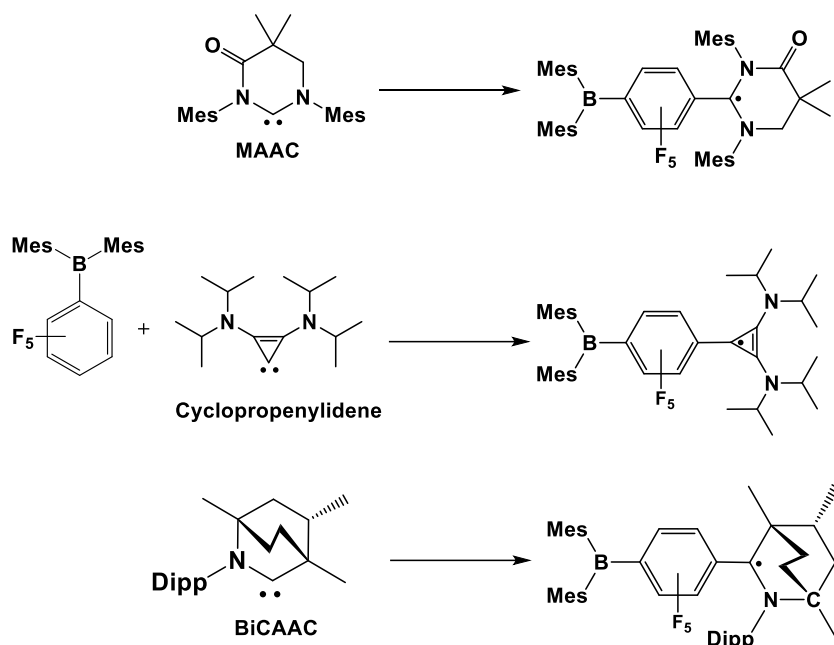


Figure 86. Future carbenes to attach to triaryl borane

4.2 Synthesis and Characterization of MAAC-Triarylboranyl Radicals

MAAC structurally very similar to the carbene DAC. However, there is only one amido group whereas DAC has 2. Even though DAC didn't add successfully to the triaryl borane, we predict this one will due to the shift in HOMO levels. DAC's HOMO level is -6.105 eV while MAAC's is -5.683, which doesn't seem like that much of a difference at first glance. However, this value is almost halfway in between the DAC and CAAC HOMO levels and is higher than both the IPr and SIMes HOMO levels. IPr and SIMes both added with little to no difficulty so theoretically MAAC will also be able to add to the triaryl borane. MAAC is much more nucleophilic in comparison to DAC based on its HOMO level. Because the addition of the carbene to the triaryl borane is a nucleophilic aromatic substitution, it's very important that the carbene is nucleophilic enough for this reaction to proceed. The following figure shows the proposed final radical structure of this series of reactions.



Figure 87. Proposed synthesis of MAAC-triaryl borane radical

4.3 Synthesis and Characterization of Cyclopropenylidene-Triarylboryl Radicals

Cyclopropenylidene is a good candidate for making a radical due to where its HOMO/LUMO levels lie in comparison to SIMes. The HOMO of cyclopropenylidene lies at -5.306 eV and the LUMO lies at -0.26 eV. The HOMO and LUMO of SIMes are very similar albeit slightly different at -5.723 eV and -0.329 eV respectively. The structure of cyclopropenylidene is much different when compared to the other carbenes discussed in this thesis, but the two nitrogens surrounding the double bond don't have electron withdrawing groups near them. This also allows the carbene carbon's lone pair to be more donating due to resonance. The following figure shows the predicted radical that would be obtained from adding cyclopropenylidene and the triaryl borane and reducing.

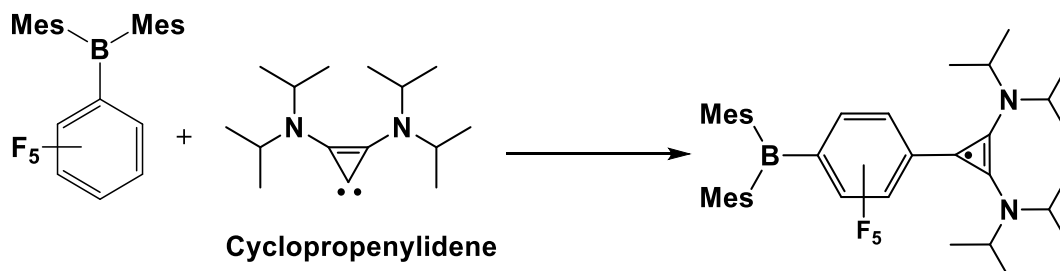


Figure 88. Proposed synthesis of cyclopropenylidene-triaryl borane radical

4.4 Synthesis and Characterization of BiCAAC-Triarylboranyl Radicals

BiCAAC is a good donor molecule due to high HOMO level. With a HOMO level of -4.971 eV, BiCAAC has the highest level of all the carbenes chosen for this project and is also the most nucleophilic of the grouping. We theorize that this carbene would add very easily due to this. With the triaryl borane being a Lewis acid, the types of molecules needed to insert easily are donor types.

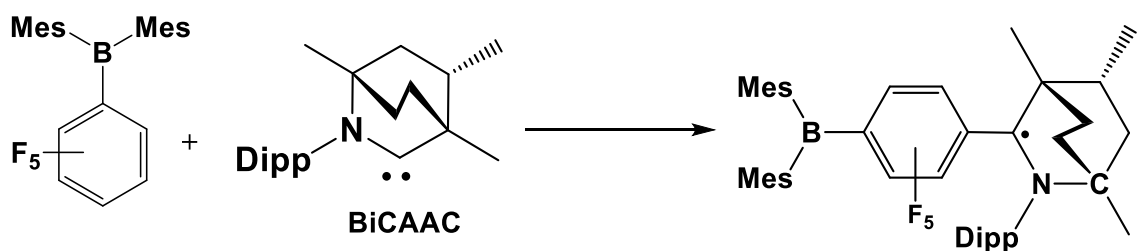


Figure 89. Proposed synthesis of BiCAAC-triaryl borane radical

4.5 Synthesis and Characterization of a Carbene-Substituted Oxoboranthracene Derivatives

Another future direction for this project is to construct a complex similar to Okamoto, Takeya, and Yamaguchi's boron stabilized neutral π -radical system. This will be completed by the multistep synthesis shown in Figure 90. This product would be a different direction from the previous reactions but still take advantage of carbene to change the emission, and a boron for the radical to cling to. Because it is a planar molecule, this may also make the potential OLED device more efficient.

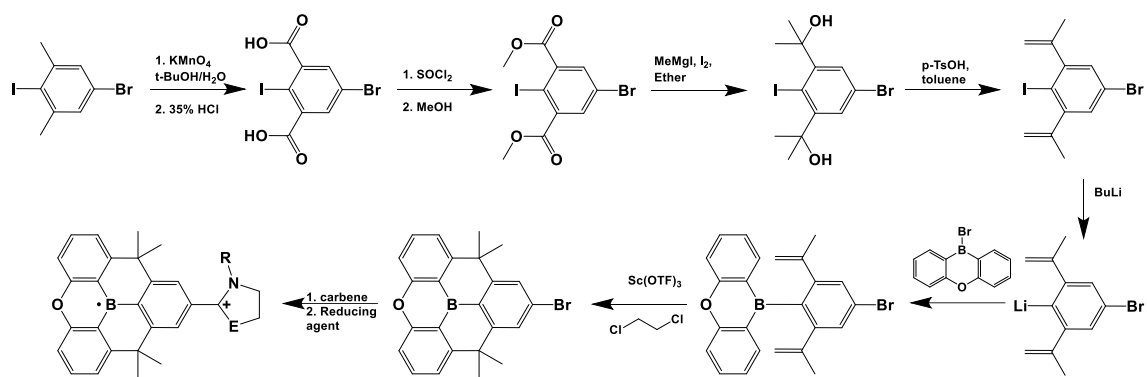
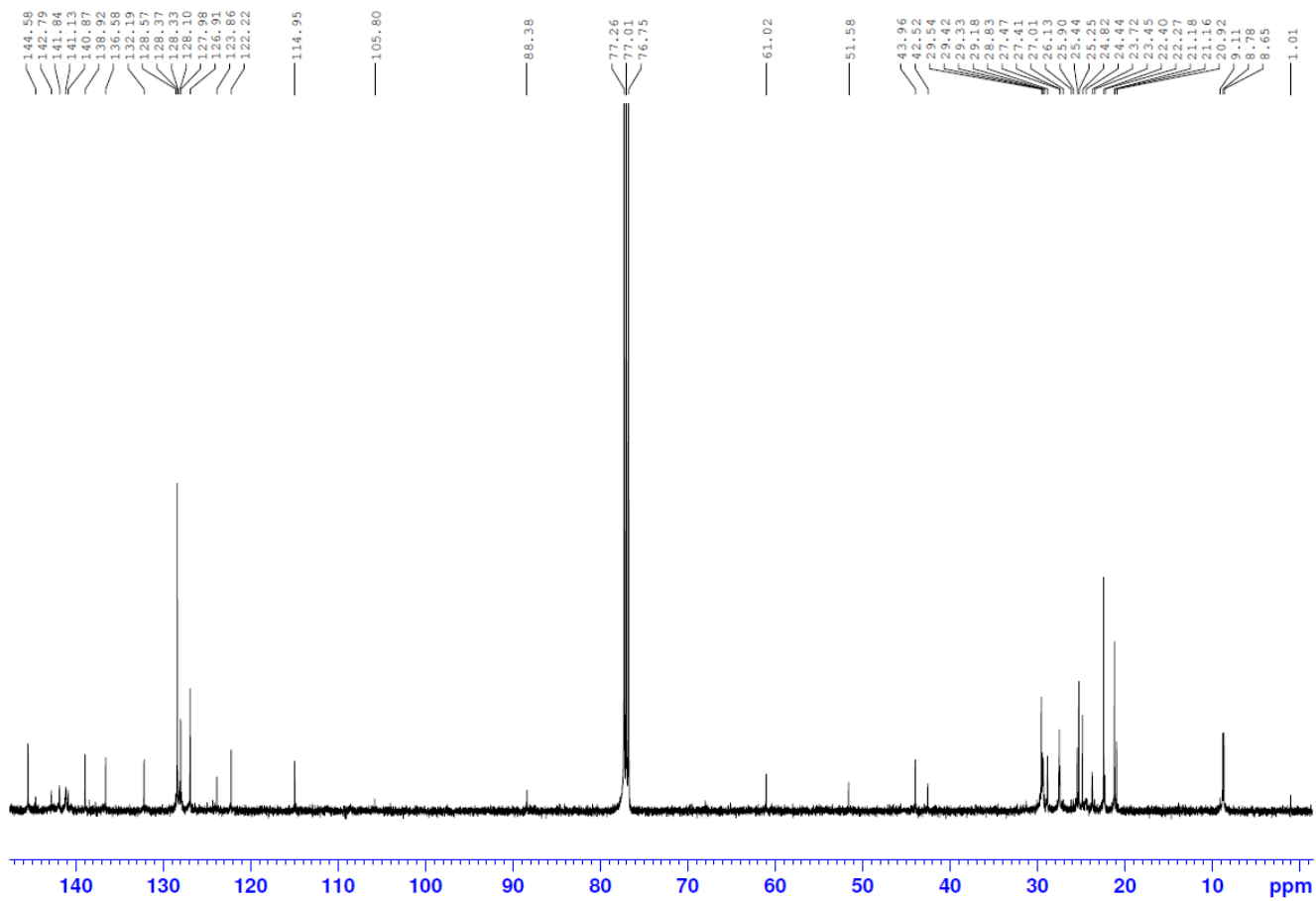


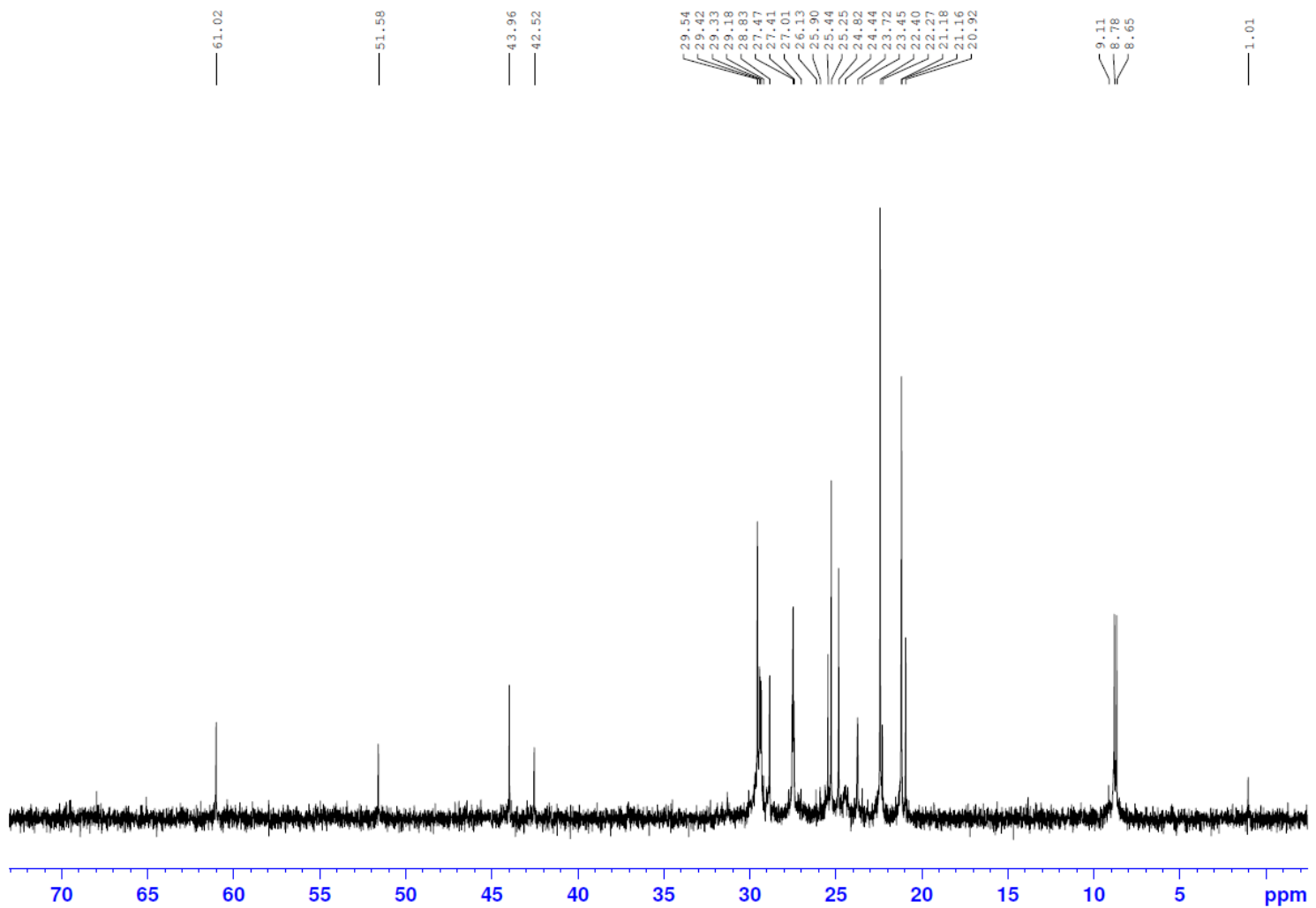
Figure 90. Proposed synthesis of π -radical system with carbene

APPENDIX SECTION

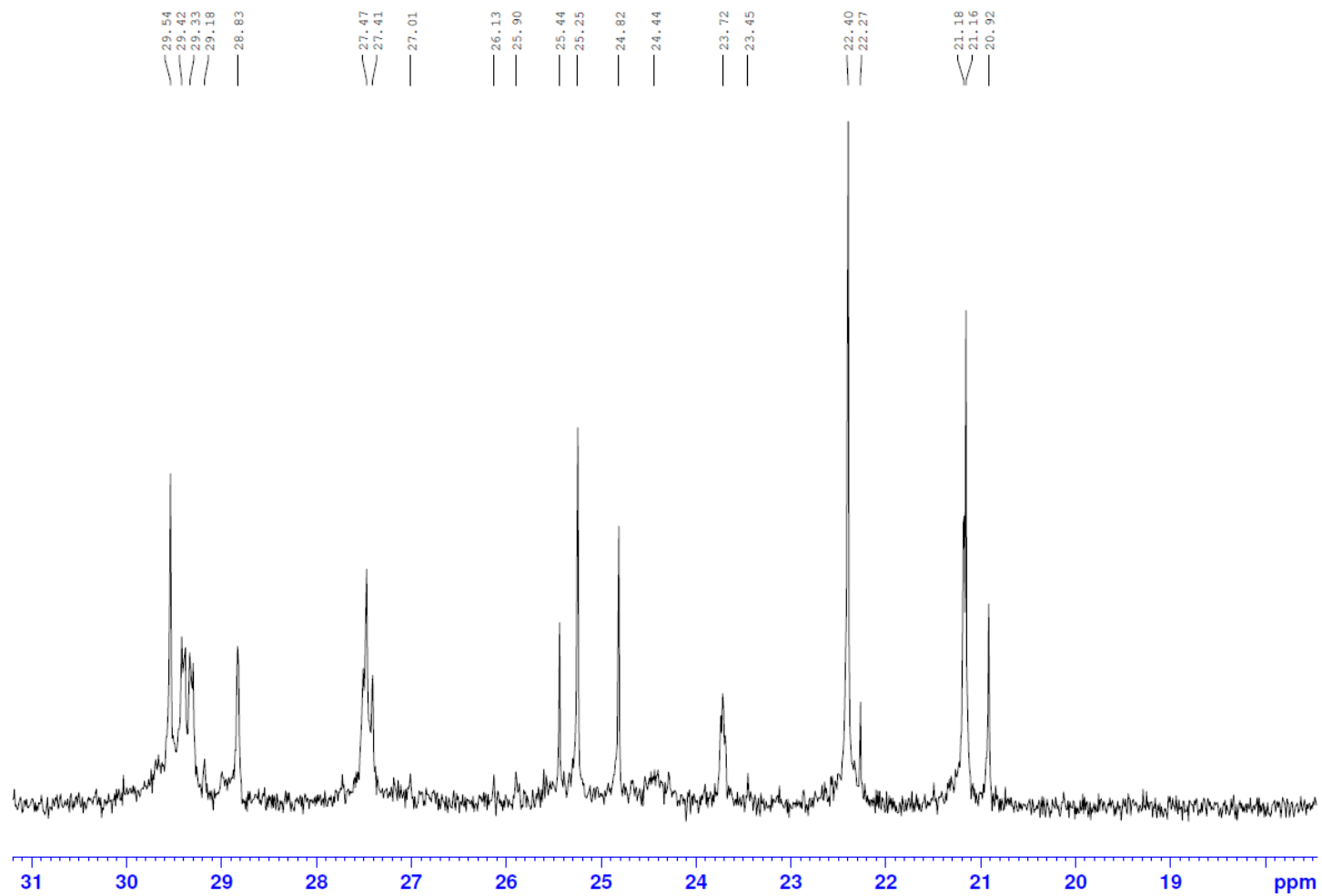
CAAC-BF ¹³C NMR in CDCl₃

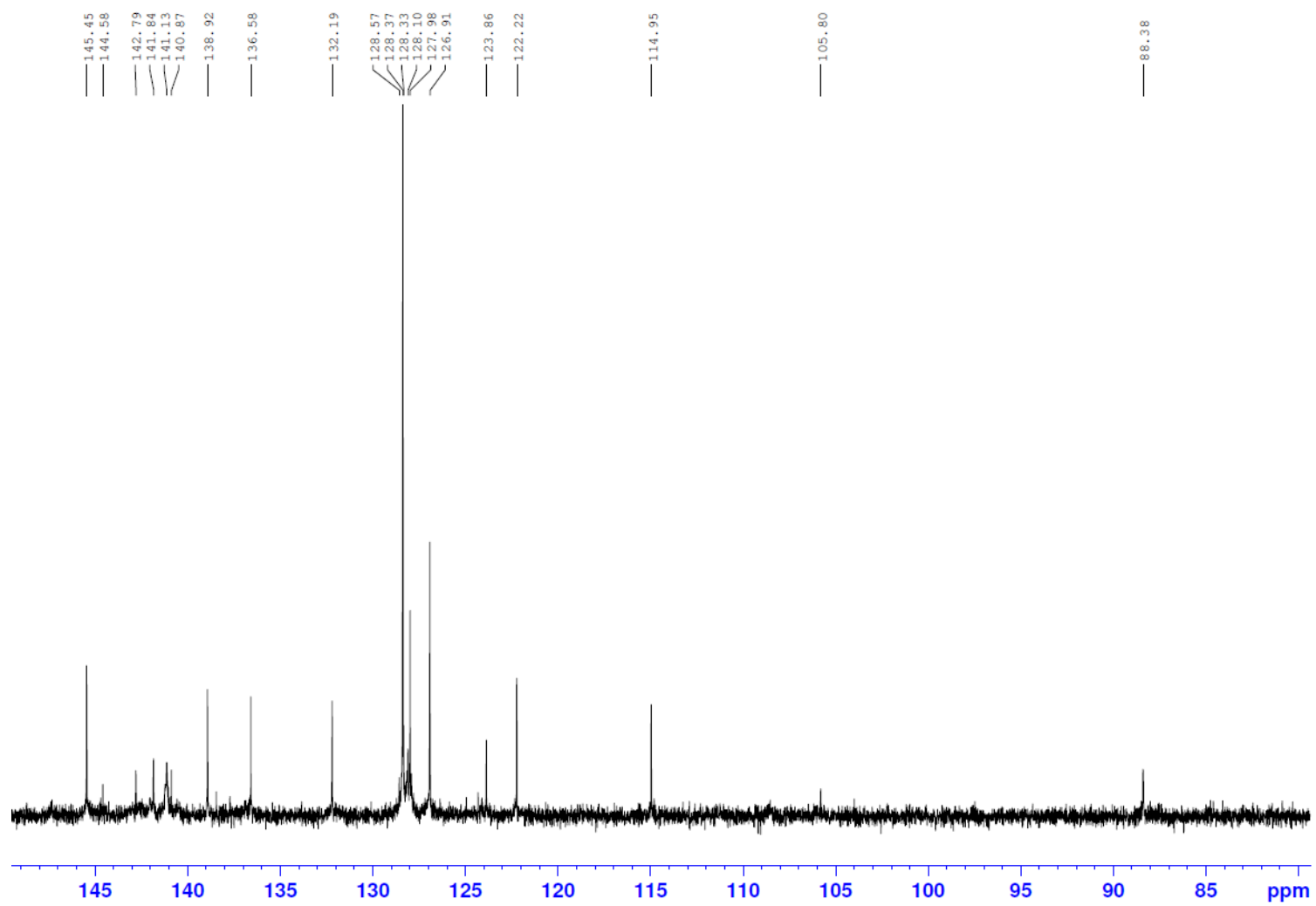


CAAC-BF ¹³C NMR in CDCl₃ (0-75ppm)

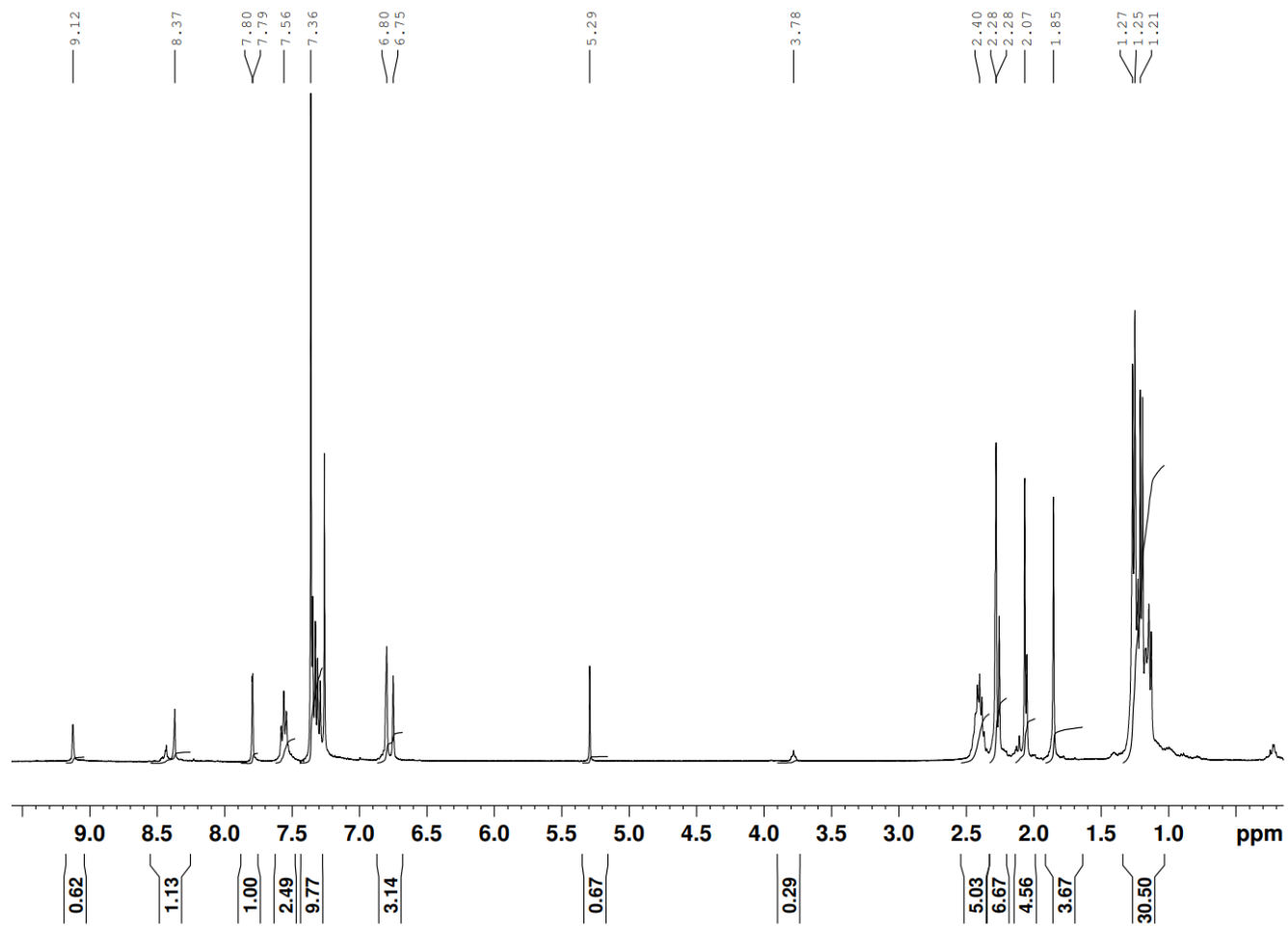


CAAC-BF ¹³C NMR in CDCl₃ (18-31ppm)



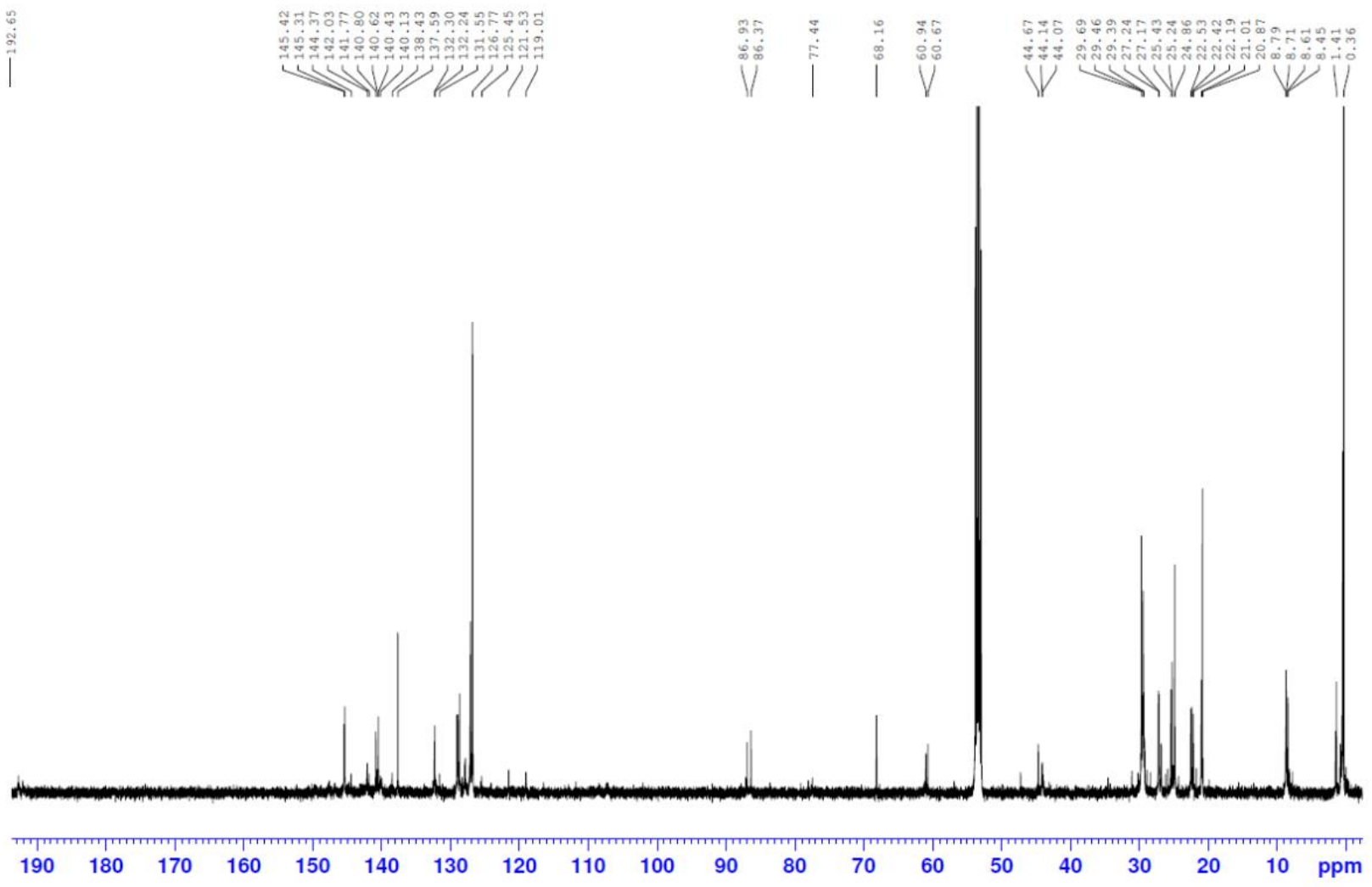
CAAC-BF ^{13}C NMR in CDCl_3 (80-150ppm)

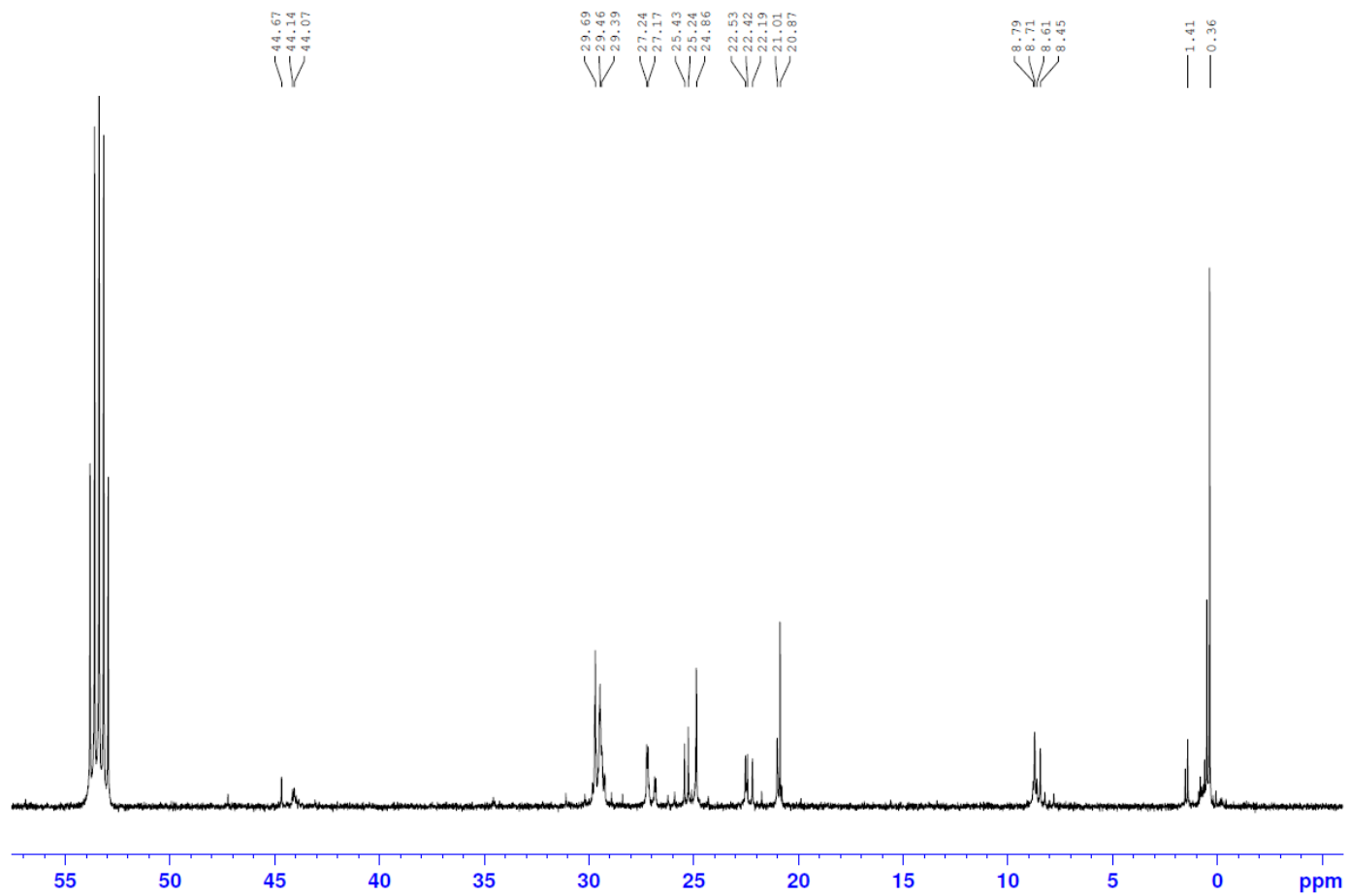
CAAC-BF ¹H NMR in CDCl₃

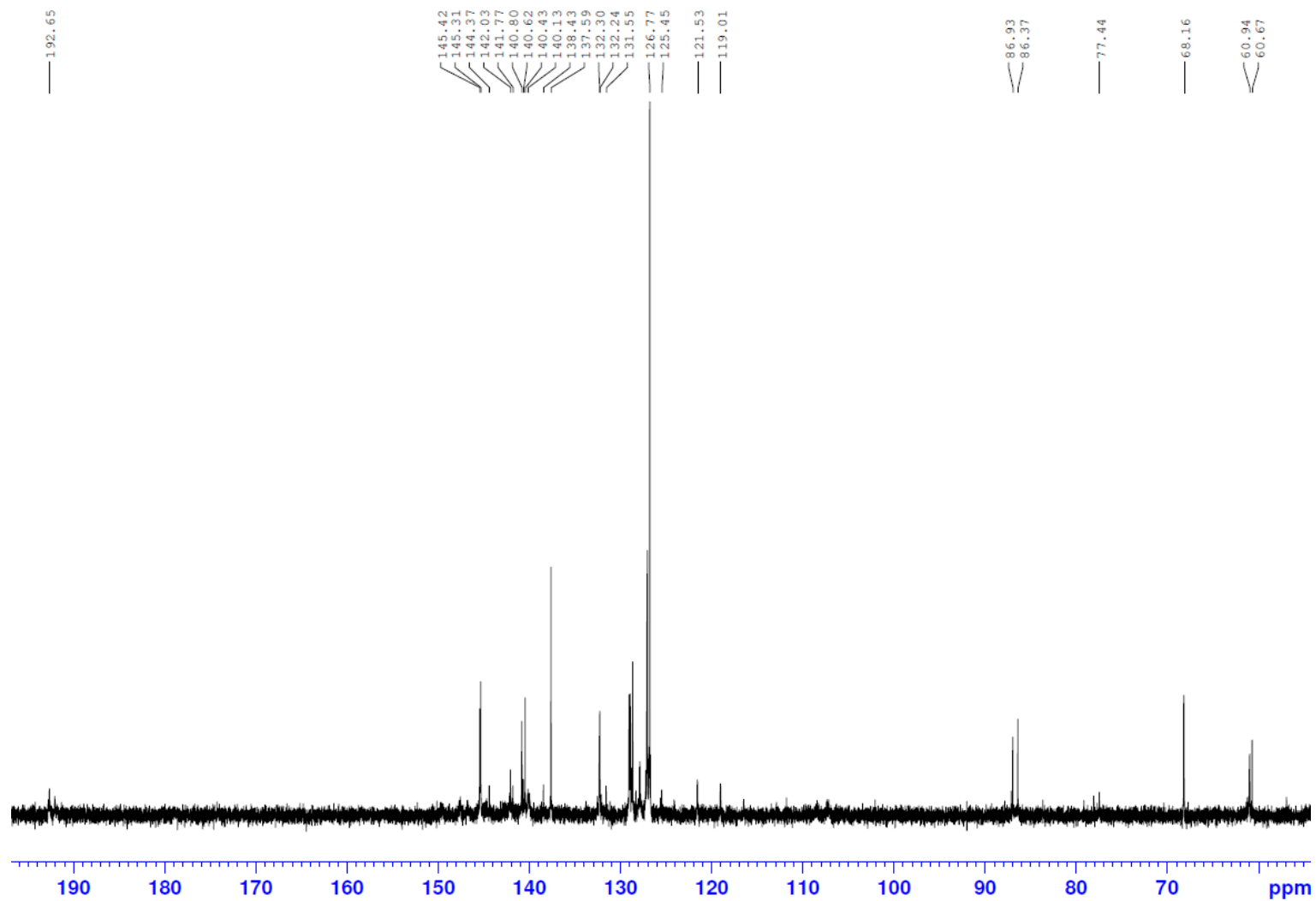


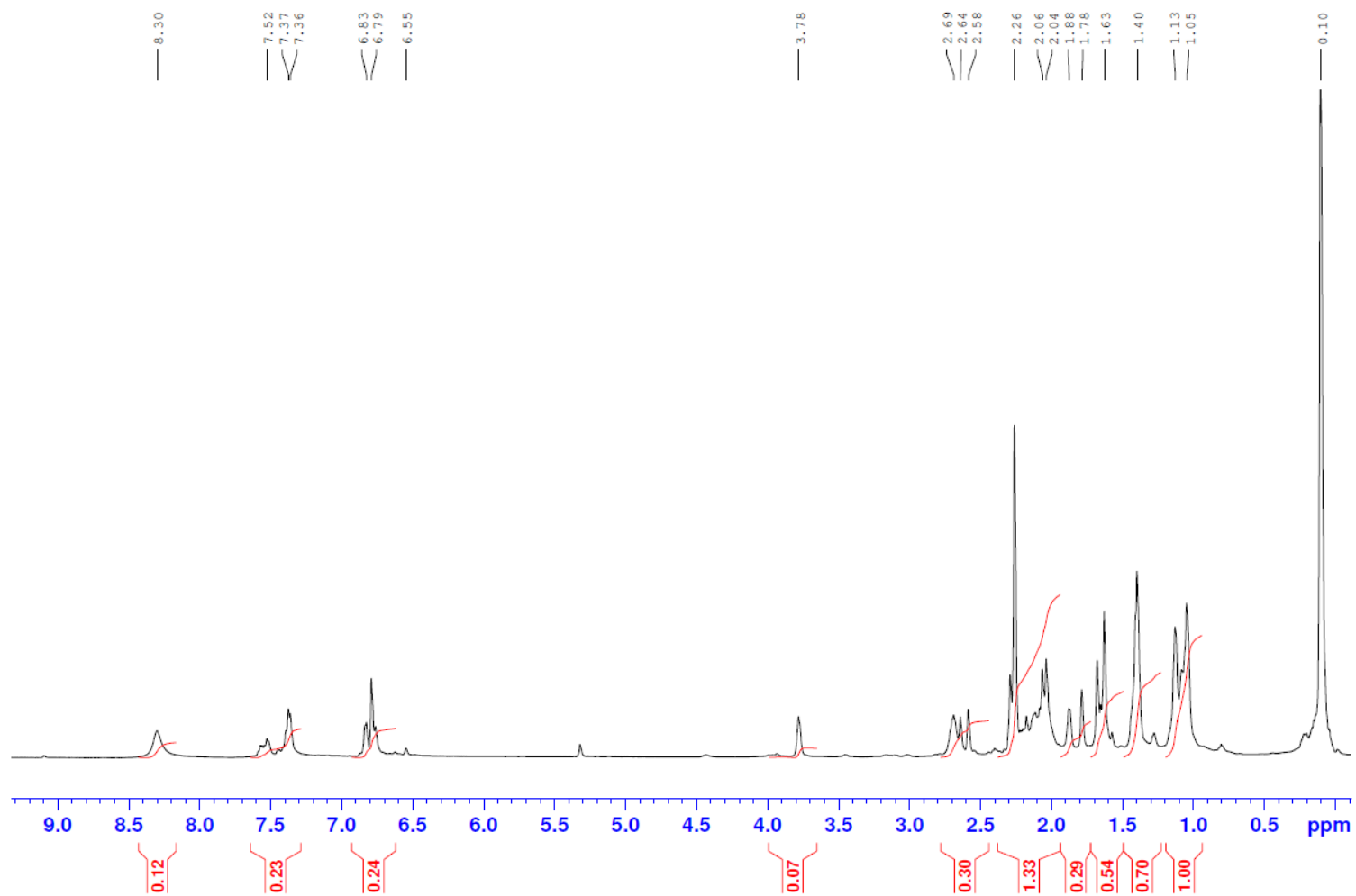
LL

CAAC-OTf- ¹³C NMR in CD₂Cl₂

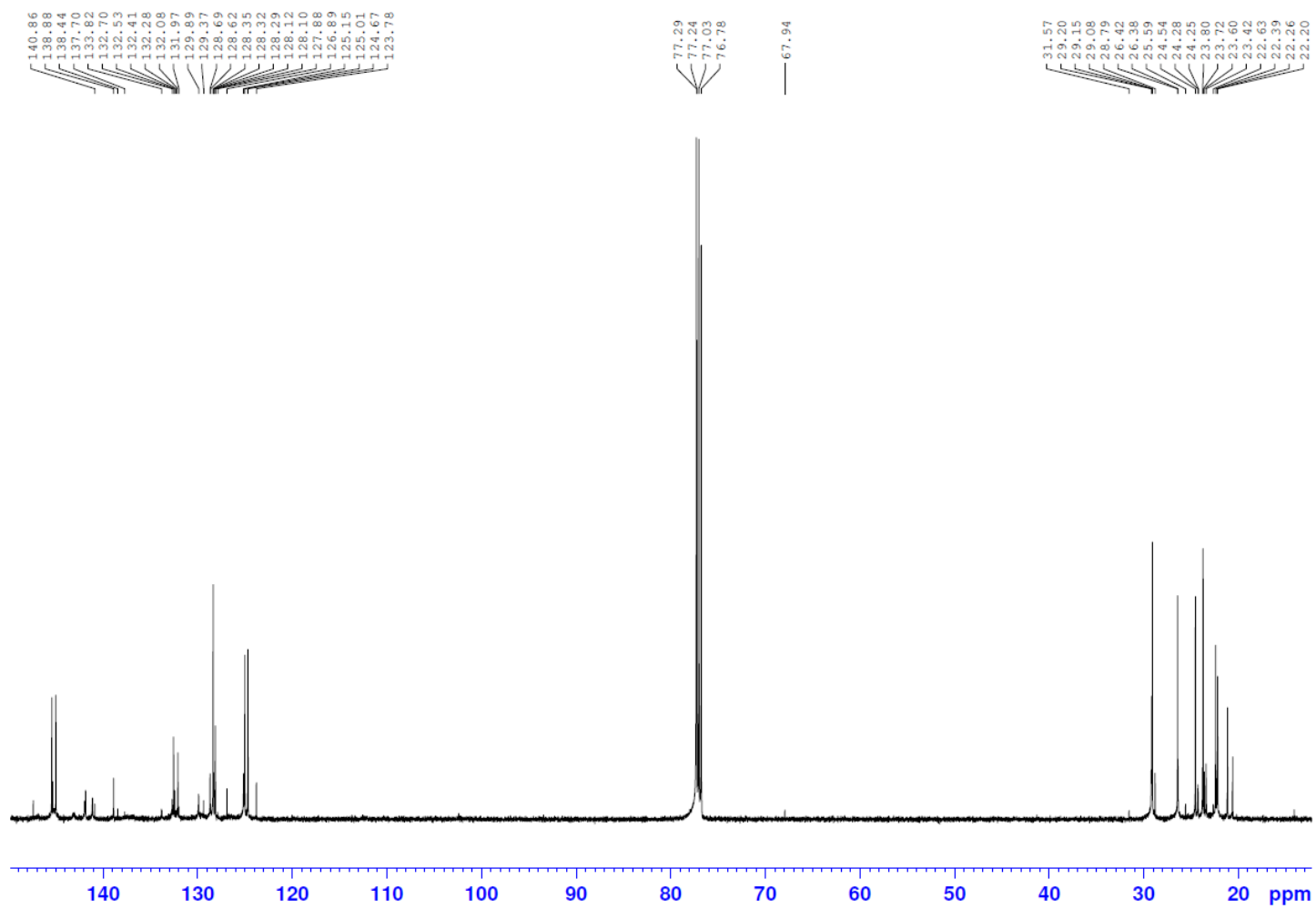


CAAC-OTf-¹³C NMR in CD₂Cl₂ (0-55 ppm)

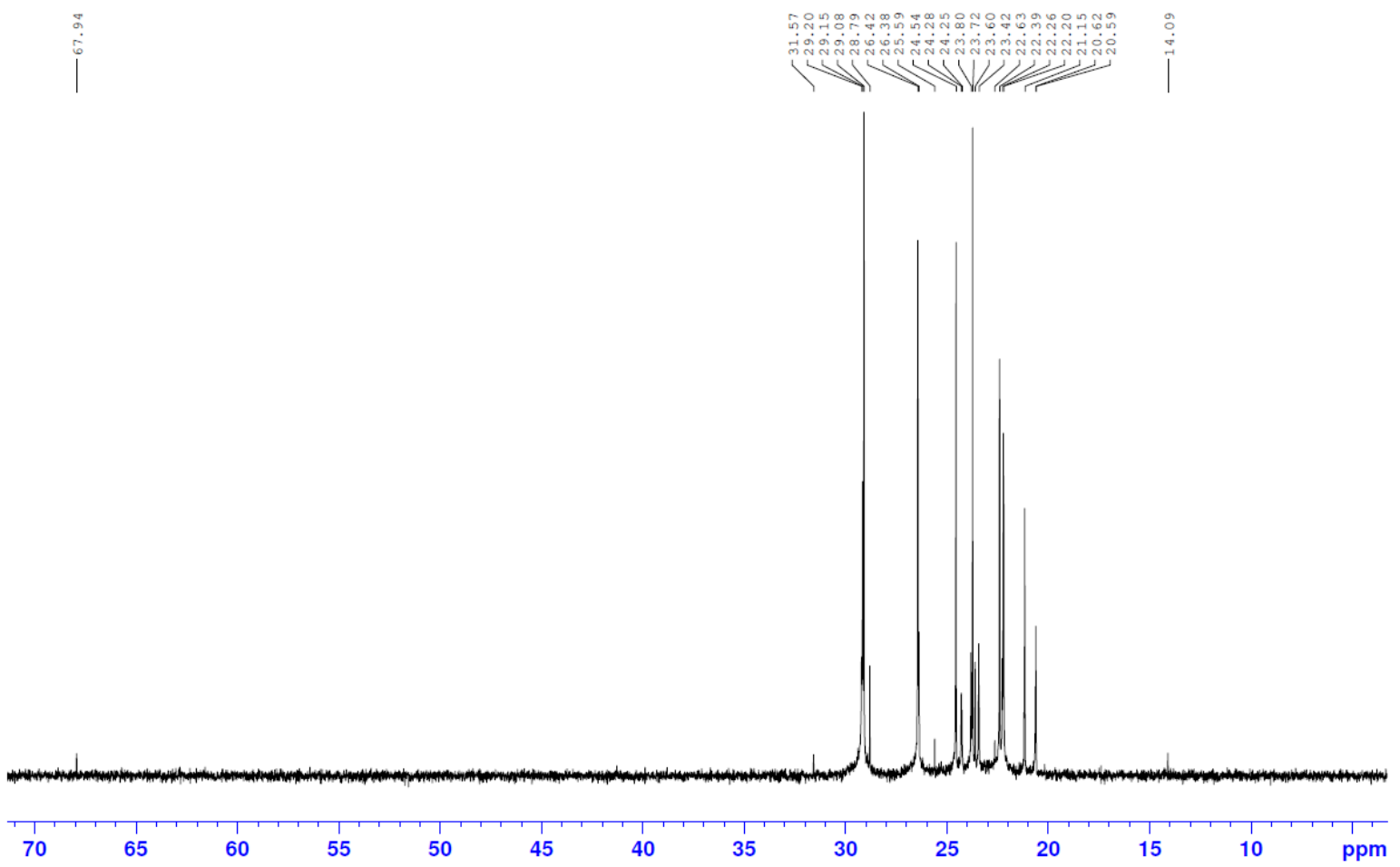
CAAC-OTf-¹³C NMR in CD₂Cl₂ (80-195 ppm)

CAAC-OTf- ^1H NMR in CD_2Cl_2 

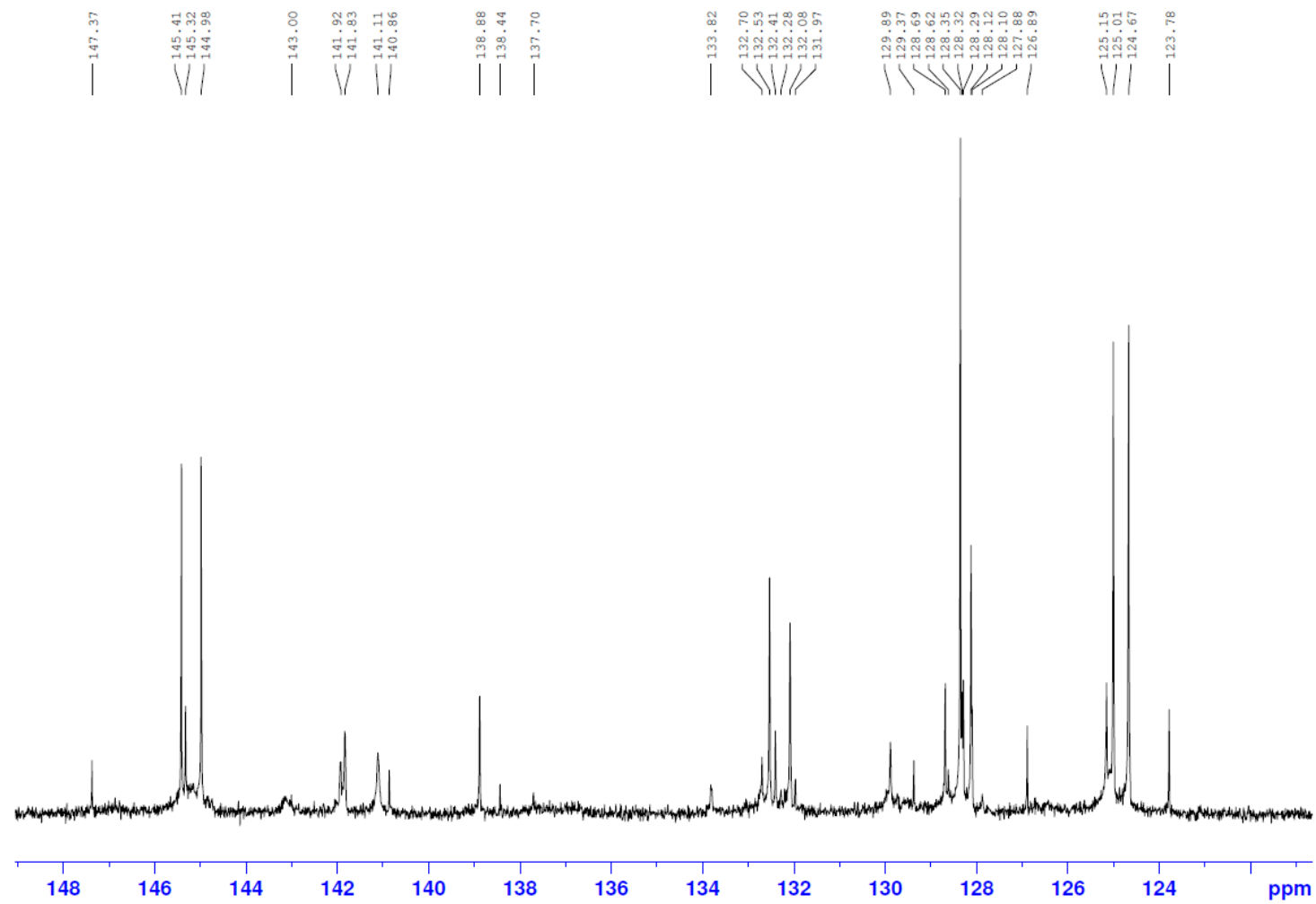
IPr-BF ¹³C NMR in CDCl₃



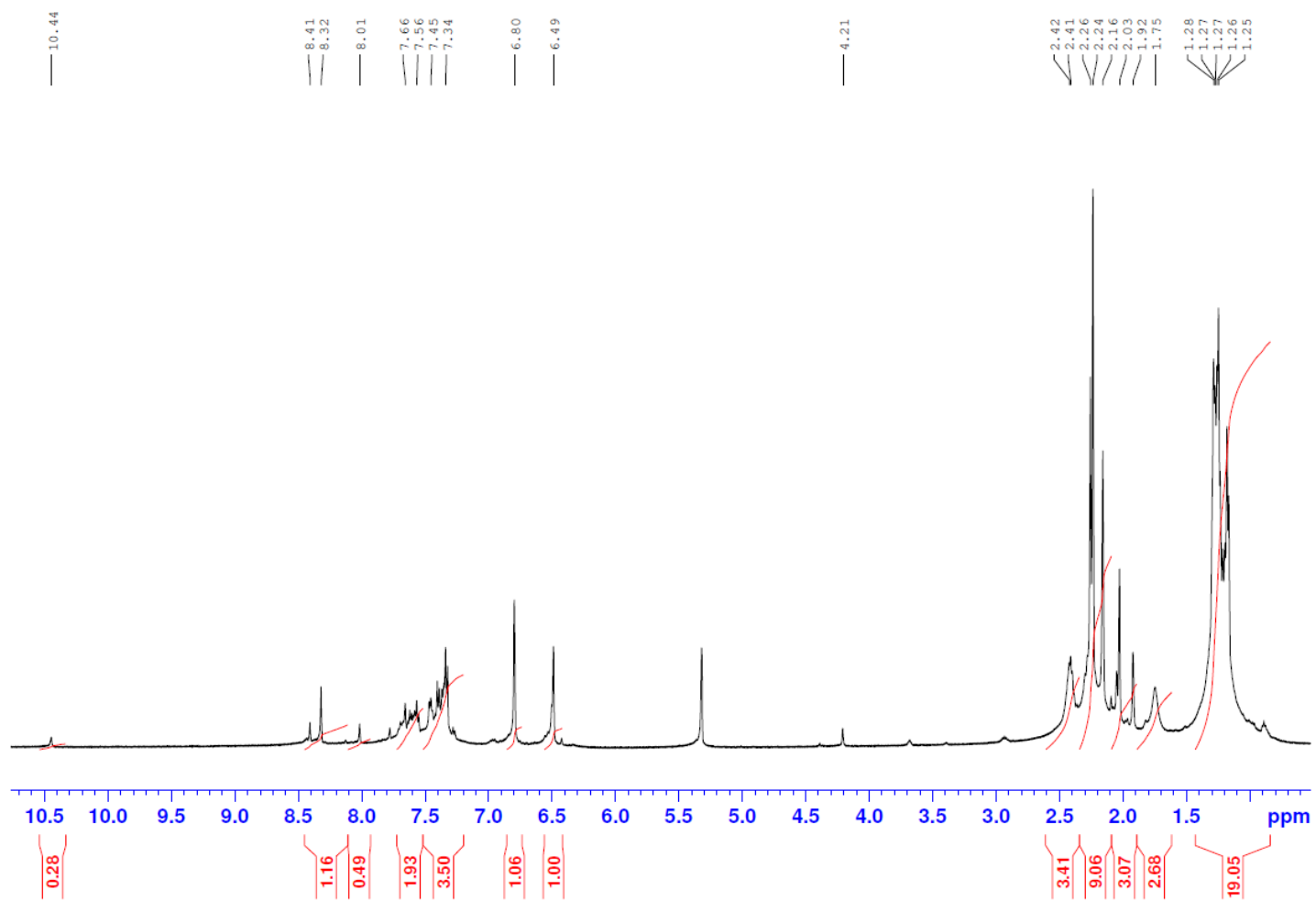
IPr-BF ¹³C NMR in CDCL₃ (0-70 ppm)



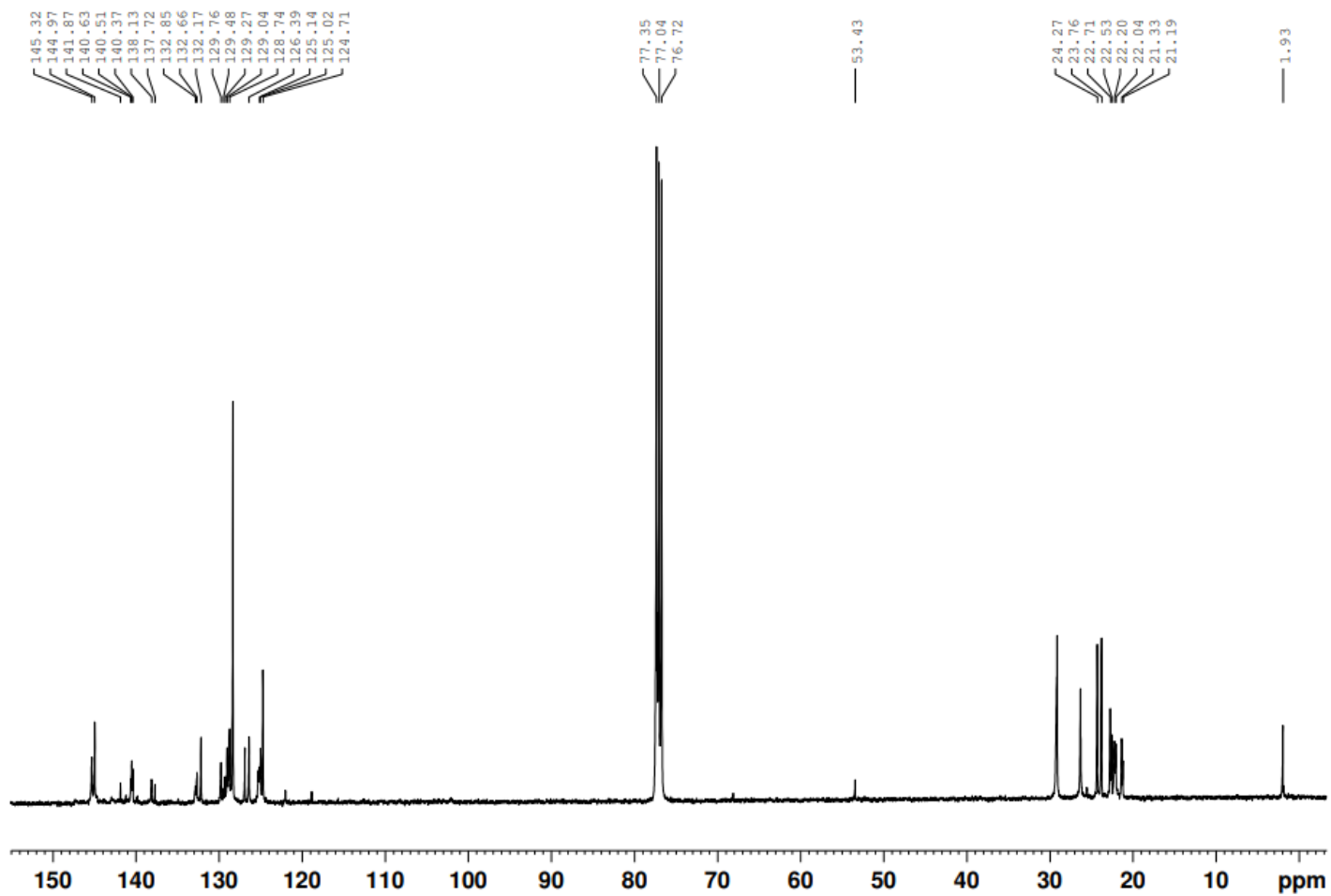
IPr-BF ¹³C NMR in CDCl₃ (120-150ppm)



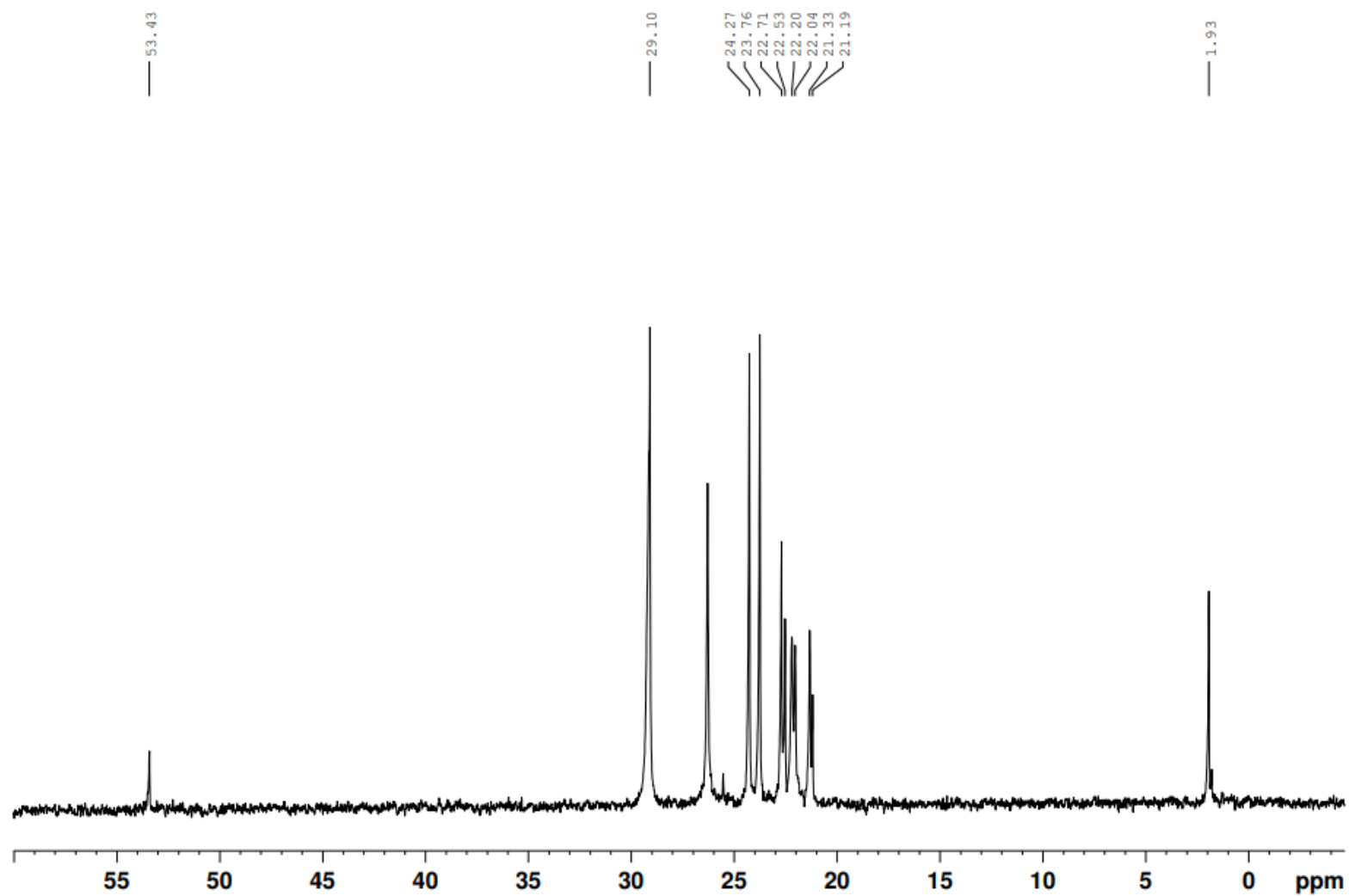
IPr-BF ¹H NMR in CDCl₃



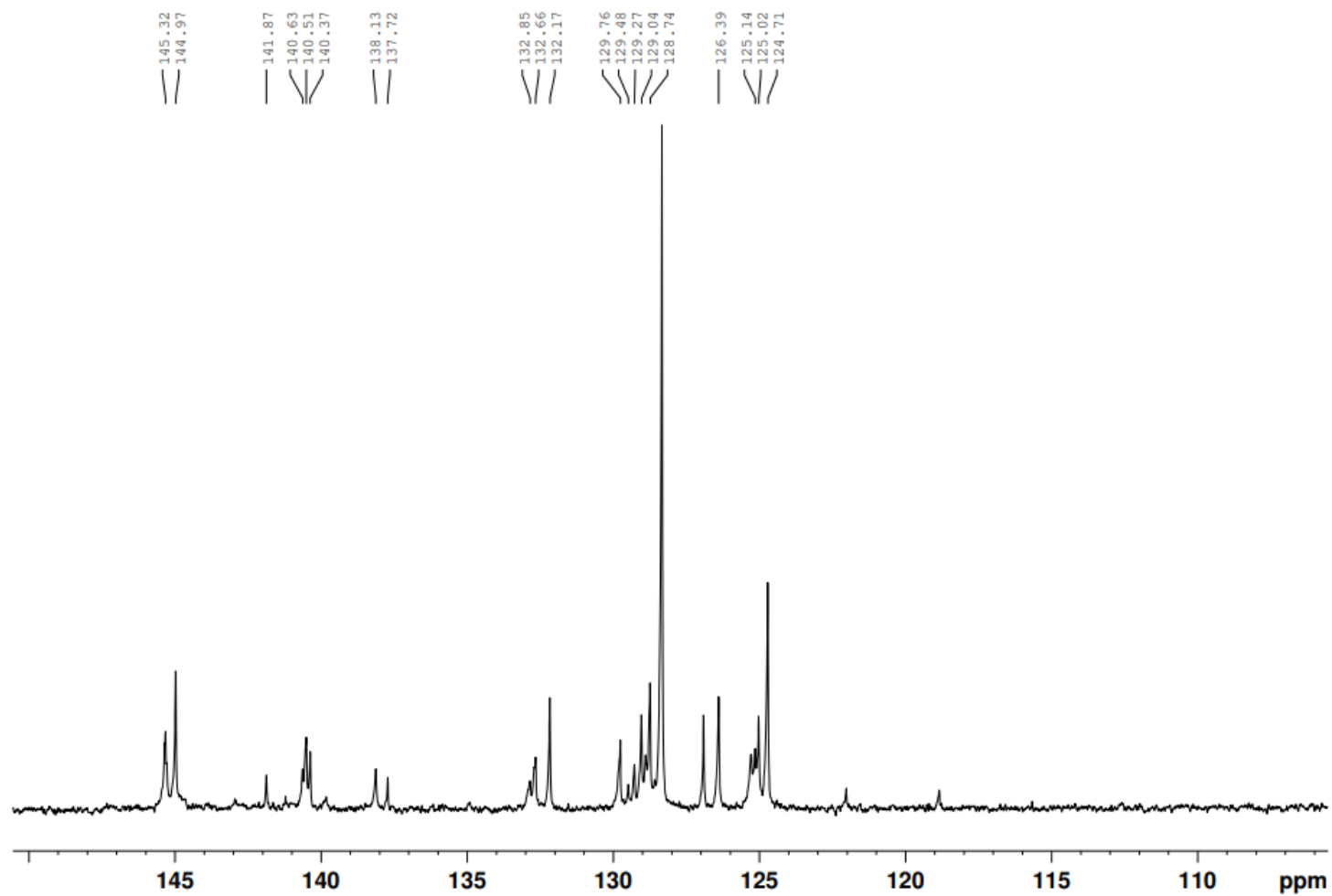
IPr-OTf- ^{13}C NMR in CDCl_3



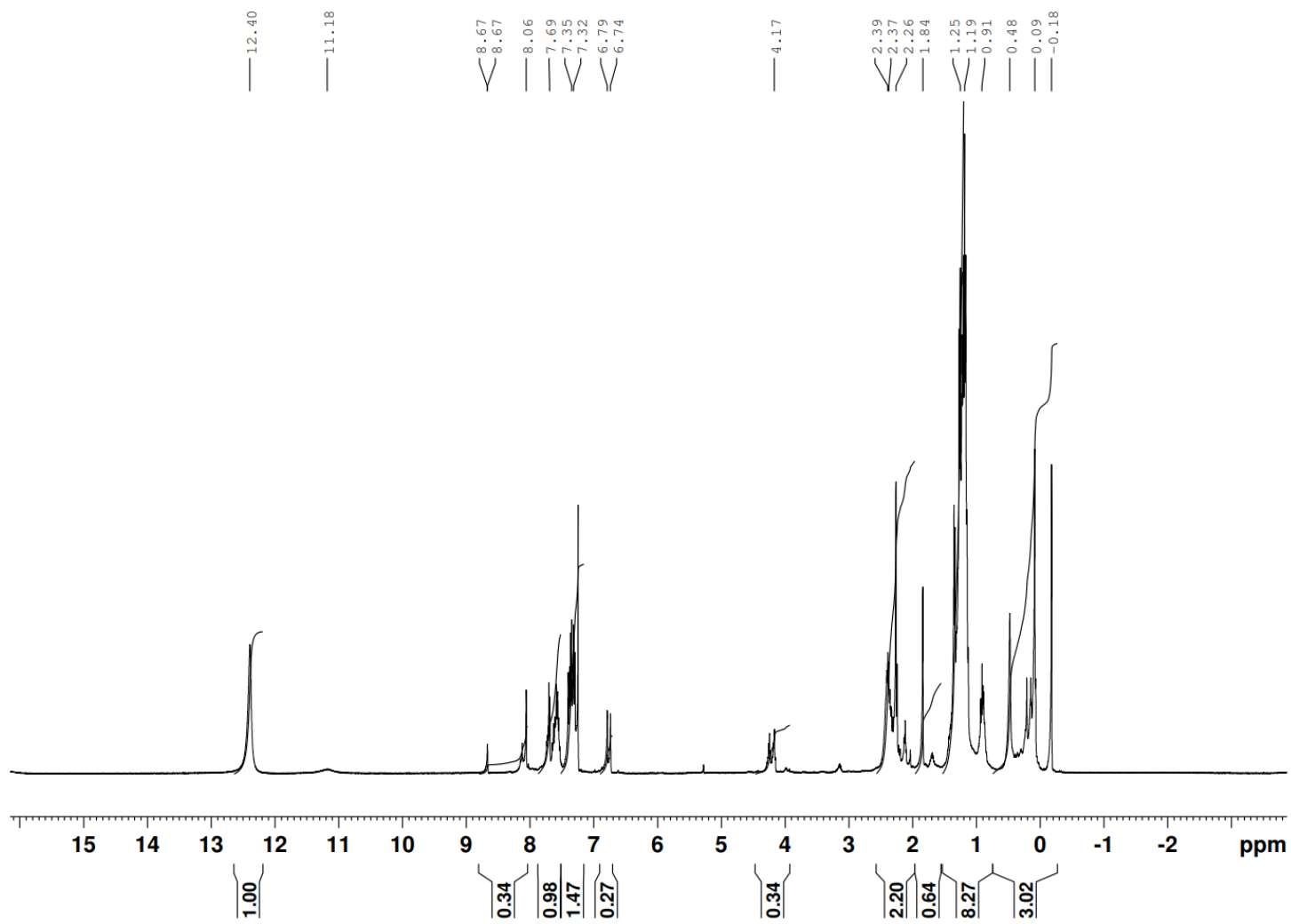
IPr-OTf-¹³C NMR in CDCl₃ (0-60 ppm)



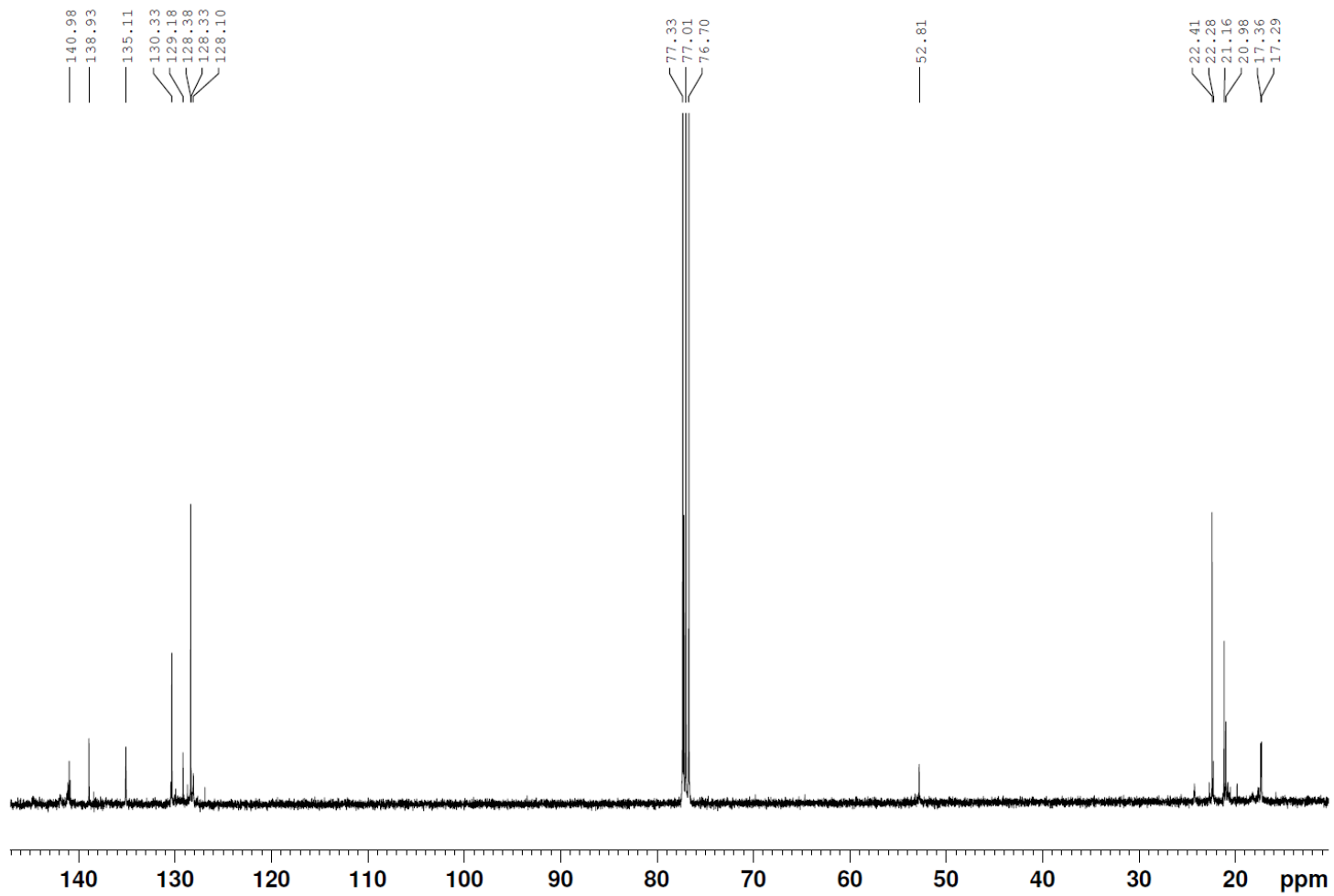
IPr-OTf-¹³C NMR in CDCl₃ (100-150 ppm)



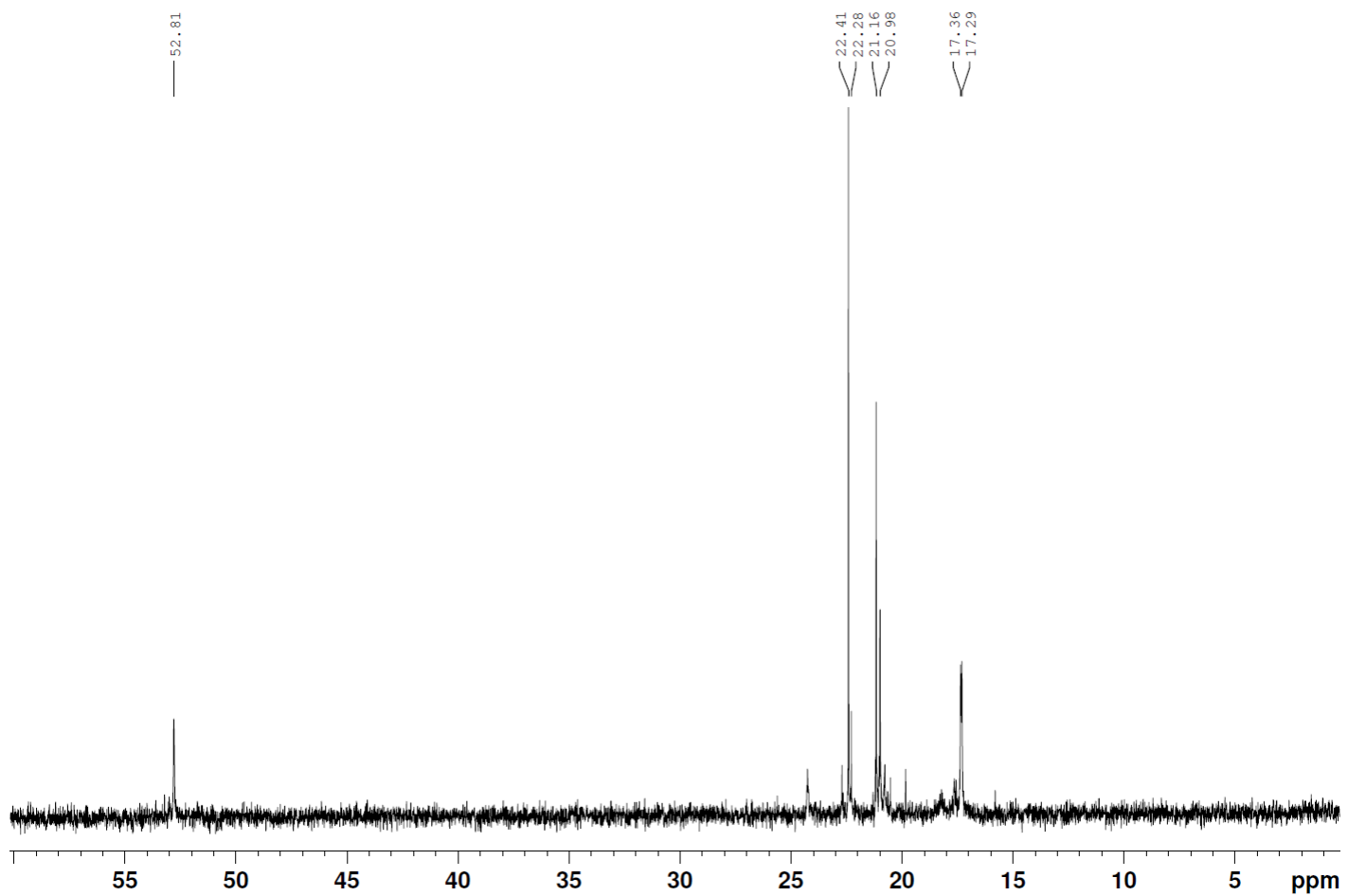
IPr-OTf-¹H NMR in CDCl₃



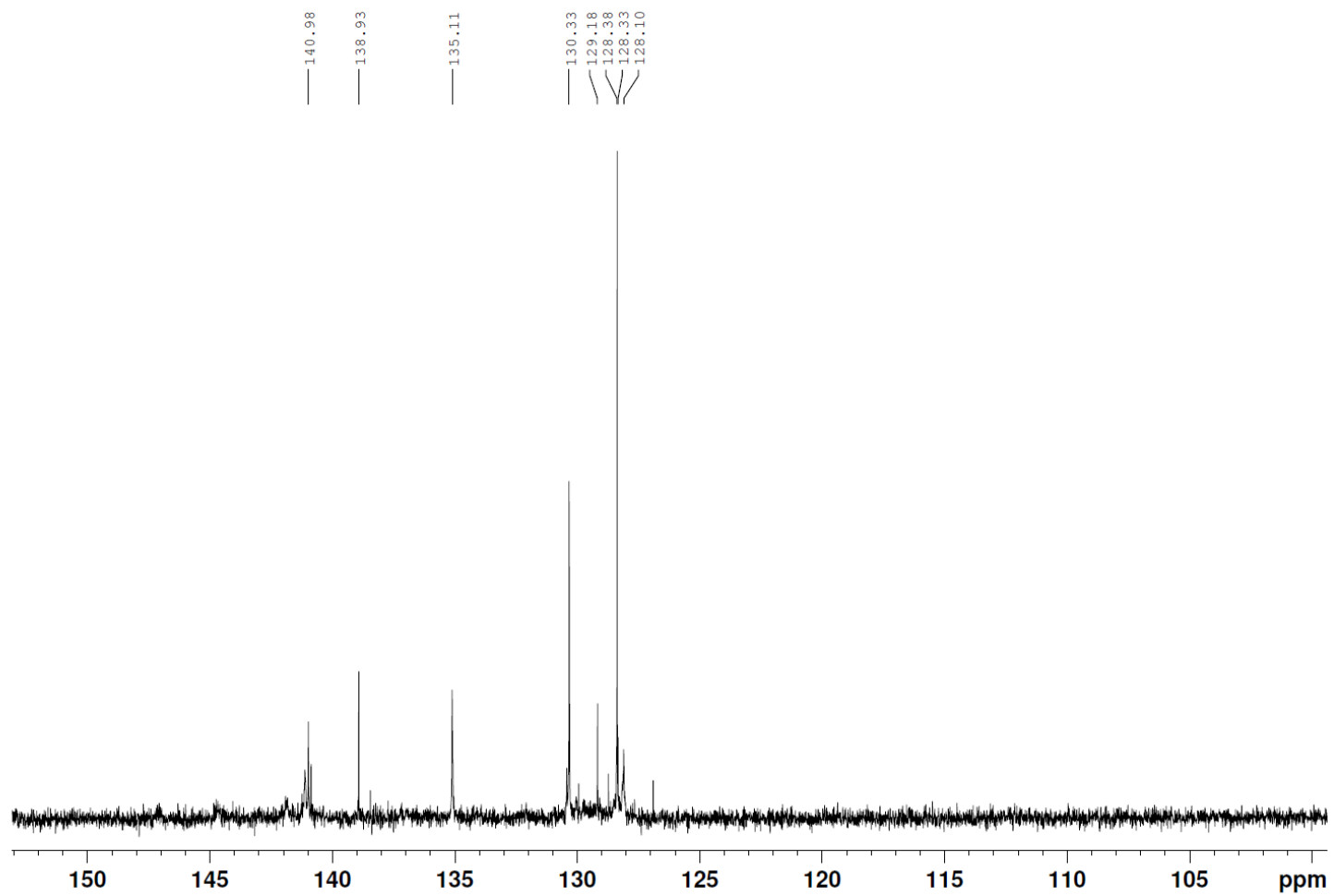
SIMes-BF ¹³C NMR in CDCl₃



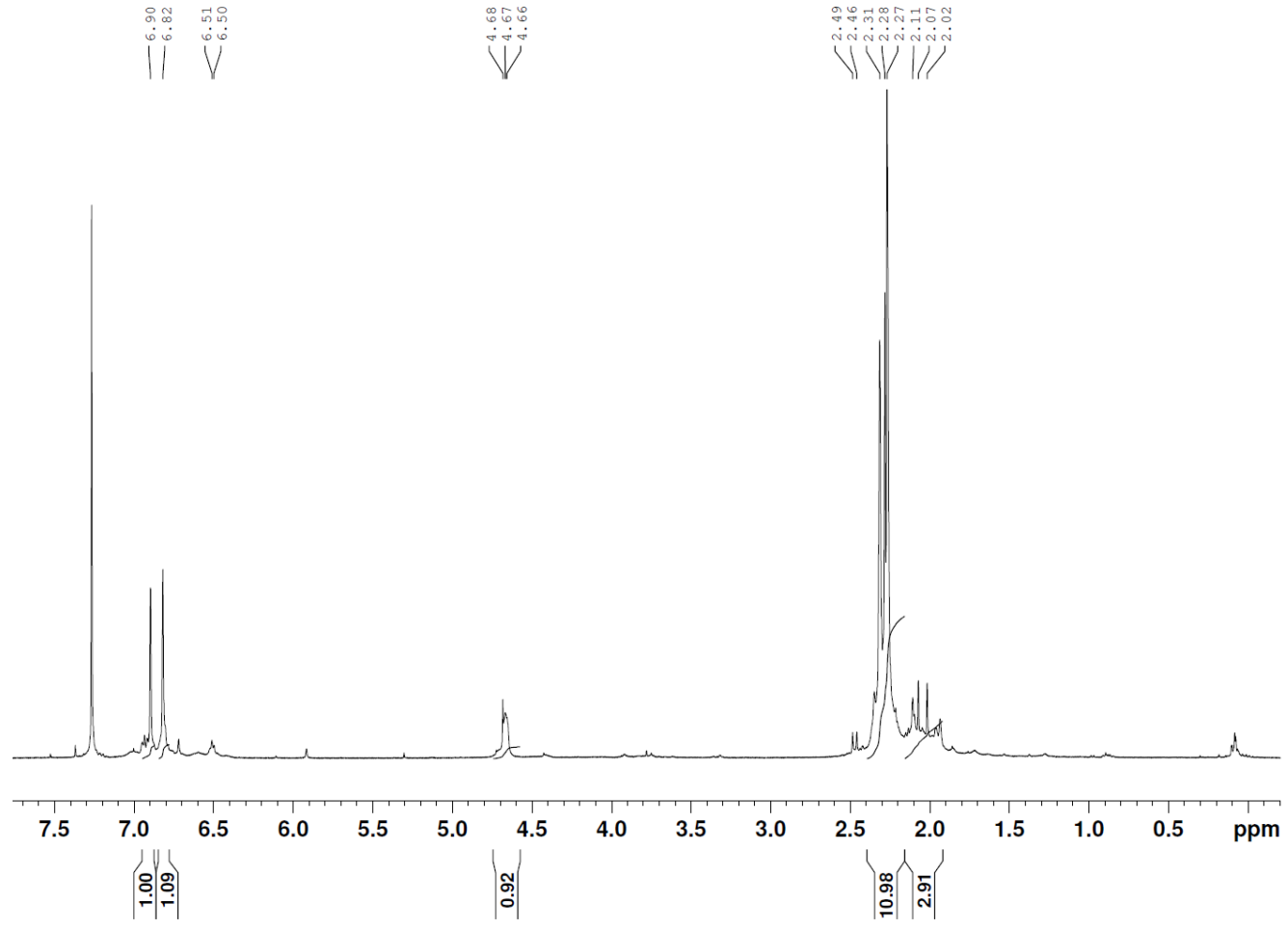
SIMes-BF ¹³C NMR in CDCL₃ (0-60ppm)



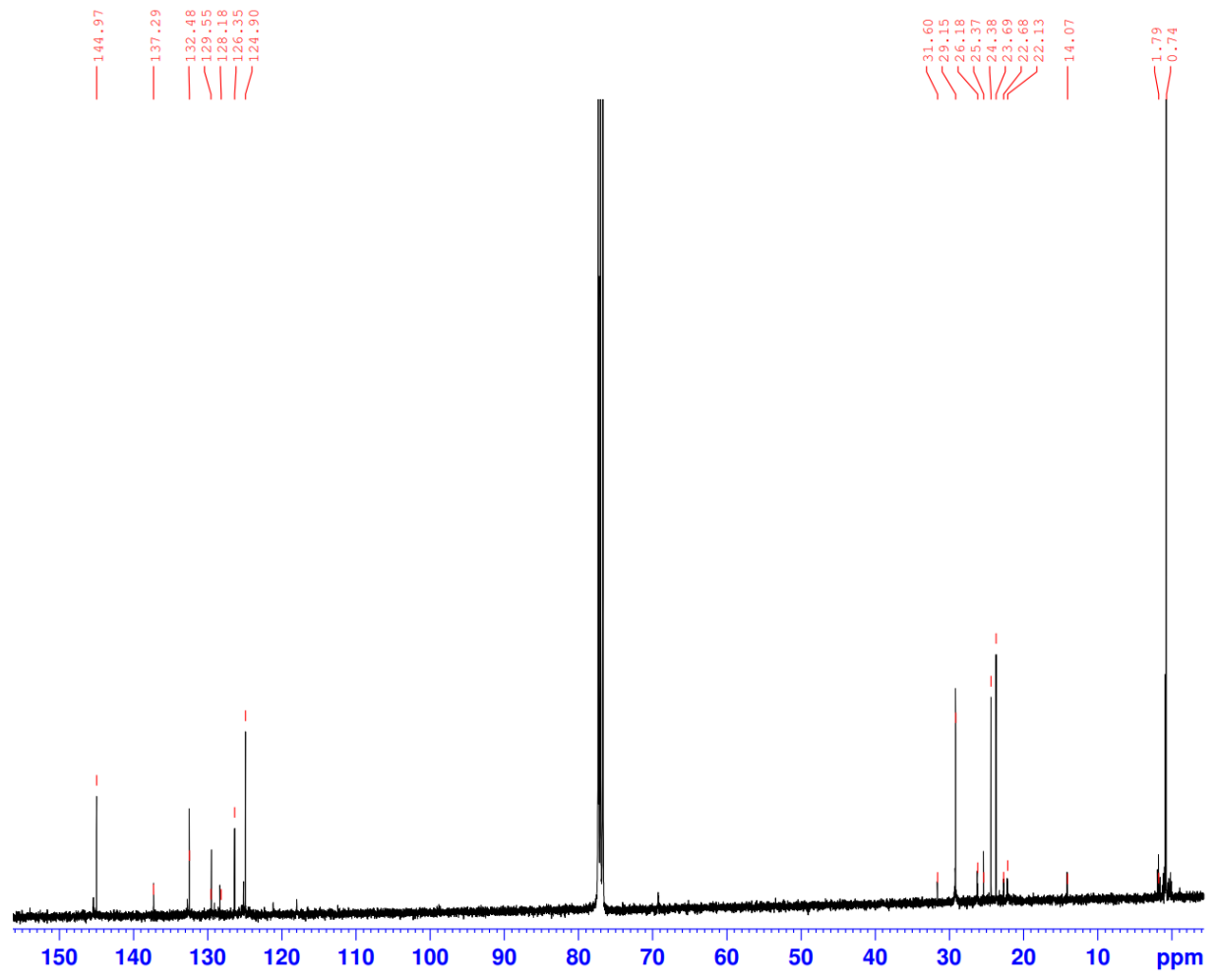
SIMes-BF ¹³C NMR in CDCl₃ (100-155 ppm)

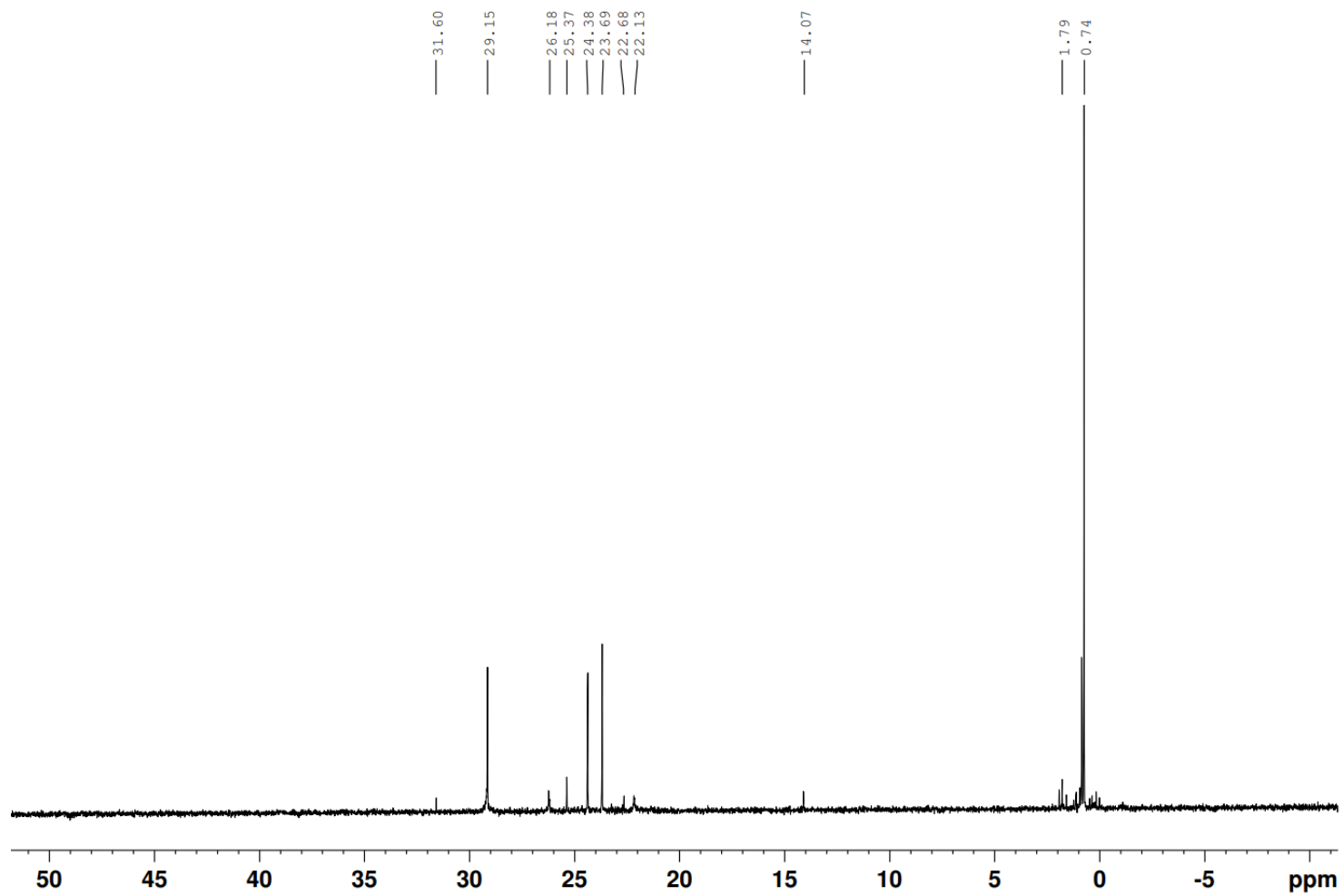


SIMes-BF ¹H NMR in CDCl₃

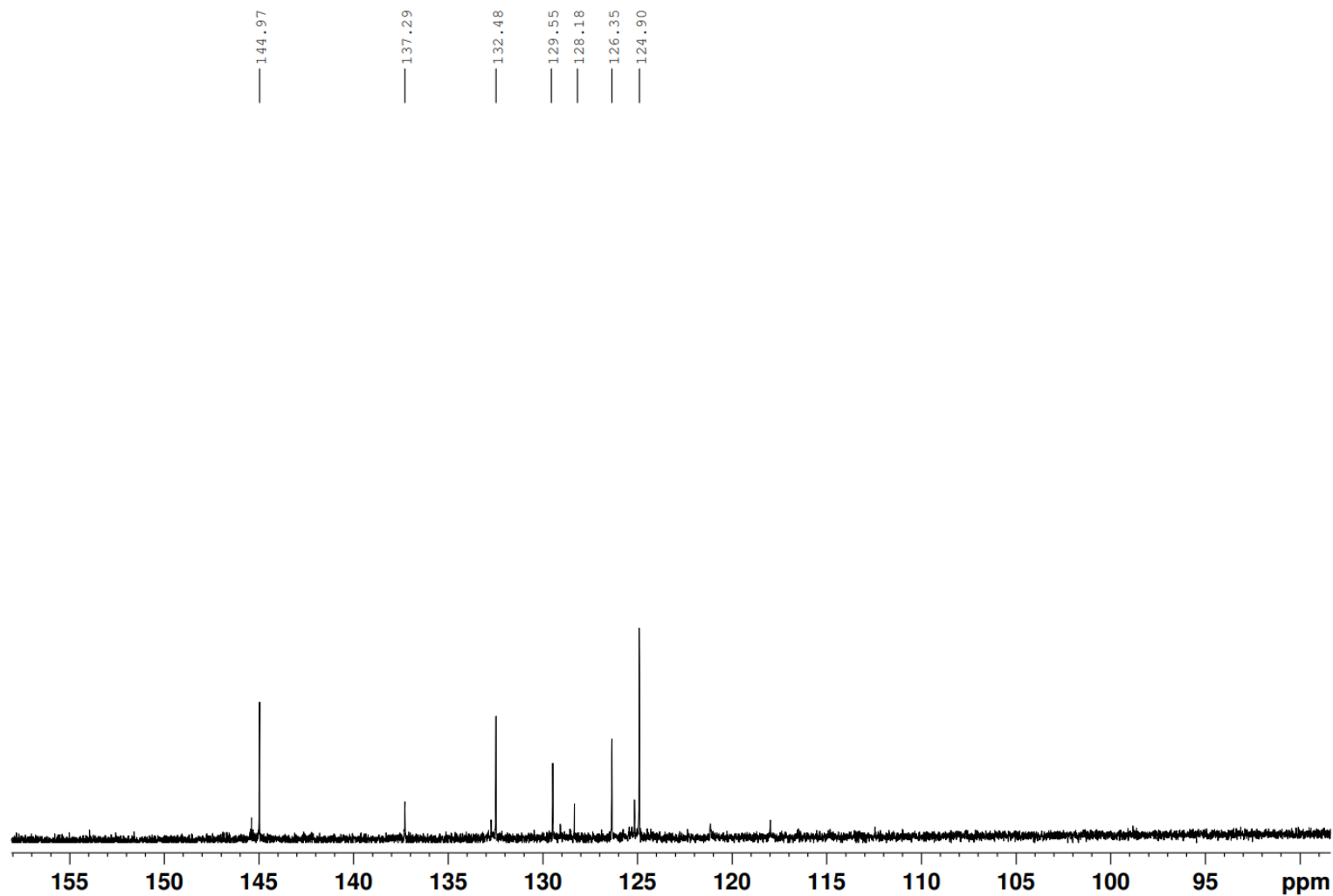


SIMes-OTf- ¹³C NMR in CD₂Cl₂

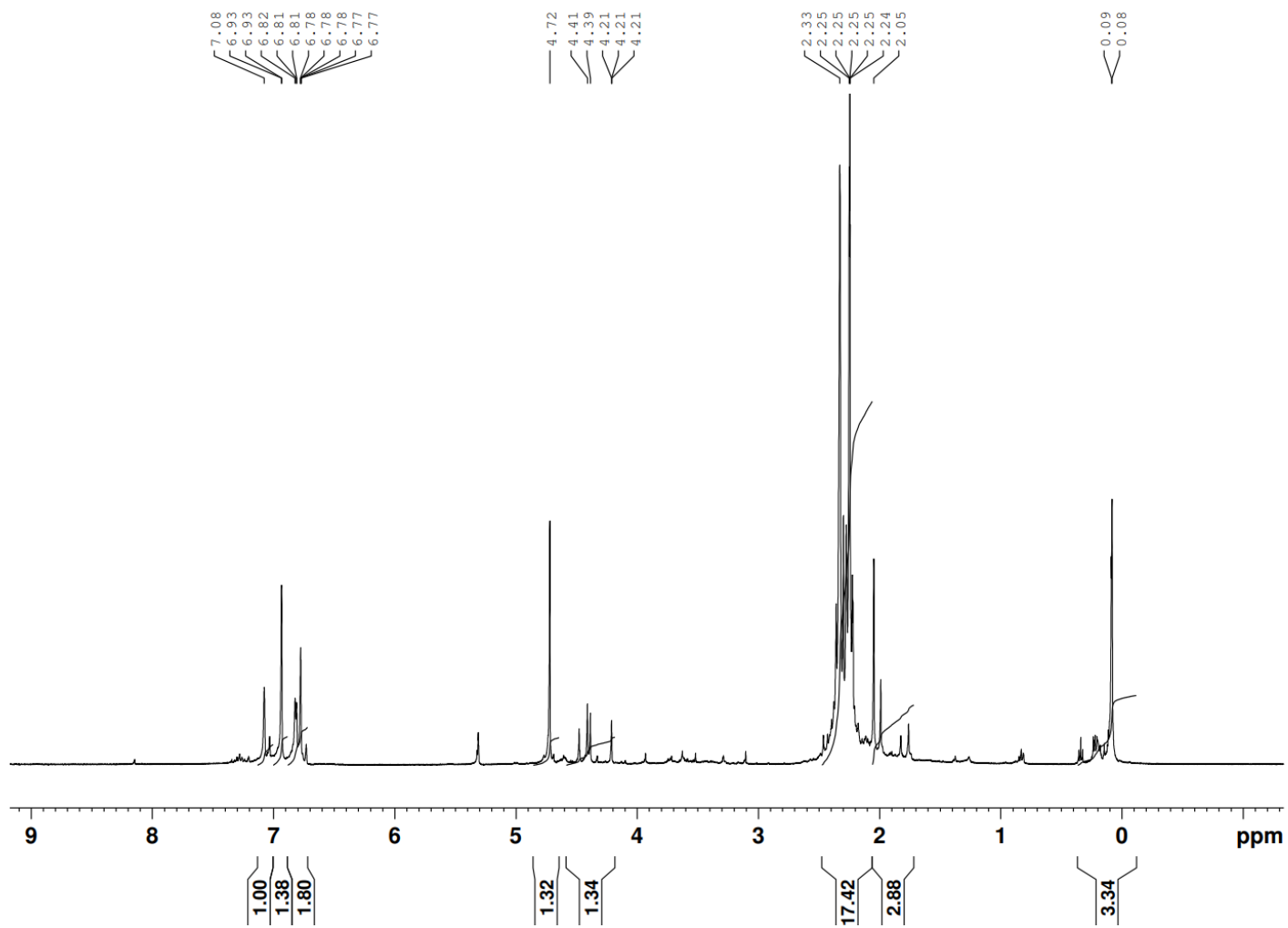


SIMes-OTf-¹³C NMR in CD₂Cl₂ (0-50 ppm)

SIMes-OTf-¹³C NMR in CD₂Cl₂ (85-160 ppm)



SIMes-OTf- ^1H NMR in CD_2Cl_2



LITERATURE CITED

- (1) Freudenrich, C. How OLEDs Work. <https://electronics.howstuffworks.com/oled.htm> (accessed March 9, 2020)
- (2) Kodan, M. *OLED displays and lighting*; John Wiley & Sons: Chichester, 2017.
- (3) Why your next TV should be OLED. <https://www.popularmechanics.co.za/tech/next-tv-oled/> (accessed Mar 9, 2020).
- (4) Lin Ke, Peng; Ramadas, K.; Burden, A.; Soo-Jin, C. "Indium-Tin-Oxide-Free Organic Light-Emitting Devices". *Transactions on Electron Devices*, **2006**, 53 (6): 1483–1486.
- (5) A. Endo; M. Ogasawara; A. Takahashi; D. Yokoyama; Y. Kato; C. Adachi. "Thermally Activated Delayed Fluorescence from Sn (4+)-porphyrin complexes and their application to organic light emitting diodes--a novel mechanism for electroluminescence". *Adv. Mater.* **2009**, 21 (47): 4802–4806.
- (6) Adachi, C.; Baldo, M. A.; Thompson, M. E.; Forrest, S. R. "Nearly 100% internal phosphorescence efficiency in an organic light-emitting device". *J. App. Phys.* **2001**, 90 (10): 5048.
- (7) Tang, C. W.; Vanslyke, S. A. "Organic electroluminescent diodes". *App Phys Lett.* **1987**, 51 (12): 913.
- (8) Kenneth S. Krane. *Introductory Nuclear Physics*. Wiley. **1987**, ISBN 978-0-471-80553-3.
- (9) What is the Jablonski diagram? <https://www.quora.com/What-is-the-Jablonski-diagram> (accessed Mar 13, 2020).
- (10) Granite. Jablonski Diagram: What is it? <https://www.edinst.com/blog/jablonski-diagram/>
- (11) Bernanose, A.; Comte, M.; Vouaux, P. (1953). "A new method of light emission by certain organic compounds". *J. Chem. Phys.* 50: 64.

- (12) Pope, M.; Kallmann, H. P.; Magnante, P. (1963). "Electroluminescence in Organic Crystals". *J. Chem Phys.* 38 (8): 2042.
- (13) Burroughes, J. H.; Bradley, D. D. C.; Brown, A. R.; Marks, R. N.; MacKay, K.; Friend, R. H.; Burns, P. L.; Holmes, A. B. "Light-emitting diodes based on conjugated polymers". *Nature*. **1990**, 347 (6293): 539–541.
- (14) J. Kido, K. Hongawa, K. Okuyama, K. Nagai. *Appl. Phys. Lett.* **1994**, 64, 815-817.
- (15) T. Wakimoto, R. Murayama, K. Nagayama, Y. Okuda, H. Nakada, T. Tohma, *SID 96 Digest*, 849 (1996)
- (16) M.A. Baldo, D. F. O'Brian, Y. You, A. Shoustikov, S. Sibley, M. E. Thompson, S. R. Forrest, *Nature*, **1993** 395, 151-154.
- (17) Freudenrich, C. How OLEDs Work.
<https://electronics.howstuffworks.com/oled5.htm> (accessed Mar 16, 2020).
- (18) An introduction to OLED displays. <https://www.oled-info.com/oled-introduction> (accessed Mar 16, 2020).
- (19) LG's 65" Rollable OLED TV R Boasts 100-watt Dolby Atmos Speaker System, Hits CES 2019. <https://www.techeblog.com/lg-rollable-oled-tv-ces-2019/> (accessed Mar 16, 2020).
- (20) Bagher, A. M. OLED Display Technology. *Am. J. Optics Photonics* **2014**, 2 (3), 32.
- (21) Tarantola, A. Why Is OLED Different and What Makes It So Great?
<https://gizmodo.com/why-is-oled-different-and-what-makes-it-so-great-1654102034>.
- (22) Tremblay, J.-F. The rise of OLED displays. <https://cen.acs.org/articles/94/i28/rise-OLED-displays.html>.

- (23) After three decades, OLED technology continues to evolve.
<https://www.ledsmagazine.com/leds-ssl-design/article/16695600/after-three-decades-oled-technology-continues-to-evolve-magazine> (accessed Mar 16, 2020).
- (24) M. Pope, C. E. Swenberg, *Electronic Processes in Organic Crystals and Polymers*, Oxford University Press, Oxford, 1999
- (25) A. Obolda, X. Ai, M. Zhang, F. Li. . **2016**, 8(51), 35472-35478
- (26) Minaev, B., Baryshnikov, G., & Agren, H. Principles of phosphorescent organic light emitting devices. *Phys. Chem. Chem. Phys.*, **2014**, 16(5), 1719–1758.
- (27) Fukagawa, H.; Shimizu, T.; Kamada, T.; Yui, S.; Hasegawa, M.; Morii, K.; Yamamoto, T. Highly efficient and stable organic light-emitting diodes with a greatly reduced amount of phosphorescent emitter. *Nature*. **2015**, 5, 1
- (28) Adachi, C.; Baldo, M. A.; Thompson, M. E.; Forrest, S. R. Nearly 100% internal phosphorescence efficiency in an organic light-emitting device. *J. App. Phys.*, **2001**. 90 (10): 5048.
- (29) Schmidbauer, S.; Hohenleutner, A.; König, B. Studies on the Photodegradation of Red, Green and Blue Phosphorescent OLED Emitters. *Beilstein J. Org. Chem.*, **2013**, 9, 2088–2096.
- (30) Ai, X., Evans, E.W., Dong, S. et al. Efficient radical-based light-emitting diodes with doublet emission. *Nature*, **2015** 563, 536–540.
- (31) Reineke, S. Radically more stable. *Nat. Mater.* **2019**, 18, 917–918
- (32) Hattori, Y., Kusamoto, T., & Nishihara, H. Luminescence, Stability, and Proton Response of an Open-Shell (3,5-Dichloro-4-pyridyl)bis(2,4,6-trichlorophenyl)methyl Radical. *Angew. Chem. Int. Ed.* **2015**. 53(44), 11845–11848.

- (33) Peng, Q.; Obolda, A.; Zhang, M.; Li, F. Organic Light-Emitting Diodes Using a Neutral π Radical as Emitter: The Emission from a Doublet. *Angew. Chem. Int. Ed.* **2015**, 54 (24) 7091-7095.
- (34) Gomberg, M. An instance of trivalent carbon: triphenylmethyl. *J. Am. Chem. Soc.* **1900**, 22 (11) 757-771.
- (35) Gomberg, M. On trivalent carbon. *J. Am. Chem. Soc.* **1902**, 24 (7) 597-628.
- (36) Kimera, S. H.; Kusamoto, T.; Tanushi, A.; Kochi, S. Isolable Bis(Triarylamine) Dications: Analogues of Thiele's, Chichibabin's, and Müller's Hydrocarbons. *Chem. Sci.* **2018**, 9 (7).
- (37) A. E. Tschitschibabin (1907), "Über einige phenylierte Derivate des *p, p*-Ditolyls." *Berichte der Deutschen Chemischen Gesellschaft*, volume 40, pages 1810–1819
- (38) Caneschi, A., Gatteschi, D., Sessoli, R., & Rey, P. Toward molecular magnets: the metal-radical approach. *Acc. Chem. Res.*, **1989**, 22(11), 392–398.
- (39) Nakahara, K.; Oyaizu, K.; Nishide, H. Organic radical battery approaching practical use. *Chem. Lett.* **2011**, 40 (3), 222–227.
- (40) Sung, S. H.; Bajaj, N.; Rhoads, J. F.; Chiu, G. T.; Boudouris, B. W. Radical Polymers Improve the Metal-Semiconductor Interface in Organic Field-Effect Transistors. *Org. Electron.* **2016**, 37, 148–154.
- (41) Mukherjee, S.; List, B. Radical catalysis. *Nature.* **2007**, 447, 152-153
- (42) Ai, X.; Chen, Y.; Feng, Y.; Li, F. A stable room-temperature luminescent biphenylmethyl radical. *Angew. Chem. Int. Ed.* **2018**, 57, 1-6.

- (43) Kimura, S.; Tanushi, A.; Kusamoto, T.; Kochi, S.; Sato, T.; Nishihara, H., A luminescent organic radical with two pyridyl groups: high photostability and dual stimuli-responsive properties, with theoretical analyses of photophysical processes. *Chem. Sci.* **2018**, 9 (7), 1996-2007.
- (44) Kimura, S.; Tanushi, A.; Kusamoto, T.; Kochi, S.; Sato, T.; Nishihara, H. A Luminescent Organic Radical with Two Pyridyl Groups: High Photostability and Dual Stimuli-Responsive Properties, with Theoretical Analyses of Photophysical Processes. *Chem. Sci.* **2018**, 9 (7), 1996–2007.
- (45) Guo, H.; Peng, Q.; Chen, X.-K.; Gu, Q.; Dong, S.; Evans, E. W.; Gillett, A. J.; Ai, X.; Zhang, M.; Credginton, D.; Coropceanu, V.; Friend, R. H.; Brédas, J.-L.; Li, F. High Stability and Luminescence Efficiency in Donor–Acceptor Neutral Radicals Not Following the Aufbau Principle. *Nature Materials.* **2019**, 18 (9), 977–984.
- (46) Shuto, A.; Kushida, T.; Fukushima, T.; Kaji, H.; Yamaguchi, S. π -Extended Planarized Triphenylboranes with Thiophene Spacers. *J. Am. Chem. Soc.* **2013**, 135 (24), 62234-6237
- (47) Martin, D.; Melaimi, M.; Soleilhavoup, M.; Bertrand, G.; Gabbai, F. A Brief Survey of Our Contribution to Stable Carbene Chemistry. *Organometallics* **2011**, 30 (20), 5304–5313.
- (48) Priv, V. Neues *Uber Carbene.* **1961**, No. 5.
- (49) Smith, A. D.; Woods, P. A. N-Heterocyclic Carbene Based Catalysts for the Kinetic Resolution of Alkyl Aryl Alcohols. *J. Am. Chem. Soc.* **2012**, 1.
- (50) Wang, Y.; Robinson, G. H. N-Heterocyclic Carbene—Main-Group Chemistry: A Rapidly Evolving Field. *Inorg. Chem.* **2014**, 53 (22), 11815–11832.

- (51) Glorius, F. *N-Heterocyclic Carbenes in Transition Metal Catalysis*; Springer Berlin Heidelberg: Berlin, Heidelberg, 2007.
- (52) Barynmaalz, D.; Siure, D.; Hyacinthengeruch, V.; Untereuchungen, M.; Mittheilung, V.; Kohlenwaeseretoffe, B.; Toluol, M.; Xvii, D. B.; Xviii, D. B. Buchner Und Th. Curtius: Ueber Die Einwirkun# von DiazoessigBther. 2377–2379.
- (53) Wanzlick, H.-W.; Schikora, E. Ein Neuer Zugang Zur Carben-Chemie. *Angew. Chemie* **1960**, 72 (14), 494–494.
- (54) Igau, A.; Grutzmacher, H.; Baceiredo, A.; Bertrand, G. Analogous α, α' -Bis-Carbenoid Triply Bonded Species: Synthesis of a Stable Λ^3 -Phosphinocarbene- Λ^5 -Phosphaacetylene. *J. Am. Chem. Soc.* **1988**, 110 (10), 6463–6466.
- (55) Berthon-Gelloz, G.; Siegler, M. A.; Spek, A. L.; Tinant, B.; Reek, J. N. H.; Markó, I. E. IPr* an Easily Accessible Highly Hindered N-Heterocyclic Carbene. *Dalton Trans.* **2010**, 39 (6), 1444–1446.
- (56) Fantasia, S.; Petersen, J. L.; Jacobsen, H.; Cavallo, L.; Nolan, S. P. Electronic Properties of N-Heterocyclic Carbene (NHC) Ligands: Synthetic, Structural, and Spectroscopic Studies of (NHC)Platinum (II)Complexes *Organometallics*. **2007**, 26 (24), 5880–5889.
- (57) Lavallo, V. Cyclopropenylienes: From Interstellar Space to an Isolated Derivative in the Laboratory. *Science* **2006**, 312 (5774), 722–724.
- (58) Lavallo, V.; Canac, Y.; Praesang, C.; Donnadieu, B.; Bertrand, G. Stable Cyclic (Alkyl)(Amino)Carbenes as Rigid or Flexible, Bulky, Electron-Rich Ligands for Transition-Metal Catalysts: A Quaternary Carbon Atom Makes the Difference. *ChemInform* **2006**, 37 (1).

- (59) Torres, A. J.; Dorsey, C. L.; Hudnall, T. W. Preparation and Use of Carbonyl-Decorated Carbenes in the Activation of White Phosphorus. *J. Visualized Exp.* **2014**, No. 92.
- (60) Tomás-Mendivil, E.; Hansmann, M. M.; Weinstein, C. M.; Jazzar, R.; Melaimi, M.; Bertrand, G. Bicyclic (Alkyl)(Amino)Carbenes (BICAACs): Stable Carbenes More Ambiphilic than CAACs. *J. Am. Chem. Soc.* **2017**, *139* (23), 7753–7756.
- (61) Viehe, H. G.; Janousek, Z.; Merenyi, R. ChemInform Abstract: Captodative Substituent Effects. Part 44. Captodative Substituent Effect in Synthesis. *ChemInform* **1990**, *21* (12).
- (62) Wang, Y.; Robinson, G. H. Carbene Stabilization of Highly Reactive Main-Group Molecules. *Inorg. Chem.* **2011**, *50* (24), 12326–12337.
- (63) Viehe, H. G.; Janousek, Z.; Merenyi, R. ChemInform Abstract: Captodative Substituent Effects. Part 44. Captodative Substituent Effect in Synthesis. *ChemInform* **1990**, *21* (12).
- (64) Rogawski, R.; Sergeyev, I. V.; Zhang, Y.; Tran, T. H.; Li, Y.; Tong, L.; Mcdermott, A. E. NMR Signal Quenching from Bound Biradical Affinity Reagents in DNP Samples. *J. Phys. Chem. B* **2017**, *121* (48), 10770–10781.
- (65) Piers, W. E.; Chivers, T. “Pentafluorophenylboranes: from Obscurity to Applications”, *Chem. Rev.* **1997**, *26*, 345-354
- (66) Bonn, A. G.; Wenger, O. S. Charge Transfer Emission in Oligotriarylamine–Triarylborane Compounds. *J. Org. Chem.* **2015**, *80* (8), 4097–4107.
- (67) Kumar, G. R.; Sarkar, S. K.; Thilagar, P. Aggregation-Induced Emission and Sensing Characteristics of Triarylborane-Oligothiophene-Dicyanovinyl Triads. *Chem. - Eur. J.* **2016**, *22* (48), 17215–17225.

- (68) Segawa, Y.; Suzuki, Y.; Yamashita, M.; Nozaki, K. Chemistry of Boryllithium: Synthesis, Structure, and Reactivity. *J. Am. Chem. Soc.* **2009**, *131* (27), 9600–9600.
- (69) Cummings, S. A.; Imura, M.; Harlan, C. J.; Kwaan, R. J.; Trieu, I. V.; Norton, J. R.; Bridgewater, B. M.; Jäkle, F.; Sundararaman, A.; Tilset, M. An Estimate of the Reduction Potential of B(C₆F₅)₃ from Electrochemical Measurements on Related Mesityl Boranes. *Organometallics* **2006**, *25* (7), 1565–1568.
- (70) Turkoglu, G.; Cinar, M. E.; Ozturk, T. Triarylborane-Based Materials for OLED Applications. *Molecules* **2017**, *22* (9), 1522.
- (71) Yang, K.; Zhang, G.; Song, Q. Four-Coordinate Triarylborane Synthesis via Cascade B–Cl/C–B Cross-Metathesis and C–H Bond Borylation. *Chem. Sci.* **2018**, *9* (39), 7666–7672.
- (72) Schaub, T. A.; Padberg, K.; Kivala, M. Bridged Triarylboranes, -Silanes, -Amines, and -Phosphines as Minimalistic Heteroatom-Containing Polycyclic Aromatic Hydrocarbons: Progress and Challenges. *J. Phys. Org. Chem.* **2019**, *33* (2).
- (73) Kitamoto, Y.; Kobayashi, F.; Suzuki, T.; Miyata, Y.; Kita, H.; Funaki, K.; Oi, S. Investigation of the Lewis Acidic Behaviour of an Oxygen-Bridged Planarized Triphenylborane toward Amines and the Properties of Their Lewis Acid–Base Adducts. *Dalton Transactions* **2019**, *48* (6), 2118–2127.
- (74) Stephan, D. W.; Erker, G. Frustrated Lewis Pair Mediated Hydrogenations. *Topics in Current Chemistry Frustrated Lewis Pairs I* **2013**, 85–110.
- (75) Thakur, A.; Vardhanapu, P. K.; Vijaykumar, G.; Bhatta, S. R. Investigation on Reactivity of Non-Classical Carbenes with Sterically Hindered Lewis Acid, B(C₆F₅)₃ under Inert and Open Conditions. *J. Chem. Sci.* **2016**, *128* (4), 613–620.

- (76) Styra, S.; Melaimi, M.; Moore, C. E.; Rheingold, A. L.; Augenstein, T.; Breher, F.; Bertrand, G. Crystalline Cyclic (Alkyl)(Amino)Carbene-Tetrafluoropyridyl Radical. *Chem. - Eur. J.* **2015**, *21* (23), 8441–8446.
- (77) Fluorine shifts overview. <https://www.chem.wisc.edu/areas/reich/nmr/11-f-data.htm>
- (78) Foris, A. *On ¹⁹F NMR Spectra of BF₂ and BF Complexes and Related Compounds*; **2016**.
- (79) Perrio, C.; Schmitt, S.; Pla, D.; Gabbai, F. P.; Chansaenpak, K.; Mestre-Voegtle, B.; Gras, E. [18F]-Fluoride Capture and Release: Azeotropic Drying Free Nucleophilic Aromatic Radiofluorination Assisted by a Phosphonium Borane. *Chem. Comm.* **2017**, *53* (2), 340–343.
- (80) The Relationship Between UV-VIS Absorption and Structure of Organic Compounds. <https://www.shimadzu.com/an/uv/support/uv/ap/apl.html> (accessed Apr 4, 2020).
- (81) Jones, R. N. The Ultraviolet Absorption Spectra of Aromatic Hydrocarbons. *Chem. Reviews.* **1943**, *32* (1), 1–46.
- (82) Engelen, D. L. V.; Thomas, L. C.; Piepmeier, E. H. Ultraviolet Spectrometric Detection for Gas Chromatography of Polynuclear Aromatic Compounds with Repetitive Spectral Scans Using Absorbance and Concurrent Fluorescence Measurements. *J. Chromatography A* **1987**, *405*, 191–202.
- (83) Cummings, S. A.; Iimura, M.; Harlan, C. J.; Kwaan, R. J.; Trieu, I. V.; Norton, J. R.; Bridgewater, B. M.; Jäkle, F.; Sundararaman, A.; Tilset, M. An Estimate of the Reduction Potential of B(C₆F₅)₃ from Electrochemical Measurements on Related Mesityl Boranes. *Organometallics* **2006**, *25* (7), 1565–1568.

- (84) Brandt, J. R.; Lee, E.; Boursalian, G. B.; Ritter, T. Mechanism of Electrophilic Fluorination with Pd (Iv): Fluoride Capture and Subsequent Oxidative Fluoride Transfer. *Chem. Sci.* **2014**, 5 (1), 169–179.
- (85) Kim, Y.; Lee, E. *Chem. Comm.* **2016**, 52 (72), 10922–10925.